NASA Contractor Report 198231

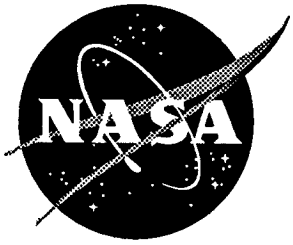

Empirical Modeling of Environment-Enhanced Fatigue Crack Propagation in Structural Alloys for Component Life Prediction

Edward Richey III
University of Virginia, Charlottesville, Virginia

Grant NAG1-745

(NASA-CR-198231) EMPIRICAL MODELING OF ENVIRONMENT-ENHANCED FATIGUE CRACK PROPAGATION IN STRUCTURAL ALLOYS FOR COMPONENT LIFE PREDICTION Final Report (Virginia Univ.) 173 p

N96-15122

Unclas

G3/24 0079427

October 1995

National Aeronautics and
Space Administration
Langley Research Center
Hampton, Virginia 23681-0001

Empirical Modeling of Environment-Enhanced Fatigue Crack Propagation in Structural Alloys for Component Life Prediction

Executive Summary

This research aims to develop the methods and understanding needed to incorporate time and loading variable dependent environmental effects on fatigue crack propagation (FCP) into computerized fatigue life prediction codes such as NASA FLAGRO. In particular, the effect of loading frequency on FCP rates in $\alpha + \beta$ titanium alloys exposed to an aqueous chloride solution is investigated. The approach couples empirical modeling of environmental FCP rates with corrosion fatigue experiments.

Three different computer models have been developed and incorporated in the DOS executable program, UVAFAS. A multiple power law model is available, and can fit a set of fatigue data to a multiple power law equation. A model has also been developed which implements the Wei and Landes linear superposition model, as well as an interpolative model which can be utilized to interpolate trends in fatigue behavior based on changes in loading characteristics (stress ratio, frequency, and hold time).

Ti-6Al-4V in aqueous chloride was chosen as the material/environment system utilized to test the computer models. Ti-6Al-4V was chosen because it is the most studied $\alpha + \beta$ titanium alloy, with some data available in the literature. Ti-6Al-4V was also chosen because of the complex, time dependent fatigue behavior exhibited by the alloy in NaCl solution. Unfortunately, sufficient literature data were not available to test the computer models.

In order to generate data to test the computer models, environment assisted cracking

experiments were conducted on Ti-6Al-4V in aqueous chloride. Constant crack mouth opening displacement rate experiments were conducted on fracture mechanics compact tension specimens of Ti-6Al-4V in the mill-annealed, extra low interstitial (ELI) condition in moist air and a 3.5% NaCl solution at a fixed electrode potential of -500 mV_{SCE}. The fracture toughness of the material (78 MPa$\sqrt{m}$) , as well as the stress corrosion cracking susceptibility of the alloy were determined. ELI grade Ti-6Al-4V exhibits a greater resistance to stress corrosion cracking than standard Ti-6Al-4V. The threshold stress intensity for crack initiation (K_{TH}) in NaCl is between 48 and 55 MPa$\sqrt{m}$ depending on loading rate. The ELI alloy also exhibits a slower stress corrosion crack velocity ($< 10^{-5}$ mm/sec) than less pure Ti-6Al-4V.

The fatigue crack propagation rates exhibited by Ti-6Al-4V (ELI) are enhanced two to fourfold in NaCl compared to moist air. The ELI grade in 3.5% NaCl(-500 mV_{SCE}) exhibits da/dN which mildly increases with frequency (f) for constant ΔK levels of 12.5 and 25 MPa$\sqrt{m}$, and frequencies in the range of 0.03 to 40 Hz. Specifically, da/dN is proportional to $f^{0.1 \text{ to } 0.2}$. Unlike standard Ti-6Al-4V, the ELI grade does not exhibit the frequency "crossover" effect for ΔK values below 25 MPa$\sqrt{m}$, due to the increased stress corrosion cracking resistance of the ELI grade. For frequencies less than 200 Hz, a frequency crossover is likely to occur only at a ΔK level above 25 MPa$\sqrt{m}$.

The closure levels exhibited by ELI Ti-6Al-4V are consistent with plasticity induced crack closure, and are independent of environment. Closure levels similarly equal 0.3 for fatigue crack propagation in moist air, 1.0% NaCl (-500 mV_{SCE}), and 3.5% NaCl (-500 mV_{SCE}) at ΔK levels above 10 MPa$\sqrt{m}$. Changes in frequency in the range of 0.03 to 40 Hz

and the associated changes in exposure time have no effect on closure levels for ΔK values of 12.5 and 25 MPa$\sqrt{m}$ in 3.5% NaCl. For ΔK values below 10 MPa$\sqrt{m}$, closure levels significantly increase as ΔK decreases, perhaps due to roughness or oxide-induced closure.

Two separate computer models in UVAFAS were applied to describe fatigue crack propagation rates in Ti-6Al-4V in an aqueous NaCl solution. The Wei and Landes linear superposition model is effective for modeling the effect of loading frequency on fatigue crack propagation rates in standard grade Ti-6Al-4V in 3.5% NaCl for ΔK values where K_{max} exceeds K_{TH}. The linear superposition model is not effective for ELI grade Ti-6Al-4V due to the increased stress corrosion cracking resistance of the alloy.

An interpolative model reasonably describes the effect of stress ratio (R) on FCP rates in Ti-6Al-4V (ELI), as well as the effect of frequency on fatigue crack propagation rates in standard and ELI grade Ti-6Al-4V. The model interpolates the effect of R and f on da/dN within the range of the establishing data base. The ability of the model to predict fatigue data for load characteristics outside the data base has not been tested, and is likely to be poor.

The linear superposition and interpolative models have been tested and effectively model fatigue crack propagation rates in certain material/environment systems; these models can be incorporated in NASA FLAGRO. These empirical models , however, are only applicable to certain material/environment systems where substantial data exist. They cannot be used for widespread prediction of environmental fatigue behavior.

Table Of Contents

List of Tables

List of Figures

List Of Symbols

a ..... crack length
b ..... specimen thickness
BA ..... beta annealed
CMOD ..... crack mouth opening displacement
CT ..... compact tension
da/dN ..... fatigue crack growth rate
$(da/dN)_{fatigue}$ ..... inert environment mechanical fatigue crack growth rate
$(da/dN)_{total}$ ..... environment enhanced fatigue crack growth rate
$(da/dt)_{environment}$ ..... stress corrosion crack velocity
DCPD ..... direct current potential drop
E ..... elastic (Young's) modulus
EAC ..... environment assisted cracking
EFCP ..... environmental fatigue crack propagation
ELI ..... extra low interstitial
f_c ..... crack closure function used by the Forman equation with closure
FCP ..... fatigue crack propagation
FTA ..... Fracture Technology Associates
J_{IC} ..... critical value of J-integral required to initiate growth of a preexisting crack
K ..... stress intensity
K_C ..... plane stress fracture toughness
K_{cl} ..... closure stress intensity
K_{IC} ..... plane strain fracture toughness
K_{ISCC} ..... threshold stress intensity for stress corrosion cracking
K_{min} ..... minimum applied stress intensity during fatigue cycle
K_{max} ..... maximum applied stress intensity during fatigue cycle
K_{TH} ..... threshold stress intensity for crack initiation in environment
MA ..... mill annealed
MSE ..... Modified Sigmoidal Equation
N ..... cycle number
P ..... applied load
P_{min} ..... minimum applied load during fatigue cycle
R ..... stress ratio, ratio of minimum to maximum applied stress intensity
r^2 ..... coefficient of determination
SCC ..... stress corrosion cracking
SCE ..... saturated calomel electrode
SINH ..... Hyperbolic Sine Equation
V_{LL} ..... load line displacement
W ..... specimen width
Δa ..... crack extension
ΔK ..... stress intensity range, $K_{max} - K_{min}$
ΔK_{eff} ..... effective stress intensity range when closure is present, $K_{max} - K_{cl}$

ΔK_{SCC} ..... ΔK value associated with the onset of "cyclic" stress corrosion cracking
ΔK_{th} ..... threshold stress intensity range for fatigue growth
σ_{ys} ..... yield strength
τ ..... hold time at K_{max} during fatigue cycle
f ..... fatigue loading frequency

Acknowledgements

The author would like to thank Professor Richard P. Gangloff for his time, patience, and aid in the completion of this thesis. Also, a special thanks to fellow graduate students Mark Mason, Jennifer Grandle, Brian Somerday, and Mike Haynes for their assistance in conducting the experiments completed during this research. Financial support was contributed by NASA Langley Research Center, monitored by Dr. Robert S. Piascik, and by NASA Johnson Space Center, monitored by Dr. Royce G. Forman.

Chapter 1: Background

1.1 Problem

Coupling an aggressive environment with cyclic plastic deformation can significantly reduce the fatigue life of an aerospace alloy. Environmental effects, however, have not adequately been incorporated in computer life prediction codes such as NASA FLAGRO, which addresses fatigue crack propagation (FCP) from the fracture mechanics damage tolerance perspective. NASA FLAGRO describes environmental enhancements of FCP rates on a material/environment case-by-case basis. Using data to describe environmental effects on fatigue behavior, however, requires extensive information and is useful only for well characterized material/environment systems.

This research seeks to develop the methods and understanding to incorporate time and loading variable dependent environmental effects on fatigue behavior in NASA FLAGRO. This research seeks to test the Wei and Landes linear superposition model and an interpolative model, and to suggest improvements to these models based on an improved understanding of the time dependencies which affect environmental fatigue crack propagation (EFCP) in structural alloys. In particular the alloy Ti-6Al-4V is studied in the mill annealed (MA), extra low interstitial (ELI) condition due to its complex, time-dependent environmental fatigue behavior.

1.2 Introduction

1.2.1 Fracture Mechanics Methodology

Fracture mechanics provides an effective methodology for predicting the damage tolerant fatigue life of metallic alloy components. This approach is critical because structural alloys and components contain defects which eliminate the crack nucleation stage of fatigue life. The approach relies on the concept of similitude in order to utilize laboratory data to predict the fatigue life of a component.

Figure 1.1 illustrates the fracture mechanics approach for describing FCP. FCP rates are measured in a laboratory experiment using precracked specimens according to ASTM standardized procedures.[1] The crack length (a) is measured as a function of load cycle number (N). These data are analyzed to determine the average fatigue crack growth rate per unit cycle (da/dN) as a function of applied stress intensity range, ΔK. ΔK is defined as K_{max} - K_{min}, where K_{max} is the maximum applied stress intensity and K_{min} is the minimum applied stress intensity for a given fatigue load cycle.

Paris experimentally demonstrated the validity of the similitude concept, which states that equal FCP rates are produced by equal stress intensity ranges, regardless of the load, crack size, and specimen geometry.[2] Paris demonstrated this concept for metallic alloys in moist air. The concept was extended by Wei and coworkers to include corrosion fatigue.[3-4] The concept of similitude allows the integration of laboratory data to predict the fatigue life of a structural component. If da/dN is written as a function (f) of ΔK, the life of a component can be calculated as follows:

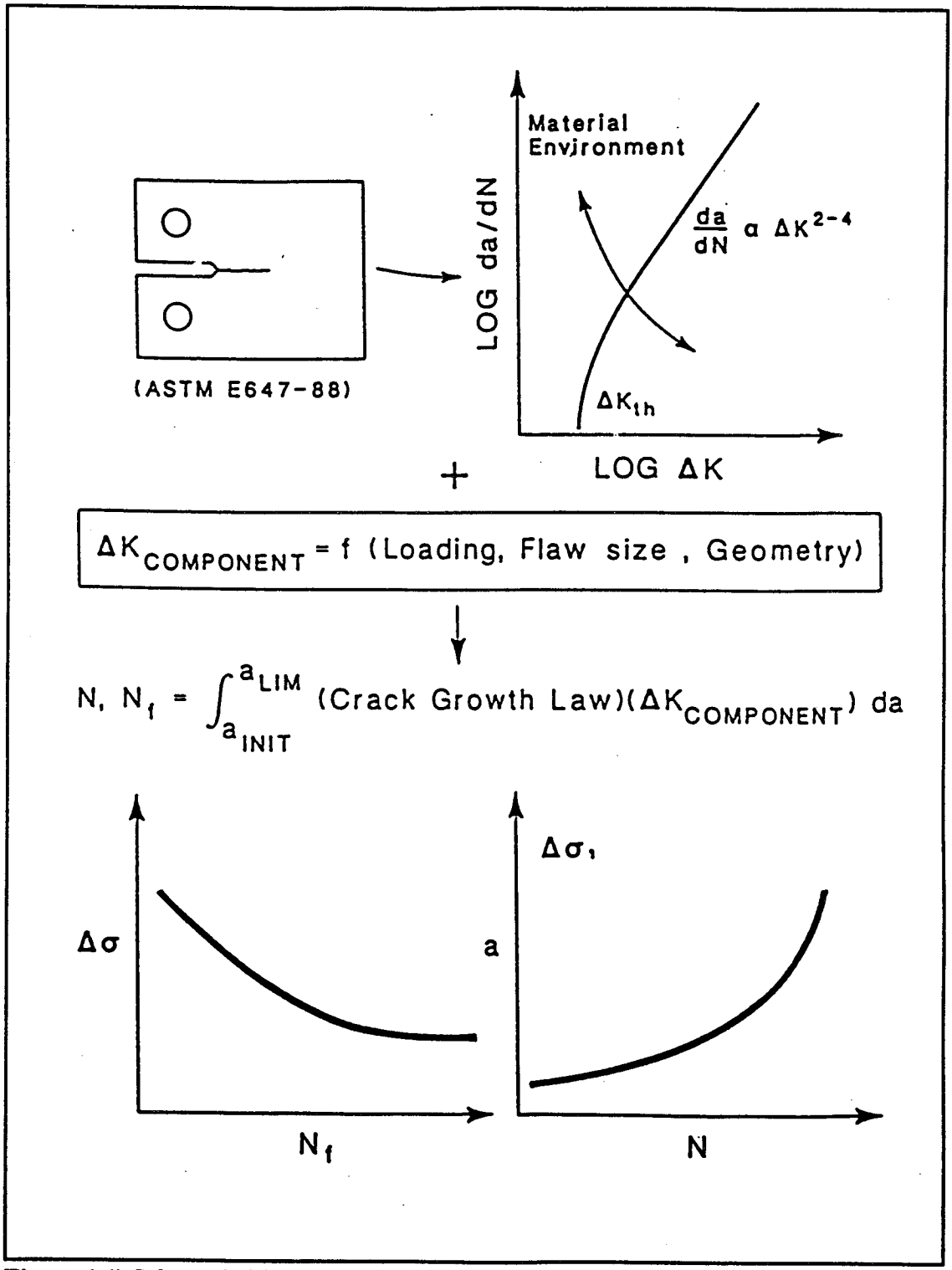

Figure 1.1: Schematic illustrating fracture mechanics approach for describing FCP and predicting component life. After Gangloff.[5]

$$\frac{da}{dN} = f(\Delta K) \Rightarrow dN = \frac{da}{f(\Delta K)} \tag{1.1}$$

$$N_f = \int_{o}^{N_f} dN = \int_{a_o}^{a_f} \frac{da}{f(\Delta K)} \tag{1.2}$$

where N_f is the number of cycles to failure, a_o is the initial crack size, and a_f is the final crack size. Equation 1.2 predicts the lower plots in Figure 1.1.

1.2.2 NASA FLAGRO Software

The fracture mechanics approach is incorporated in computerized damage tolerant fatigue life prediction codes such as NASA FLAGRO. NASA FLAGRO provides an automated method for calculating stress intensity factors, computing critical crack sizes from fracture toughness considerations, and calculating the fatigue life of structures which contain crack like defects.[6] This program includes an extensive library of stress intensity solutions for various geometries and loading, and extensive tabulation of material data in the form of da/dN versus ΔK and the stress ratio, R ($R = K_{min}/K_{max}$).

NASA FLAGRO describes fatigue crack growth rates with a modified Forman Equation of the form:

$$\frac{da}{dN} = \frac{C\,(1 - f_c)^n\,\Delta K^n \left(1 - \frac{\Delta K}{\Delta K_{th}}\right)^p}{(1 - R)\left(1 - \frac{\Delta K}{(1 - R)\,K_C}\right)^q} \tag{1.3}$$

where K_C is the critical value of the stress intensity and ΔK_{th} is the threshold value of the

stress intensity range. C, n, p, and q are empirical constants, and f_c is a function used to describe the effect of plasticity induced crack closure.

Crack closure is a phenomena associated with premature contact of fatigue crack surfaces upon unloading at K levels higher than K_{min}.[7] Since the crack surfaces touch at a K level, K_{cl}, higher than K_{min}, there is a reduced driving force for fatigue. FCP is then controlled by ΔK_{eff}, where $\Delta K_{eff} = K_{max} - K_{cl}$. Loading below K_{cl} to K_{min} does not add additional plastic strain, and thus no fatigue damage. This behavior is illustrated in Figure 1.2, and was initially referred to as plasticity induced closure.[7] Material that has been permanently deformed in the crack tip plastic zone becomes the wake of the advancing crack and interferes on unloading.[8]

Shown in Figure 1.3 is an example of the NASA FLAGRO Forman Equation fit to fatigue data for 300 M steel. Data for a R of 0 were fit empirically, while the model (Equation 1.3) was used to predict da/dN versus ΔK at higher and lower stress ratios. The predicted effect of R agrees with measurements. The data and crack growth rate model used in NASA FLAGRO have focused on FCP in benign moist air, where da/dN is only a function of ΔK and R. Load characteristics such as frequency (f), wave form, and hold time (τ) do not affect FCP in inert environments, often including somewhat aggressive moist air.

1.2.3 Environmental Effects on Fatigue Crack Propagation

Aggressive environments significantly increase FCP rates in structural alloys.[5,9] Examples are iron and nickel based superalloys in high pressure gaseous hydrogen, high strength alloy steels in water vapor, as well as aluminum, titanium, and ferrous alloys in

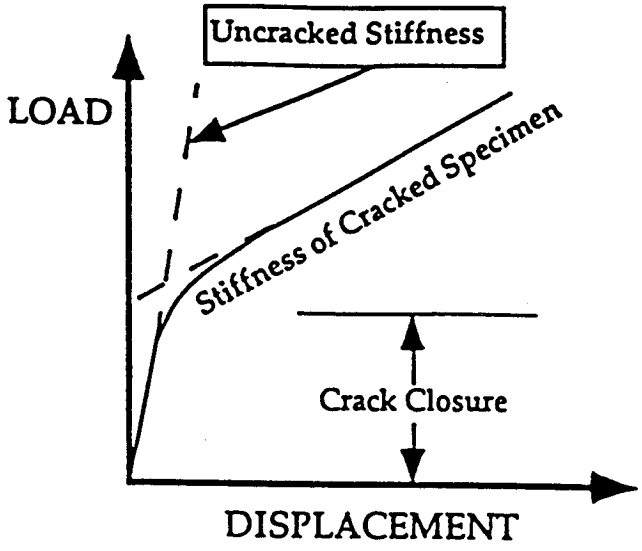

(a) Load-displacement behavior.

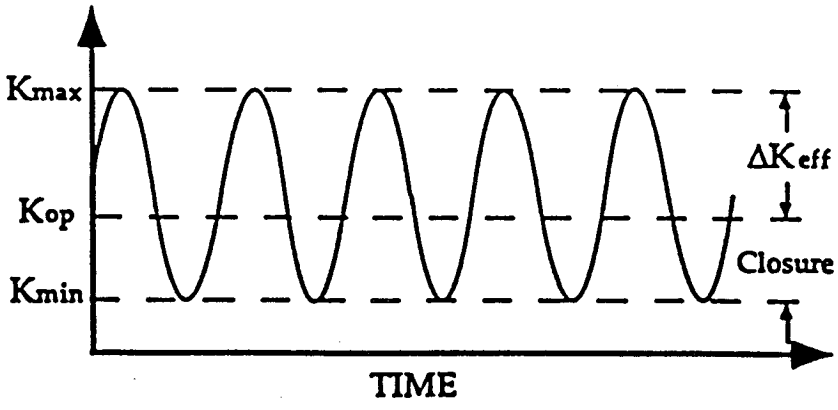

(b) Definition of effective stress intensity range.

Figure 1.2: Schematic illustrating crack closure during fatigue crack growth. Crack faces contact at a positive load greater than P_{min} (a), resulting in a lower driving force for fatigue, ΔK_{eff} (b). After Anderson.[10]

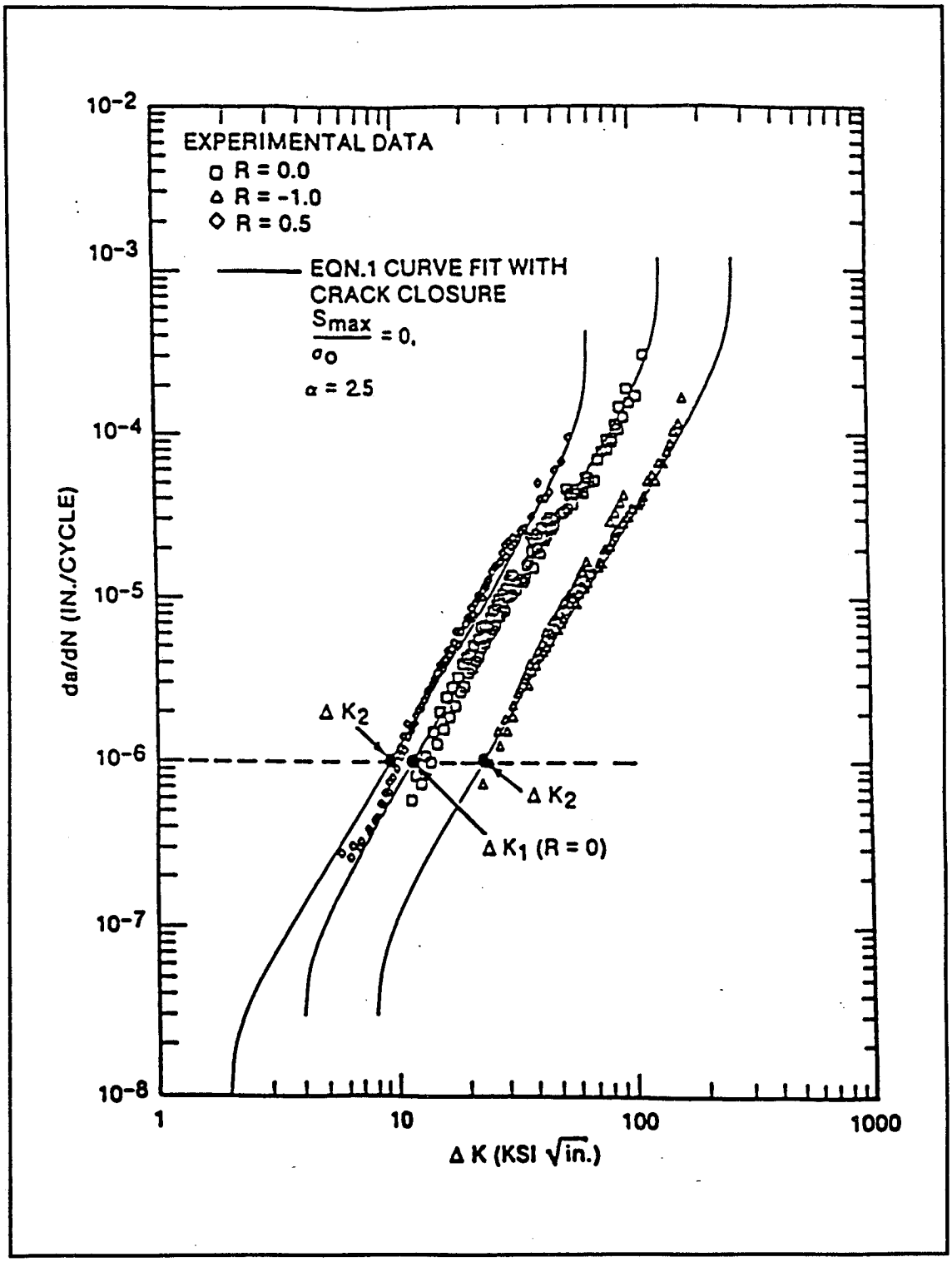

Figure 1.3: Example of a FLAGRO generated fit of the Forman Equation to fatigue data for 300 M steel. After Forman *et. al.* [11]

aqueous chloride solutions. This is particularly true for environments capable of producing atomic hydrogen through reactions with the metal.[5,12] Figure 1.4 shows an extreme example of the deleterious effect of environment on fatigue behavior for 4130 steel. Relative to FCP in vacuum, da/dN is enhanced by up to three orders of magnitude by gaseous hydrogen or NaCl solution.

Unlike FCP in inert environments, environmental effects on fatigue behavior are influenced by a wide range of mechanical, metallurgical, and chemical variables.[5,13-14] Mechanical and metallurgical variables include loading frequency, loading wave form, crack size, crack geometry, alloy composition, stress ratio, and yield strength. Chemical factors include electrode potential, solution pH, ionic composition, impurity content, conductivity, temperature, and halogen and sulfide content.[14] Figure 1.5 contains a list of the important factors which affect EFCP of aerospace aluminum alloys in aggressive moist gas and electrolyte environments.

Environmental subcritical crack growth, referred to as stress corrosion cracking (SCC), occurs in corrosive environments without necessarily involving cyclic loads. The stress intensity is constant or monotonically changing, and a time-based crack growth rate is often observed for the metal in the corrosive environment. This crack growth rate, $(da/dt)_{environment}$, is the change in crack length per unit time (t). This crack growth occurs at stress intensity levels well below the fracture toughness, but only in the presence of environmental embrittlement. For vacuum, da/dt is zero provided there is no crack tip creep damage. For the environmental case, static loads cause localized plasticity at the crack tip. A chemical reaction between the material and environment causes crack propagation by

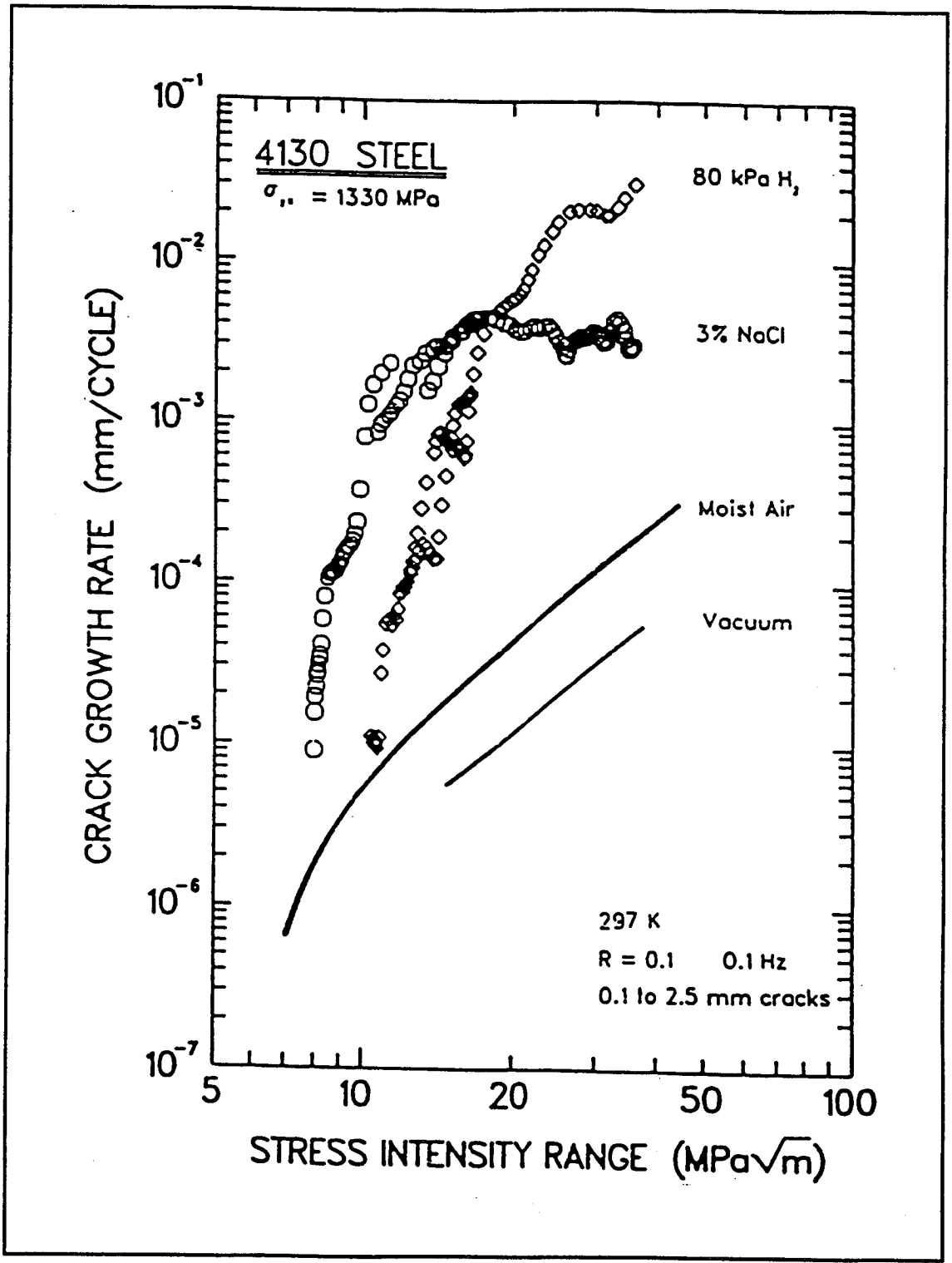

Figure 1.4: Example of deleterious effect of various environments on the fatigue behavior of 4130 steel. After Gangloff and Kim. [9]

MECHANICAL, ENVIRONMENT CHEMISTRY AND METALLURGICAL VARIABLES AFFECTING ENVIRONMENTAL FATIGUE IN ALUMINUM ALLOYS	
STRESS INTENSITY RANGE	MEAN STRESS
CRACK SIZE AND SHAPE	SPECIMEN THICKNESS
LOADING FREQUENCY	SPECIMEN ORIENTATION
LOADING SEQUENCE	LOADING WAVE FORM
SOLUTION Cl^-,H^+, O_2, S^{-2}	WATER VAPOR PRESSURE
ELECTRODE POTENTIAL	OXYGEN CONTAMINATION
ALLOY MICROSTRUCTURE	ALLOY COMPOSITION
GRAIN/SUBGRAIN SIZE	ALLOY YIELD STRENGTH
SLIP MORPHOLOGY	ALLOY TEXTURE
PRECIPITATES	TEMPERATURE

Figure 1.5: Mechanical, chemical and metallurgical factors which affect EFCP of aluminum alloys. After Gangloff and Kim.[9]

either hydrogen embrittlement or film rupture with transient dissolution.

When irreversible cyclic plastic deformation occurs in conjunction with localized chemical or electrochemical reactions, environment enhanced fatigue occurs. The rate of crack growth is then represented by $(da/dN)_{total}$ and is not generally described by a simple power law.

Despite substantial advances over the past three decades in such areas as small crack advance and crack closure, the fracture mechanics approach to damage tolerant fatigue life prediction has not been adequately developed to incorporate environmental effects in computer codes such as NASA FLAGRO. These codes must ultimately account for a plethora of variables which interactively affect EFCP kinetics while making quantitative estimates of the flaw tolerance of aerospace structures. The complex time dependent nature of EFCP must be researched and understood so that short-term da/dN versus ΔK data can be

effectively used to predict the long-life performance of structural components.

1.3 Objective

The general objective of this research is to develop a method for estimating environmental effects on FCP rates in metals for use in NASA FLAGRO. Specific goals of the research are:

- Develop a set of computer programs which model the effect of an aggressive environment on the relationship between da/dN and ΔK, as well as the loading characteristics. Specifically:
  - Develop a computer program which implements the Wei and Landes linear superposition model.
  - Develop a curve-fitting based interpolative computer modeling program, extending the approach used in NASA FLAGRO.
  - Develop a computer program which allows the user to fit a multiple power law equation to fatigue data.
  - Define the problems that limit these empirical modeling approaches.
- Determine the time dependent environment assisted cracking (EAC) behavior of Ti-6Al-4V as a model system to test the computer programs.
  - Determine the stress corrosion cracking susceptibility of Ti-6Al-4V in a 3.5% NaCl solution.
  - Determine the effect of loading frequency on EFCP in Ti-6Al-4V in 3.5% NaCl.

- Determine the effect of environmental exposure on crack closure in Ti-6Al-4V.

1.4 Approach

One aim of this thesis is to develop a set of computer programs which model the ΔK, R, frequency, and load-wave form dependencies of EFCP rates. Three separate models were used during this research, a linear superposition model, an interpolative model, and a multiple power law model. The models and the associated computer program are discussed in Chapter 2.

In order to test the models, data were needed for a specific material/environment system. Ti-6Al-4V was chosen as the material, and a NaCl solution was chosen as the environment. Ti-6Al-4V was chosen for three reasons. First, it is the most widely studied titanium alloy, thus there should be extensive data in the literature. Unfortunately, sufficient data could not be located in the literature, so tests were conducted during this research to generate more sufficient data to test the computer models. Second, Ti-6Al-4V exhibits complex effects of R and frequency on da/dN in NaCl solutions, which makes computer modeling of FCP rates challenging. Third, Ti-6Al-4V was chosen because of its relevance to structural applications. Ti-6Al-4V and alloys similar to Ti-6Al-4V are used in high speed aircraft airframes, in spacecraft pressure vessels, as well as in fasteners for aerospace and marine structures. ELI grade Ti-6Al-4V is also used in medical implants.

Experiments were conducted to determine the effect of stress ratio and frequency on da/dN, as well as to determine the SCC susceptibility of Ti-6Al-4V. K-gradient experiments

for EFCP, and constant crack mouth opening displacement (CMOD) rate experiments for SCC were performed on the alloy in the L-T orientation in moist air and a 3.5% NaCl solution, at a fixed electrode potential of -500 mV_{SCE}. EFCP experiments were also preformed at constant ΔK levels and varying frequencies in order to determine the effect of frequency on da/dN in the aqueous chloride solution. Crack closure is measured throughout all fatigue experiments. Procedures are presented in Chapter 3 and the results of these experiments are compared to literature data for standard grade Ti-6Al-4V in Chapter 4.

The computer models were bench marked for accuracy and tested using the fatigue data for Ti-6Al-4V (Chapter 5). Both the linear superposition and the interpolative model were tested; in particular, the interpolative model and the linear superposition model were utilized to model the effects of frequency and stress ratio on da/dN. These results are given in Chapter 6. The computer program will be provided to NASA for incorporation in NASA FLAGRO.

Chapter 2: Computer Modeling of Fatigue Crack Propagation

2.1 Aim and Approach of Computer Modeling

The aim of the computer modeling discussed in this thesis is to develop an effective method for modeling time-dependent EFCP. Three separate empirical models are discussed, a linear superposition model, an interpolative model, and a multiple power law model. The equations used by each model to relate da/dN to ΔK are discussed, along with a summary of the methods used to determine equation parameters.

2.2 Empirical Models

2.2.1 Background

2.2.1.1 Paris Equation

The Paris Equation is a power law of the form:

$$\frac{da}{dN} = C\ \Delta K^{n} \qquad (2.1)$$

where C and n are constants that are determined empirically. The Paris Equation is often only accurate for FCP over a portion of the total da/dN versus ΔK curve for an alloy. A typical FCP rate curve is divided into three regions, as shown in Figure 2.1. Region I is the near threshold region where a decrease in ΔK results in a sharp decrease in da/dN as the threshold value of ΔK (ΔK_{th}) is reached. Cyclic loads which produce ΔK less than ΔK_{th} do

not cause crack propagation. Region III is the near critical region where a small increase in ΔK produces a large increase in da/dN as K_{max} approaches K_C. Region II is a transition region between Regions I and III, and is adequately described by the Paris Equation.

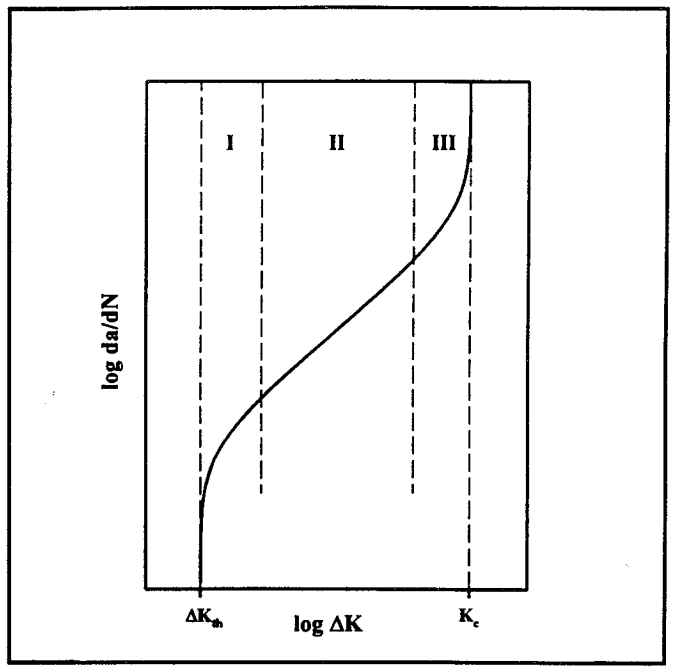

Figure 2.1: Typical curve showing three regimes of fatigue crack growth. After Hertzberg.[15]

2.2.1.2 Forman Equation With Closure

The Forman Equation with crack closure, developed by R.G. Forman, is discussed in detail in the NASA FLAGRO (Version 2.0)[16] user's manual, and is of the form:

$$\frac{da}{dN} = \frac{C\,(1 - f_c)^n\,\Delta K^n \left(1 - \dfrac{\Delta K_{th}}{\Delta K}\right)^p}{(1-R)^n \left(1 - \dfrac{\Delta K}{(1 - R)\,K_C}\right)^q} \qquad (2.2)$$

where C, n, p, and q are empirical constants which depend on material and environment.

The crack opening function, f_c, is used to calculate the effect of R on da/dN for a constant amplitude load. Newman[16] defined the function from plasticity induced crack closure considerations as:

$$f_c = \frac{K_{op}}{K_{max}} = \max\ (R\ ,\ A_o + A_1 R + A_2 R^2 + A_3 R^3) \quad R \geq 0$$
$$A_o + A_1 R \quad -2 \leq R < 0 \qquad (2.3)$$

where:

$$A_o = (0.825 - 0.34\alpha + 0.05\alpha^2)\left[\cos\left(\frac{\pi}{2}\frac{S_{max}}{\sigma_0}\right)\right]^{\frac{1}{\alpha}} \qquad (2.4a)$$

$$A_1 = (0.415 - 0.071\,\alpha)\frac{S_{max}}{\sigma_o} \qquad (2.4b)$$

$$A_2 = 1 - A_o - A_1 - A_3 \qquad (2.4c)$$

$$A_3 = 2A_o + A_1 - 1 \qquad (2.4d)$$

and K_{op} is the opening stress intensity, below which the crack is closed. The parameter α describes the condition of plane stress or plane strain, and S_{max}/σ_o is the ratio of the maximum applied stress to the flow stress, where the flow stress is the average of the ultimate tensile strength and the yield strength. The parameter α is a material constant ranging from 1 for plane stress to 3 for plane strain. S_{max}/σ_o varies from experiment to experiment and is not a material constant, however, the value is taken as 0.3 for most materials incorporated in NASA FLAGRO.

Certain materials do not exhibit a large effect of R on da/dN, and the effects of crack closure need not be considered. For these materials α is set to 5.845 and S_{max}/σ_o to 1.0. The parameter f_c is then zero for $R \leq 0$ and becomes R for $0 \leq R < 1$. For positive stress ratios,

Equation 2.2 reduces to:

$$\frac{da}{dN} = \frac{C\ \Delta K^n \left(1 - \frac{\Delta K_{th}}{\Delta K}\right)^p}{\left(1 - \frac{\Delta K}{(1 - R)\ K_C}\right)^q} \tag{2.5}$$

For negative stress ratios, ΔK is replaced by K_{max}.

2.2.1.3 Forman Equation Without Closure

The Forman Equation without an explicit treatment of crack closure[17], is:

$$\frac{da}{dN} = \frac{C\ \Delta K^n\ (1 - R)^m \left(1 - \frac{\Delta K}{\Delta K_{th}}\right)^p}{\left(1 - R - \frac{\Delta K}{K_C}\right)^q} \tag{2.6}$$

The coefficient C, and the exponents m, n, p, and q are empirical constants. C, n, p, and q will not have the same values as in Equation 2.2 for a given set of data.

2.2.1.4 Hyperbolic Sine Equation

The Hyperbolic Sine (SINH) Equation was originally developed at Pratt & Whitney Aircraft, and is discussed by Haritos *et. al.*[18], Van Stone *et. al.*[19], and Miller *et. al.*[20] The equation is of the form:

$$\log\left(\frac{da}{dN}\right) = C_1\ \sinh\ (C_2\ [\ \log\ (\Delta K) + C_3\ ]) + C_4 \tag{2.7}$$

The parameters C_3 and C_4 are the horizontal and vertical locations of an inflection point,

respectively. C_1 is a scale factor for the vertical (log da/dN) axis, while C_2 is a scale factor for the horizontal (log ΔK) axis. The SINH Equation, schematically shown in Figure 2.2, is symmetric about the inflection point and does not define K_C or ΔK_{th}. The curvature is identical in both the near toughness and near threshold regimes. Since the SINH equation is nonlinear, the effects of changing the parameters are not easily seen, as illustrated for changing C_1, C_2, C_3, and C_4 in Figures 2.3 a through d.

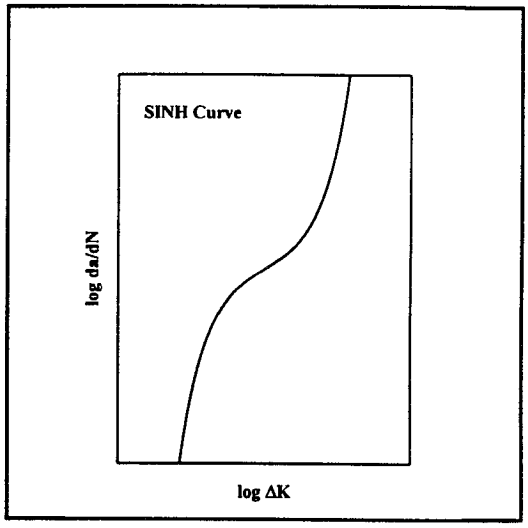

Figure 2.2: Schematic of a SINH curve.

2.2.1.5 Sigmoidal Equation

The Sigmoidal Equation was originally developed by GE Aircraft Engines, as discussed by Haritos *et. al.*[18] and Van Stone *et. al.*[19] The equation is of the form:

$$\frac{da}{dN} = e^{B}\left(\frac{\Delta K}{\Delta K_{th}}\right)^{P}\left[\ln\left(\frac{\Delta K}{\Delta K_{th}}\right)\right]^{Q}\left[\ln\left(\frac{\Delta K_C}{\Delta K}\right)\right]^{D} \qquad (2.8)$$

$$\Delta K_C = (1 - R)\, K_C$$

A schematic of a sigmoidal curve is shown in Figure 2.4. The curve fitting parameters B, P, Q, D, ΔK_{th} and ΔK_C are material/environment properties.

The parameter B translates the curve vertically, the parameter P controls the slope

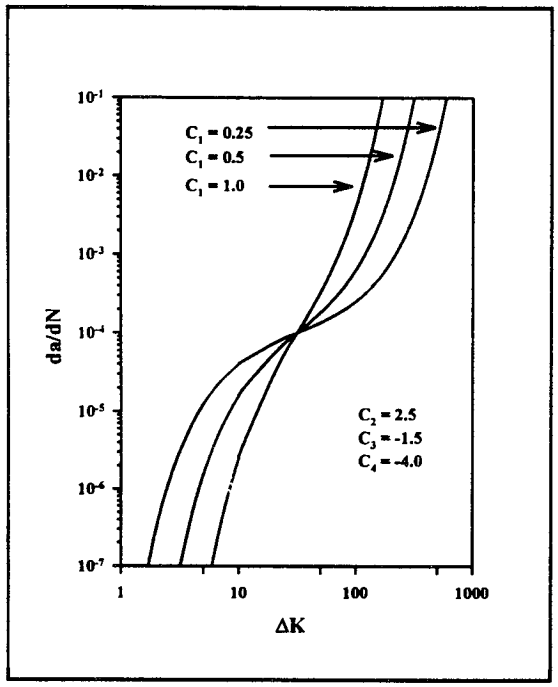

a) Effect of changing C_1.

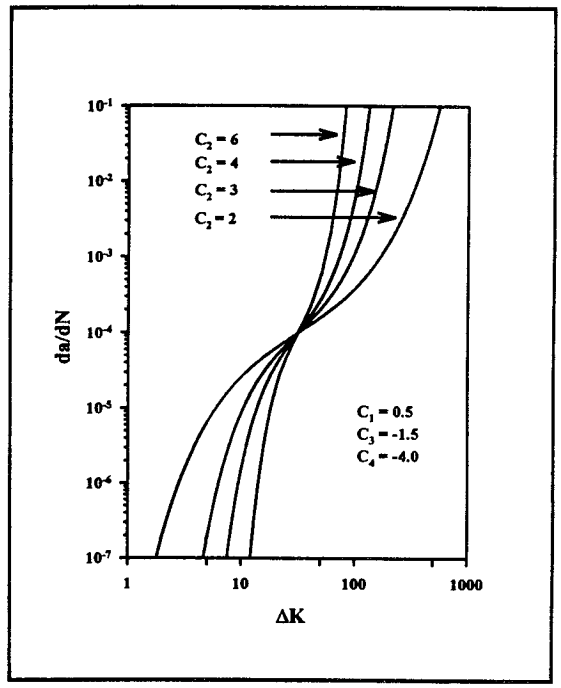

b) Effect of changing C_2.

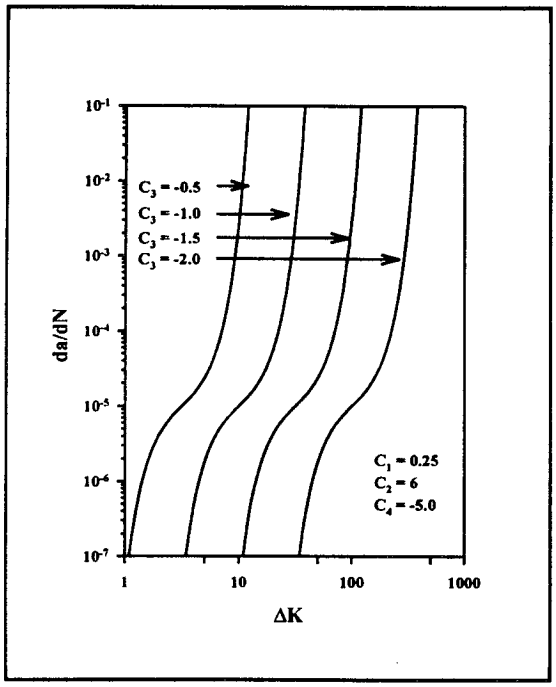

c) Effect of changing C_3.

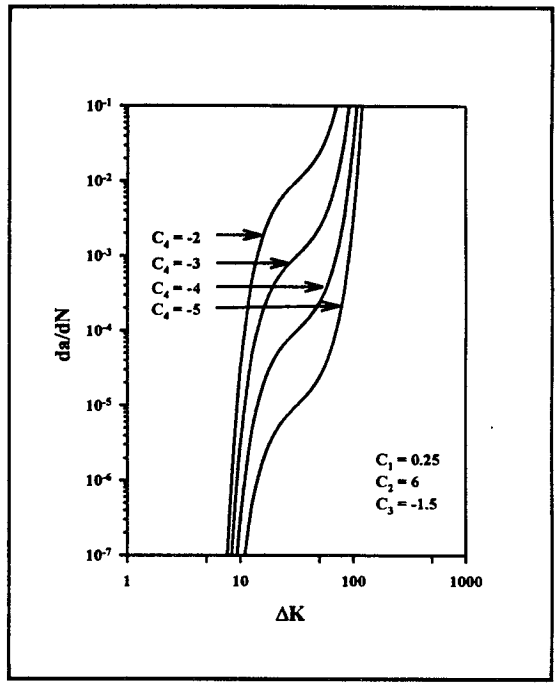

d) Effect of changing C_4.

Figure 2.3: Effect of changing C_1, C_2, C_3, and C_4 on the Hyperbolic Sine Equation.

of the curve, while the curvatures in the near threshold and the near toughness regimes are controlled by the constants Q and D, respectively. When Q and D are set to zero and ΔK_{th} is set to one, the Sigmoidal Equation is identical to the Paris Equation.

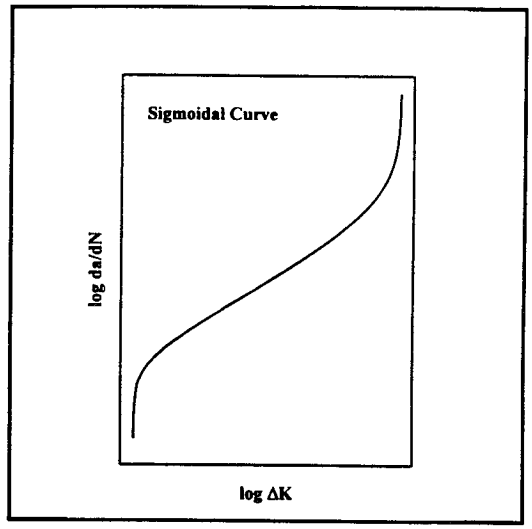

Figure 2.4: Schematic of a sigmoidal curve.

An alternate form of the Sigmoidal Equation, known as the Modified Sigmoidal Equation (MSE), can be expressed as:

$$\frac{da}{dN} = e^{B'} \left(\frac{\Delta K}{\Delta K_i} \right)^P \left[\ln \left(\frac{\Delta K}{\Delta K_{th}} \right) \right]^Q \left[\ln \left(\frac{\Delta K_C}{\Delta K} \right) \right]^D \qquad (2.9)$$

A new variable, ΔK_i, is introduced as the value of ΔK at the inflection point of the curve. The parameters Q and D control the shape of the curve between the inflection point and the upper and lower asymptotes, respectively. P controls the rotation of the curve in the vicinity of the inflection point, while B' is the vertical distance the inflection point is displaced from a da/dN value of unity.

2.2.1.6 Multiple Power Law Equation

The Multiple Power Law Equation, shown in Figure 2.5, uses the same relation between da/dN and ΔK as the Paris Equation (Equation 2.1) except the values of C and n change at various transition ΔK values. By using multiple power law segments, instead of a single Paris Equation, fatigue data can be more accurately represented in the near

threshold and near toughness regimes, where crack growth becomes asymptotic to characteristic stress intensity values. Multiple power laws are useful when modeling the complex da/dN versus ΔK behavior that often occurs due to aggressive environments. The sample multiple power law curve shown in Figure 2.5 consists of three separate power law segments, with two transition ΔK values labeled ΔK_{T1} and ΔK_{T2}. For the example, the Multiple Power Law Equation is written as:

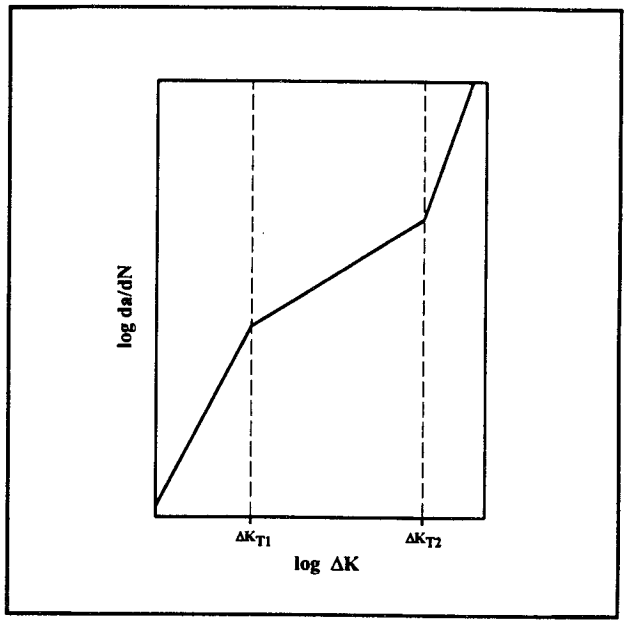

Figure 2.5: Schematic of a multiple power law curve.

$$\frac{da}{dN} = C_1 \Delta K^{n_1} \qquad \Delta K \leq \Delta K_{T1}$$

$$\frac{da}{dN} = C_2 \Delta K^{n_2} \qquad \Delta K_{T1} \leq \Delta K \leq \Delta K_{T2} \qquad \textbf{(2.10)}$$

$$\frac{da}{dN} = C_3 \Delta K^{n_3} \qquad \Delta K_{T2} \leq \Delta K$$

2.2.2 Determining Equation Parameters

2.2.2.1 Paris, Forman and Sigmoidal Equations

To determine the equation parameters in the Forman, Paris and Sigmoidal Equations, the equations are first rewritten in linear form using common logarithms so

that linear regression can be used. Using ΔK and da/dN data, a set of simultaneous linear equations is constructed involving da/dN, ΔK, and the equation parameters. These simultaneous equations are solved using Gaussian Elimination and matrix algebra to determine the equation parameters. For example, the Forman Equation without closure (Equation 2.6) is rewritten as

$$Y = A_1X_1 + A_2X_2 + A_3X_3 + A_4X_4 + A_5X_5 \tag{2.11}$$

where:

$$Y = \log\left(\frac{da}{dN}\right) \tag{2.12a}$$

$$X_1 = \log\,(1 - R) \tag{2.12b}$$

$$X_2 = \log\,(\Delta K) \tag{2.12c}$$

$$X_3 = \log\left(1 - \frac{\Delta K_{th}}{\Delta K}\right) \tag{2.12d}$$

$$X_4 = -\log\left(1 - R - \frac{\Delta K}{K_C}\right) \tag{2.12e}$$

$$X_5 = 1.0 \tag{2.12f}$$

with $A_1 = m$, $A_2 = n$, $A_3 = p$, $A_4 = q$, and $A_5 = \log C$. Similarly, the Forman Equation with closure, the Paris Equation, and the Sigmoidal Equation are written in linear form. These equations are represented in matrix form as:

$$[A]\ [X] = [Y] \tag{2.13}$$

where the A matrix contains the equation parameters such as C, n, p, q, and m, the X matrix contains the values of X_1 through X_5, and the Y matrix contains the values of log (da/dN). This equation is rewritten as:

$$[A] = [X]^{-1}\ [Y] \tag{2.14}$$

The equation parameters are then determined by Gaussian Elimination. This method minimizes the sum of the squared errors with respect to da/dN.

2.2.2.2 Hyperbolic Sine Equation

The user is given two choices in determining the equation parameters in the SINH Equation. The user can either fit C_1, C_2, C_3, and C_4, or the user can fit C_2, C_3, and C_4 with C_1 held constant at 0.5. The case of holding C_1 equal to 0.5 was included based on the results of Haritos *et. al.*[18] To determine the values of the coefficients in the SINH Equation, nonlinear regression is used. Using an algorithm from Kuester[21], which implements a procedure proposed by Marquardt[22], the parameters in the non-linear equation are determined using the method of least squares. The algorithm requires the user to input initial estimates for the equation parameters, which can be determined from a graph of da/dN versus ΔK. Upper and lower bounds are then selected for each parameter. The best value for each parameter is found by minimizing the sum of the squared errors, SSE, defined as:

$$SSE = \Sigma(Y_{Pred} - Y_{actual})^2 \tag{2.15}$$

where Y_{Pred} is the predicted value of da/dN and Y_{actual} is the actual measured value of da/dN at a given ΔK.

2.2.3 Methods of Specifying ΔK_{th} and K_C

The values for ΔK_{th} and K_C contained in NASA FLAGRO are primarily accurate for fatigue in moist air. Since the models developed during this research were developed for fatigue in embrittling environments, these values are not acceptable; thus an option has been included to optimize the values of K_C and ΔK_{th}. Presently, the computer models contain three options: (1) entering ΔK_{th} and K_C manually, (2) calculating ΔK_{th} and K_C using the equations contained in NASA FLAGRO, or (3) optimizing the values of ΔK_{th} and K_C using a cubic approximation based on input da/dN versus ΔK data. If the user decides to calculate ΔK_{th} and K_C using the equations in NASA FLAGRO, the following equations are used:[19]

$$\Delta K_{th} = \Delta K_o \left(\frac{4}{\pi} \right) \tan^{-1} (1 - R) \tag{2.16}$$

$$K_C = K_{IC} \left(1 + B_K e^{\left[\frac{A_K b}{t_o} \right]^2} \right) \tag{2.17}$$

$$t_o = 2.0 \left(\frac{K_{IC}}{\sigma_{ys}} \right)^2 \tag{2.18}$$

where b is specimen thickness, ΔK_o is the fatigue threshold at R = 0, A_K and B_K are material constants, and σ_{YS} is yield strength. If the user decides to optimize the values of K_C or ΔK_{th}, the models fit the data to a cubic equation using linear regression. The cubic equation

contains an upper and lower asymptote which correspond to K_C and ΔK_{th}, respectively.

2.3 Linear Superposition Model

2.3.1 Background

Wei and Landes first proposed that the effect of an aggressive environment on FCP in high strength steels is independent of cyclic loading.[23] The linear superposition model predicts EFCP rates by summing the contributions of inert environment mechanical fatigue, $(da/dN)_{fatigue}$, and stress corrosion cracking. In equation form:

$$\frac{da}{dN}_{total} = \frac{da}{dN}_{fatigue} + \frac{da}{dN}_{stress\ corrosion} \tag{2.19}$$

The stress corrosion crack velocity, $(da/dt)_{environment}$, is expressed as a function of stress intensity, K, and integrated over a cycle of fatigue loading to create $(da/dN)_{stress\ corrosion}$:

$$\frac{da}{dN}_{stress\ corrosion} = \int_{\alpha\tau} \left[\frac{da}{dt}[K(t)]\right] dt \tag{2.20}$$

where τ is the period of the fatigue load cycle and α is the portion of this cycle where SCC occurs. K(t) is a function of time and employs the loading parameters ΔK and R (or K_{max} and K_{min}), as well as the frequency, *f*. An example of a sinusoidal load cycle is:

$$K(t) = K_{min} + \frac{\Delta K}{2} [1 - \cos 2\pi f t\ ] \tag{2.21}$$

The success of the linear superposition model was confirmed for various material-environment combinations.[13-25] A prediction for 18Ni (250) maraging steel in gaseous hydrogen is presented in Figure 2.6. FCP rates in argon served as $(da/dN)_{fatigue}$, while

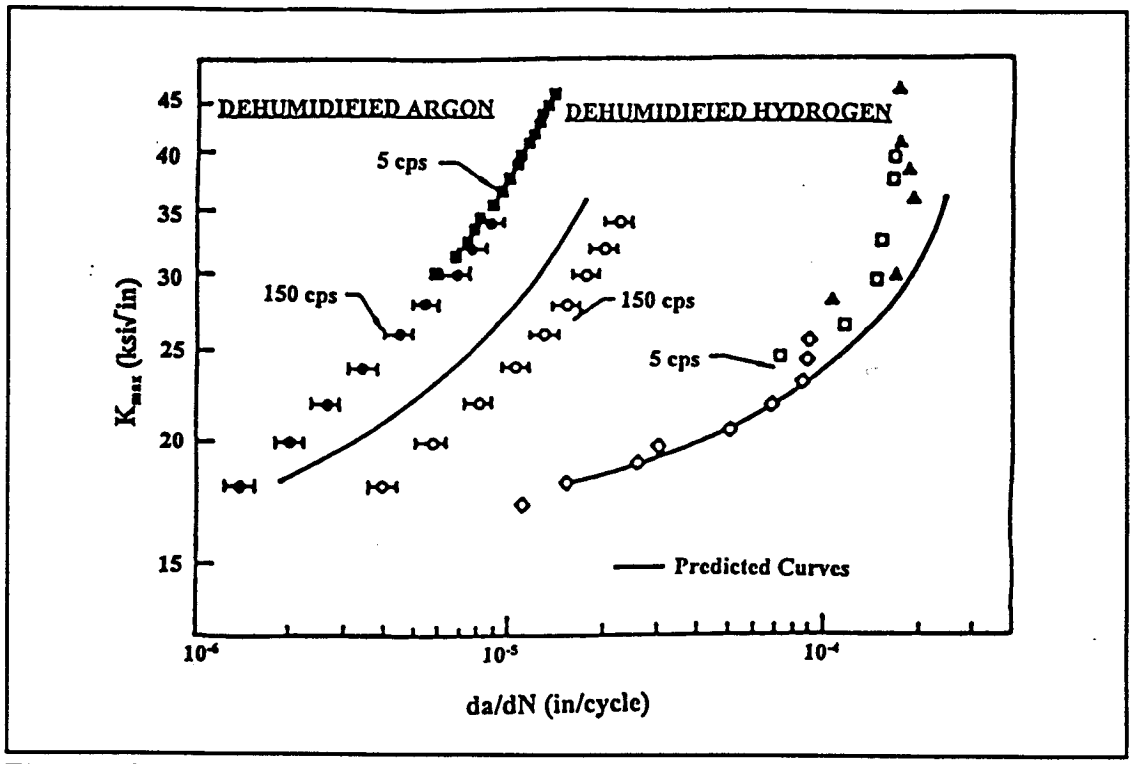

Figure 2.6: Measured and linear superposition predicted FCP rates for maraging steel in H_2. After Wei and Landes.[23]

constant load time-based crack growth rate data for this steel in dehumidified hydrogen were integrated over a cycle of loading to create the stress corrosion component.[23] The procedure reasonably predicted the absolute magnitude and frequency dependence of hydrogen enhanced FCP in 18Ni (250) maraging steel.

The effects of ΔK and f on da/dN in aluminum alloy 7079-T651 in saturated NaCl solution were predicted by Speidel using linear superposition.[24] Predictions displayed in Figure 2.7 show the accuracy of the superposition model, especially at frequencies less than 1 Hz. Mason[26] used linear superposition to predict EFCP rates for 7075-T651 in the S-L orientation in a 2.5% NaCl + 0.5% Na_2CrO_4 solution. Fatigue data for 7075 - T651 in the L-T orientation in helium constituted $(da/dN)_{fatigue}$, while the SCC component was

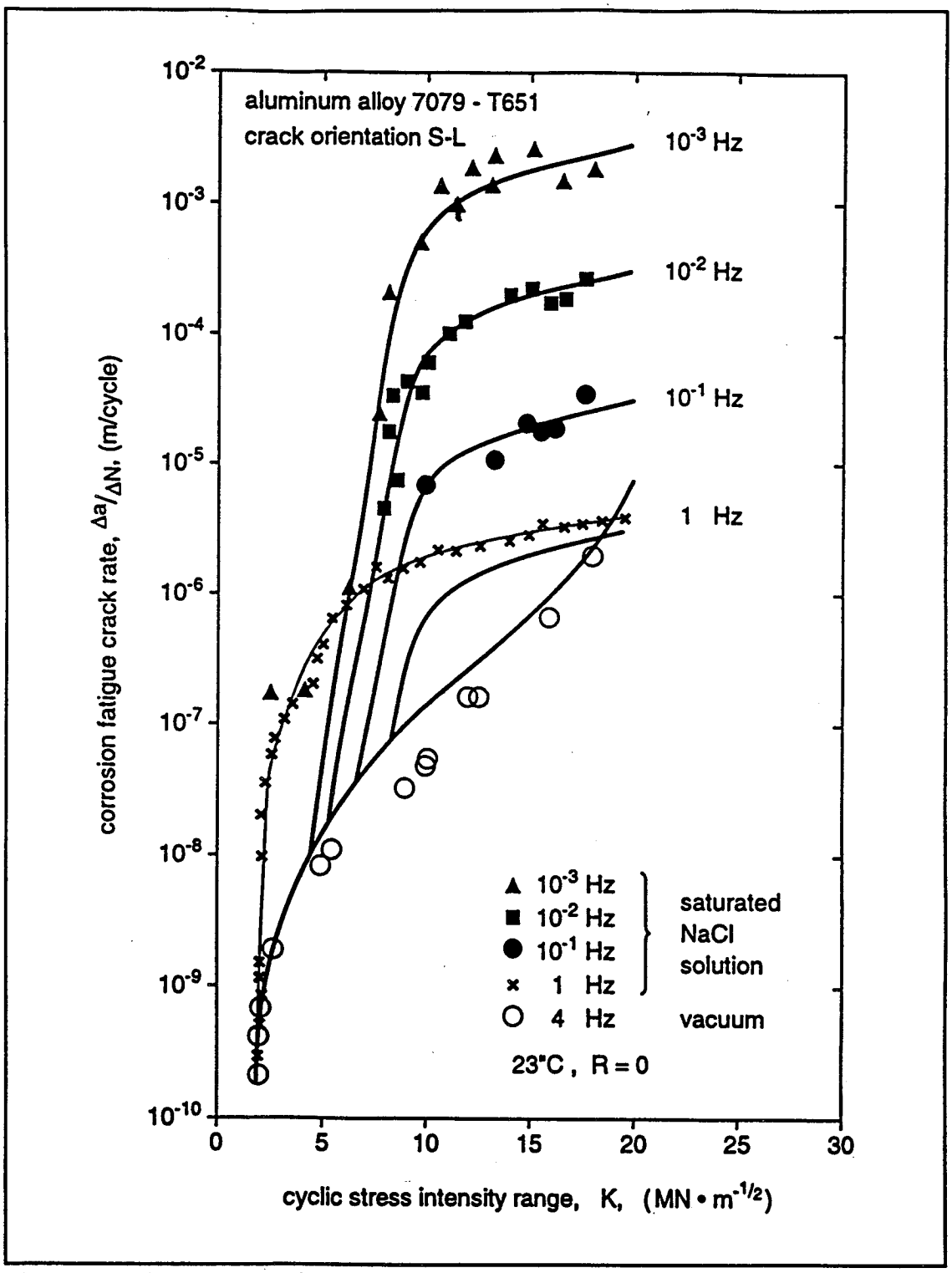

Figure 2.7: Linear superposition predicted (solid lines) and measured (data points) fatigue crack growth for SCC prone aluminum alloy 7079-T651 in NaCl. After Speidel.[24]

determined from a measured, K-independent Stage II velocity of 4×10^{-9} m/sec in NaCl, with no growth occurring below a K_{ISCC} of 5 MPa$\sqrt{m}$. Linear superposition predictions are shown in Figure 2.8. The data are for a frequency of 5 Hz, while the predictions range from 0.01 to 20 Hz. The model substantially underpredicts EFCP rates for 7075-T651 in NaCl. Mason attributed this error to the slow $(da/dt)_{environment}$ compared to the order of magnitude increase in $(da/dN)_{total}$ seen in aqueous chloride over inert helium.[26]

Harmon *et. al.* employed the linear superposition model to predict the effects of ΔK, hold time, and frequency on elevated temperature FCP rates in nickel-base superalloys, IN718 and AF115, at 1200°F.[25] The effects of hold time are reasonably modeled by linear superposition, Figure 2.9.

The preceding examples show the capability of the linear superposition method to predict FCP rates for structural alloys in gas and liquid environments, including elevated temperature. The superposition model is, however, only accurate for limited cases. Specifically, the alloy must be extremely sensitive to SCC. The contribution of stress corrosion to crack growth must be significantly greater than that of inert environment mechanical fatigue. This condition is achieved when the loading frequency is low, the stress intensity is much higher than K_{ISCC}, and $(da/dt)_{environment}$ is relatively rapid. The predictions by Speidel were for aluminum alloy 7079-T651, a material affected strongly by environment compared to other 7xxx aluminum alloys, making it a good candidate for this model.[24] The maraging steel is similarly sensitive to gaseous hydrogen embrittlement, and nickel-base superalloys are prone to sustained load crack growth at relatively low applied K. Linear superposition is not likely to be useful for most structural material/environment

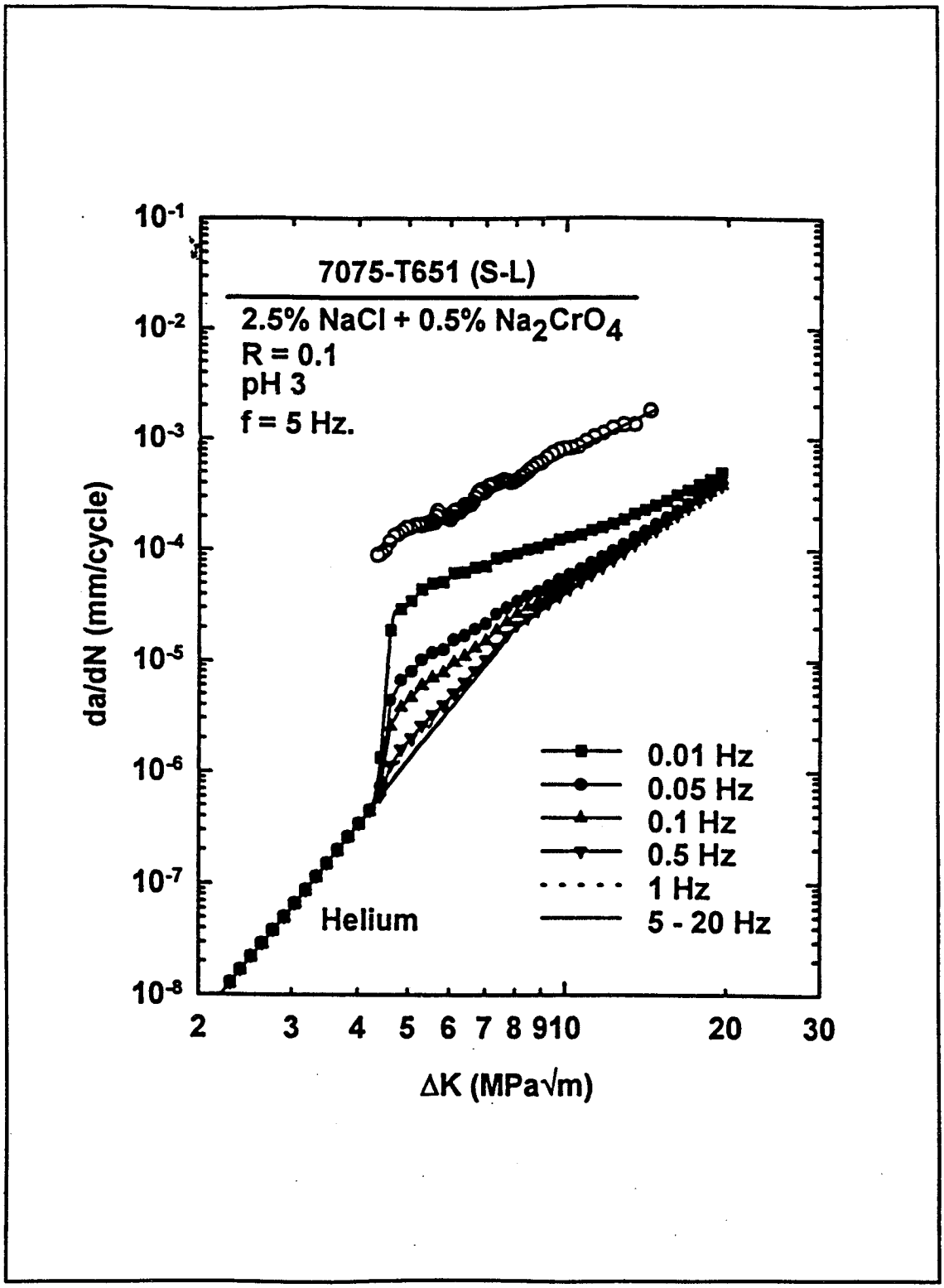

Figure 2.8: Linear superposition predictions for 7075-T651 in a 2.5% NaCl + 0.5% Na_2CrO_4 solution. After Mason.[26]

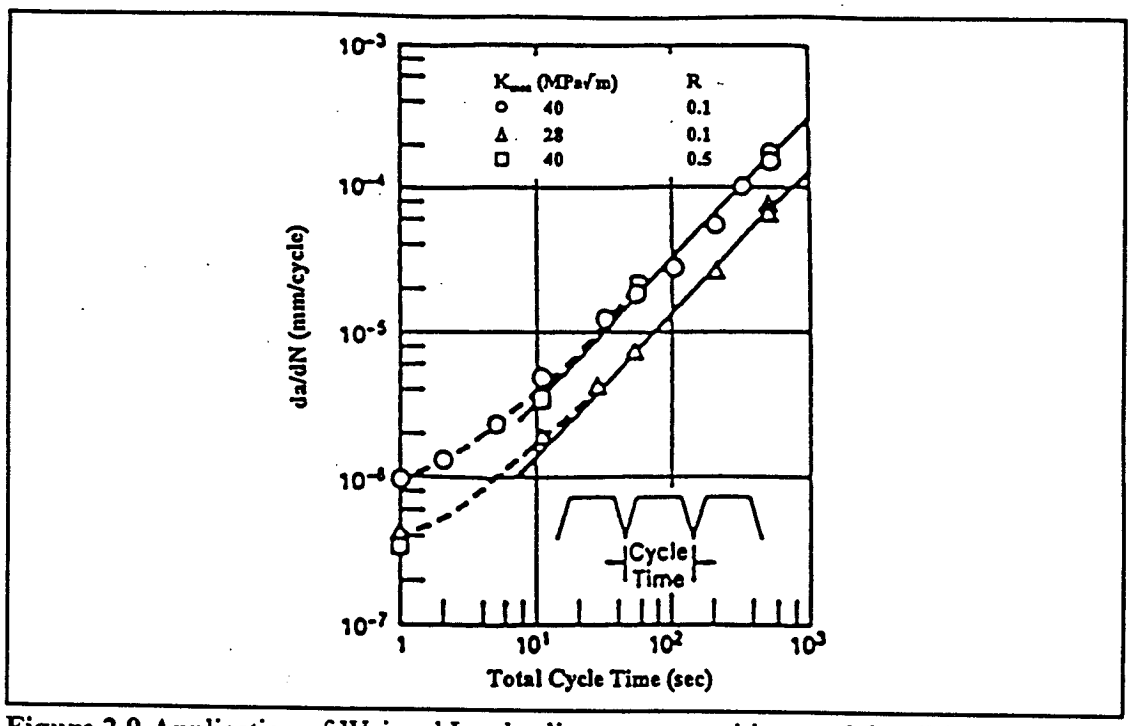

Figure 2.9 Application of Wei and Landes linear superposition model to FCP in IN718 at 1200°F with varying ΔK, R and τ. After Harmon *et. al.*[25]

systems where the material is resistant to stress corrosion cracking.[26]

2.3.2 Application of Current Model

The linear superposition model used in conjunction with this research, along with the computer program used to implement the model, were written by Allen W. Wilson at the University of Virginia, as detailed in the NASA report "Computer Modeling the Fatigue Behavior of Metals in Corrosive Environments."[27] The program was bench marked versus exact analytical calculations and tested for the same material/environment systems employed by Wei and Landes[23], Speidel[24], and Harmon *et. al.*[25] The predictions generated by the current program agreed with both analytical integration and EFCP data, although not precisely with the predictions of others.[23-25] The program yielded improved results due to a more accurate numerical integration algorithm used to calculate $(da/dN)_{stress\ corrosion}$.

2.4 Interpolative Model

2.4.1 Background

An interpolative model can be utilized to predict EFCP rates. The parameters in the crack growth rate equations discussed in Section 2.2.1 depend on stress ratio, frequency, hold time, and other load and environment characteristics. It is presently not possible to predict these dependencies based on mechanistic understanding. Rather, each crack growth rate equation parameter is defined as an empirically selected function of the load characteristics.

Interpolation was employed to describe FCP in nickel-base superalloys at elevated temperatures. Haritos *et. al.*[18] used an interpolative model in conjunction with the SINH and Modified Sigmoidal Equations to predict time-dependent fatigue crack growth in Inconel 718 at 649 °C. Haritos expressed the equation parameters in the SINH and Modified Sigmoidal Equations as functions of f, R, and hold time using the following relationship:

$$\eta = \eta_{baseline} + a_1 \log f + a_2 \log (\tau + 1) + a_3 \log \left[\frac{1-R}{0.9}\right] \qquad (2.22)$$

where η represents an equation parameter, such as C_2 in the SINH Equation, and $\eta_{baseline}$ is the value of the equation parameter for f = 1 Hz, τ = 0 seconds, and R = 0.1. The coefficients a_1, a_2, and a_3 are empirical constants.

The data used to develop the interpolation relationships, as well as the fitted MSE and SINH Equations are shown in Figure 2.10. Both equations fit the data with similar accuracy, except in the near threshold regimes where the MSE model provided better results due to a defined value for ΔK_{th}. Both equations predicted FCP rates accurately when f, R, and τ were within the range of the database used to define the constants in the SINH and MSE laws,

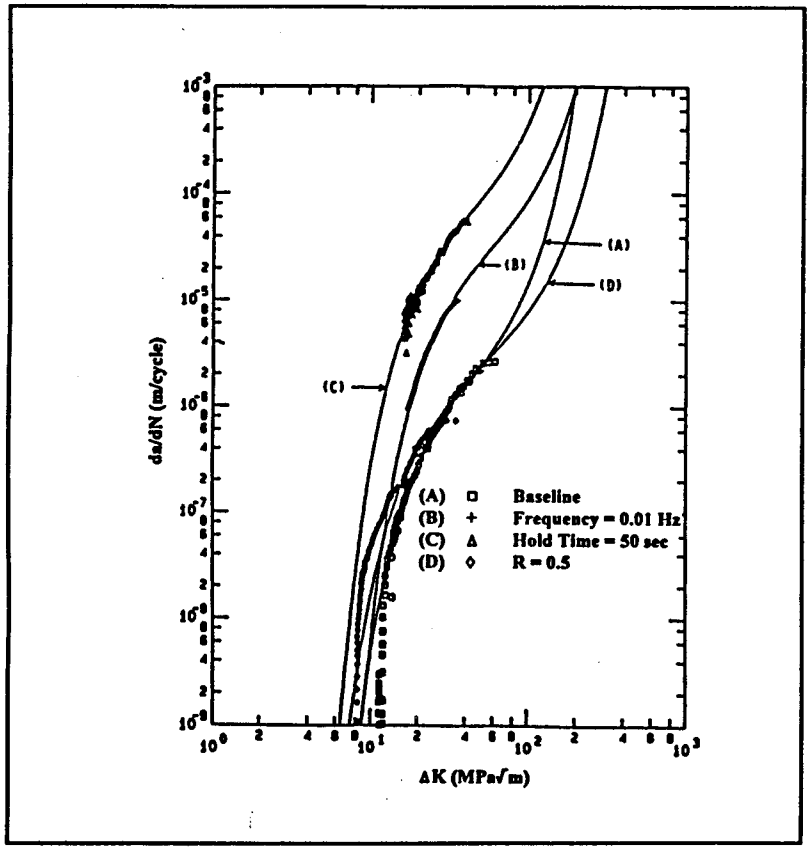

a) Fitted data using the SINH Equation.

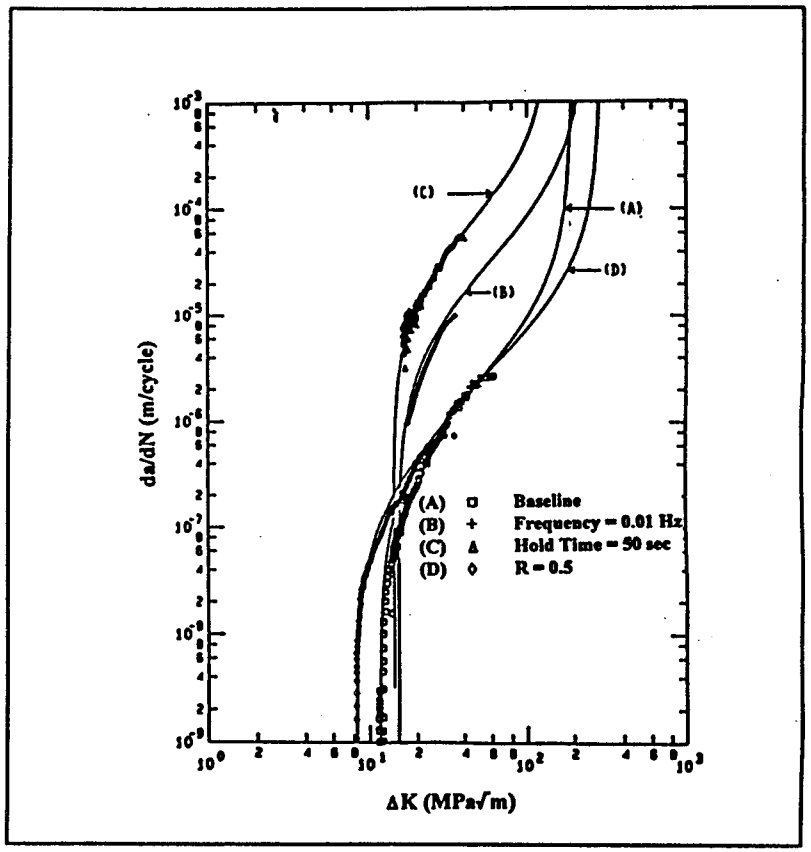

b) Fitted data using the MSE model.

Figure 2.10: Data sets and fitted equations for Inconel 718 at 649 °C using the a) SINH Equation, and b) MSE model. After Haritos *et. al.*[18]

as seen in Figure 2.11. Figure 2.12 shows that the accuracy of the model is reduced when the parameters are varied by significant amounts from the baseline case.

Van Stone *et. al.*[19] utilized an interpolative model to predict FCP rates in Rene '95 at 649°C. The Sigmoidal Equation modeled fatigue crack growth kinetics and the values of B, P, and Q were interpolated using:

$$\eta = a_1 + a_2 \ln (1-R) + a_3 \ln (1+V) + a_4 \ln (1+\tau) \qquad \textbf{(2.23)}$$

where η is B, P, or Q, and V is the cycle ramp time. The parameters a_1, a_2, a_3, and a_4 are empirical constants. K_C and D were constant, and ΔK_{th} was interpolated using:

$$\Delta K_{th} = (\Delta K_{th})_s + [K_o(1-R)^m - (\Delta K_{th})_s]\, e^{(AV-BT)} + C(1-R) \ln(1+DV+E\tau) \qquad \textbf{(2.26)}$$

where $(\Delta K_{th})_s$ is the static crack growth rate threshold, K_o, m and A through E are empirical constants. Figure 2.13 compares measured da/dN versus K_{max} with interpolative model predictions (I) for Rene '95 at 649 °C with R = 0 and hold times of 4, 30, and 300 seconds.

These examples demonstrate the capability of interpolative models to predict FCP rates when the load characteristics where data are interpolated are within the establishing data base. Interpolative models do often show substantial deviation between measured and interpolated results when the load characteristics where data are interpolated lie outside the establishing data base.[18] Interpolative models are particularly flawed when the damage mechanism for fatigue changes either within or outside the establishing data base.

2.4.2 Current Model

For the interpolative model developed as part of this research, equation constants

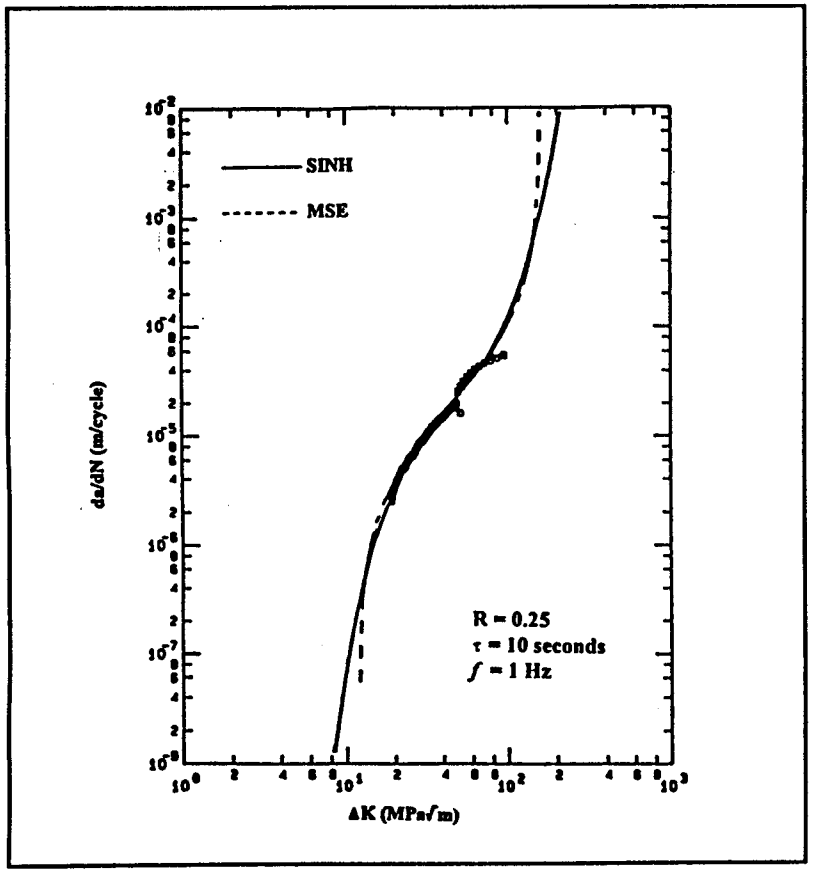

Figure 2.11: Interpolation results for Inconel 718 at 649°C using the SINH and MSE laws when f, R, and τ are inside the range of the database used to define the constants in the crack growth rate equations. After Haritos.[18]

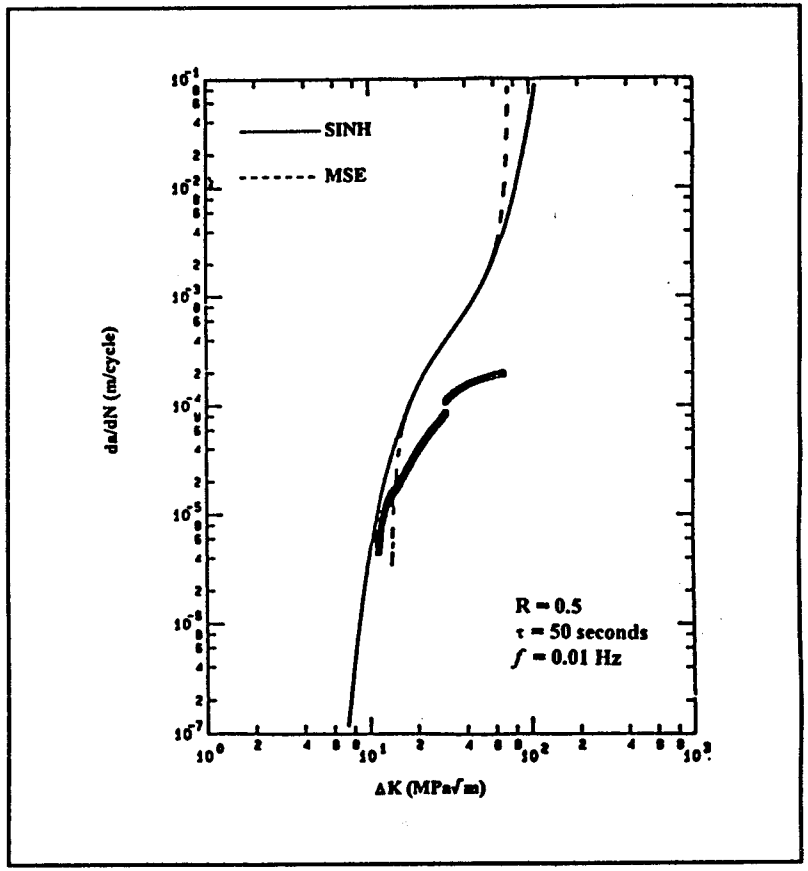

Figure 2.12: Interpolation results for Inconel 718 at 649 °C using the SINH and MSE laws when f, R, and τ vary by significant amounts from the baseline data. After Haritos.[18]

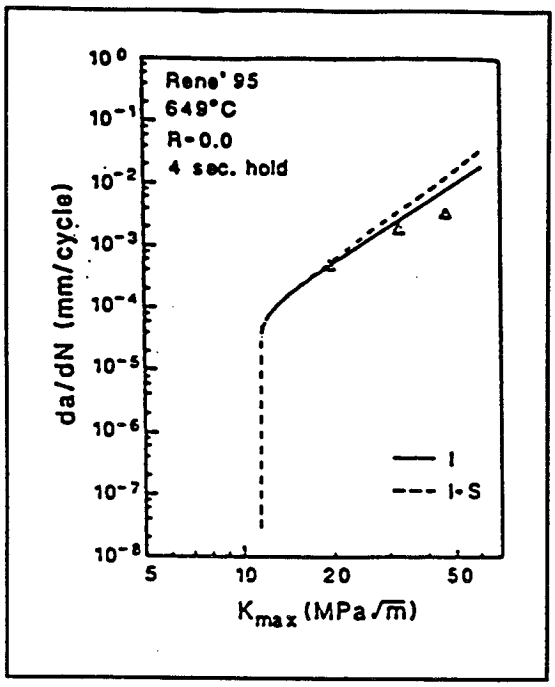

a) Interpolation results for τ = 4 seconds.

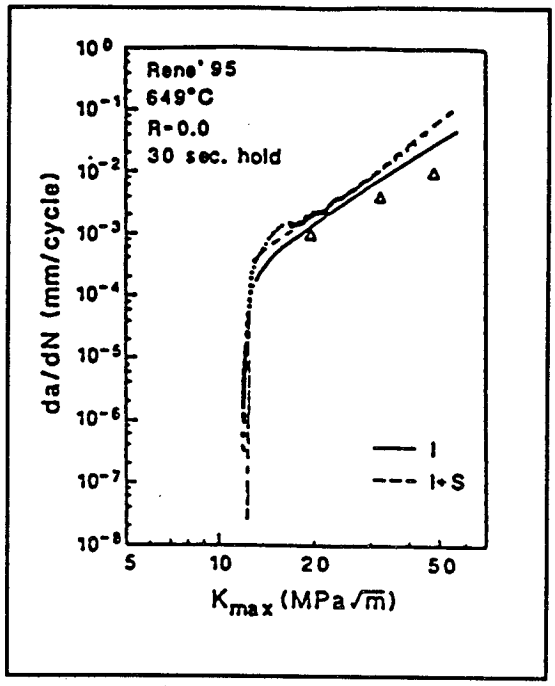

b) Interpolation results for τ = 30 seconds.

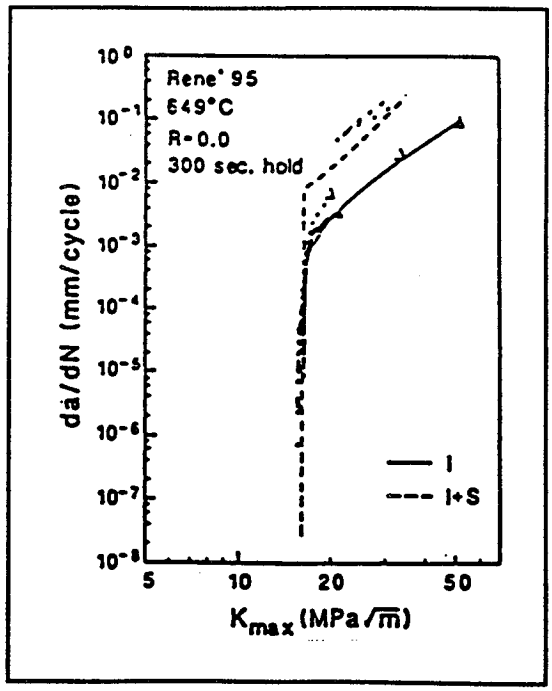

c) Interpolation results for τ = 300 seconds.

Figure 2.13: Interpolation (I) results for Rene '95 at 649°C for R = 0 and hold times of 4, 30, and 300 seconds. After Van Stone *et. al.* [19]

(such as C, n, p, and q) are set equal to linear relationships involving assumed functions of the stress ratio (or K_{max} or K_{min}), frequency and hold time. The forms of the relationships for R and τ were selected so that they would be similar to those used by Haritos *et. al.*[18] and Van Stone *et. al.*[19] The logarithmic form of the relationship for f was selected so that at lower frequencies, when there is more time for environmental reactions, the function increases in value. A relationship involving f^{α} was included based on the fatigue results for ELI Ti-6Al-4V (MA) discussed in Chapter 4.

The forms of the relationships depend on the number of data sets available and the form of the crack growth rate equation. The number of loading variables (R, τ, f, K_{max}, and K_{min}) that the equation parameters are related to must equal the number of da/dN versus ΔK data sets entered. The parameters which the users decides to fit in the crack growth rate equations are related to the load characteristics, the parameters entered by the user are not. If only one data set is entered, crack growth rate equation parameters are expressed as a function of frequency. The user may choose one of the following expressions:

$$\eta = a_1 \log\left[\left(\frac{1}{f}\right) + 1\right] \qquad \textbf{(2.25a)}$$

$$\eta = a_1 f^{\alpha} \qquad \textbf{(2.25b)}$$

where η is a fitted equation parameter (such as C or n in the Forman equation), and α is a positive or negative constant entered by the user.

If two data sets are entered, and the Forman Equation is selected, the relationship is given by one of the following expressions depending on the nature of the frequency

dependence selected by the user:

$$\eta = a_1 \log\left[\left(\frac{1}{f}\right) + 1\right] + a_2 \log\left[\frac{\tau + 1}{0.1}\right] \qquad \textbf{(2.26a)}$$

$$\eta = a_1 f^{\alpha} + a_2 \log\left[\frac{\tau + 1}{0.1}\right] \qquad \textbf{(2.26b)}$$

The effect of R is included in the original model formulated by Forman and based on plasticity induced crack closure.

If the Paris, SINH, or Sigmoidal Equation is selected and the user enters two data sets, the following relationships are used depending on the frequency dependence selected:

$$\eta = a_1 \log\left[\left(\frac{1}{f}\right) + 1\right] + a_2 \log\,(1 - R) \qquad \textbf{(2.27a)}$$

$$\eta = a_1 f^{\alpha} + a_2 \log\,(1 - R) \qquad \textbf{(2.27b)}$$

if the stress ratio is held constant. Physically, as R increases, da/dN should increase. The log (1-R) term decreases as R increases if a_2 is positive. If a_2 is negative, however, the correct trend in da/dN as a fucntion of R is predicted. If K_{max} is held constant the relationships are:

$$\eta = a_1 \log\left[\left(\frac{1}{f}\right) + 1\right] + a_2 \log\,(K_{max}) \qquad \textbf{(2.28a)}$$

$$\eta = a_1 f^{\alpha} + a_2 \log\,(K_{max}) \qquad \textbf{(2.28b)}$$

If K_{min} is held constant, K_{max} in Equation 2.28 is replaced by K_{min}. This form of the

relationship was selected so that a dependence on the stress ratio could be introduced into the Paris, SINH and Sigmoidal Equations.

The effect of hold time is not accounted for with the Paris, SINH or Sigmoidal Equations if two data sets are used. To account for τ, three data sets must be used in conjunction with one of the following relationships:

$$\eta = a_1 \log\left[\left(\frac{1}{f}\right) + 1\right] + a_2 \log\,(1 - R) + a_3 \log\left[\frac{\tau + 1}{0.1}\right] \qquad \textbf{(2.29a)}$$

$$\eta = a_1 f^{\alpha} + a_2 \log\,(1 - R) + a_3 \log\left[\frac{\tau + 1}{0.1}\right] \qquad \textbf{(2.29b)}$$

if the stress ratio is constant, depending on the frequency dependence selected. If K_{max} is held constant the relationships are:

$$\eta = a_1 \log\left[\left(\frac{1}{f}\right) + 1\right] + a_2 \log\,(K_{max}) + a_3 \log\left[\frac{\tau + 1}{0.1}\right] \qquad \textbf{(2.30a)}$$

$$\eta = a_1 f^{\alpha} + a_2 \log\,(K_{max}) + a_3 \log\left[\frac{\tau + 1}{0.1}\right] \qquad \textbf{(2.30b)}$$

depending on the frequency dependence. If K_{min} is held constant, then K_{max} in Equation 2.30 is replaced by K_{min}.

Equations 2.25 through 2.30 allow the user to interpolate da/dN data as a function of R (or K_{max} or K_{min}), f, τ, and ΔK. This is done by (1) selecting the form of the crack growth rate equation, (2) selecting the form of the frequency dependence, (3) entering one, two, or three da/dN versus ΔK data sets, and (4) determining the values of the coefficients a_1, a_2, and a_3 in Equations 2.25 through 2.30 for selected equation parameters. To determine the values

of a_1, a_2, and a_3, the equation parameters are determined for each data set entered, and a set of simultaneous equations is developed which relates the parameter values to the load characteristics. Matrix algebra and Gaussian Elimination are used to solve these equations and determine the coefficients, a_i. Values for the crack growth rate equation parameters can be determined for any *f*, R, or τ within the range of input data for the same material/environment system. Given a value of ΔK, da/dN can be calculated. Note that ΔK_{th} is an equation parameter and expressed in terms of the loading characteristics.

2.5 Multiple Power Law Model

For the multiple power law model, the user is given several alternatives for determining the equation parameters, including:

- Desired slope offset (in percent).
- Number of power law segments.
- Number of segments and approximate values of the transition stress intensity ranges.

If the user enters the desired slope offset, the program begins by fitting the first two points in the data set to a Paris Equation using linear regression, and records the value of the slope, n_1. The program then fits a Paris Equation to data points 1 through 3, and records the value of n_2. The program defines the slope offset, in percent, using the following equation:

$$Slope\ offset = \left(\frac{n_2 - n_1}{n_1} \right) X\ 100\% \qquad (2.31)$$

The program continues fitting additional data points to a Paris Equation until the slope offset

between n_i and n_{i+1} is greater than the desired slope offset. The last end point which yields a slope offset lower than that desired becomes the first temporary transition point. Starting with this first temporary transition point, the iterative process is repeated until either another temporary transition point, or the end of the data file, is reached. The final values for the transition points are determined by calculating the ΔK values where two successive power law segments intersect.

If the user enters the desired number of power law segments, the program assumes an initial slope offset of 50%. Using this initial slope offset, the corresponding number of power law segments is calculated, using the method embodied in Equation 2.31. The slope offset is then increased or decreased at successively smaller intervals until the desired number of segments is reached. If the desired number of segments can not be reached by a user specified number of iterations, the process is stopped. The transition points are calculated by determining where two successive power law segments intersect.

The final option for determining the equation parameters involves the user entering the desired number of power law segments and the approximate ΔK values of the transition points. The program uses these transition points to determine which data points are fit to each power law segment. The final values for the transition points are determined by calculating the ΔK values where two successive power law segments intersect. This option gives the user the most control in determining the equation parameters, and often yields the best results. The weakness of this approach is that the user may bias the definition of power law transitions.

The three options included in the multiple power law method are subjective. Each

requires the user to indicate or bias the number of power law segments placed through the data. A major enhancement to the algorithm would be to create a method by which the program determines the number of power law segments and transition points which yield the best fit to the data. Presently, the model calculates the coefficient of determination to indicate the accuracy of the fitted equation.

2.6 University of Virginia Fatigue Analysis Software (UVaFAS)

The three computer models utilized during this research were incorporated into a single executable computer program. The linear superposition model developed by Allen Wilson, as well as the interpolative and multiple power law models are included in the DOS executable program UVAFAS.EXE. The program was written using FORTRAN 77, and compiled with a professional, 32 bit multi-platform FORTRAN compiler from WATCOM, Inc. Some sections of the source code were taken from NASA FLAGRO, Version 2.0[16], including the material files. The program and the source code are included with this thesis. The program is discussed in detail in Appendix A.

Chapter 3: Experimental Procedure

3.1 Material

Rolled plate of Ti-6Al-4V was obtained from President Titanium in the mill-annealed (MA), extra low interstitial (ELI) condition (annealed for 8 hours at 760°C and vacuum furnace cooled). Chemical composition and mechanical properties are given in Table 3.1. The micrograph in Figure 3.1 shows that this 12.7 mm thick plate consists of equiaxed α phase, with an average grain size between 8 and 10 μm, with a small quantity of retained β. This structure is consistent with the mill-anneal process.

Table 3.1: Chemical Composition and Mechanical Properties of Ti-6Al-4V (MA,ELI)

Chemical Composition (wt. %)

Al	V	C	N	Fe	O	H	Y	Ti
6.17	4.33	0.025	0.011	0.19	0.12	0.0055	<0.0005	bal.

Mechanical Properties

Yield Strength MPa (ksi)	Tensile Strength MPa (ksi)	Elongation Percent, %	Reduction in Area, %
940 (136)	982 (142)	13	30.2

3.2 Fracture Mechanics Experiments

3.2.1 Fracture Mechanics Specimen

A closed loop servohydraulic MTS 810 Material Test System with a

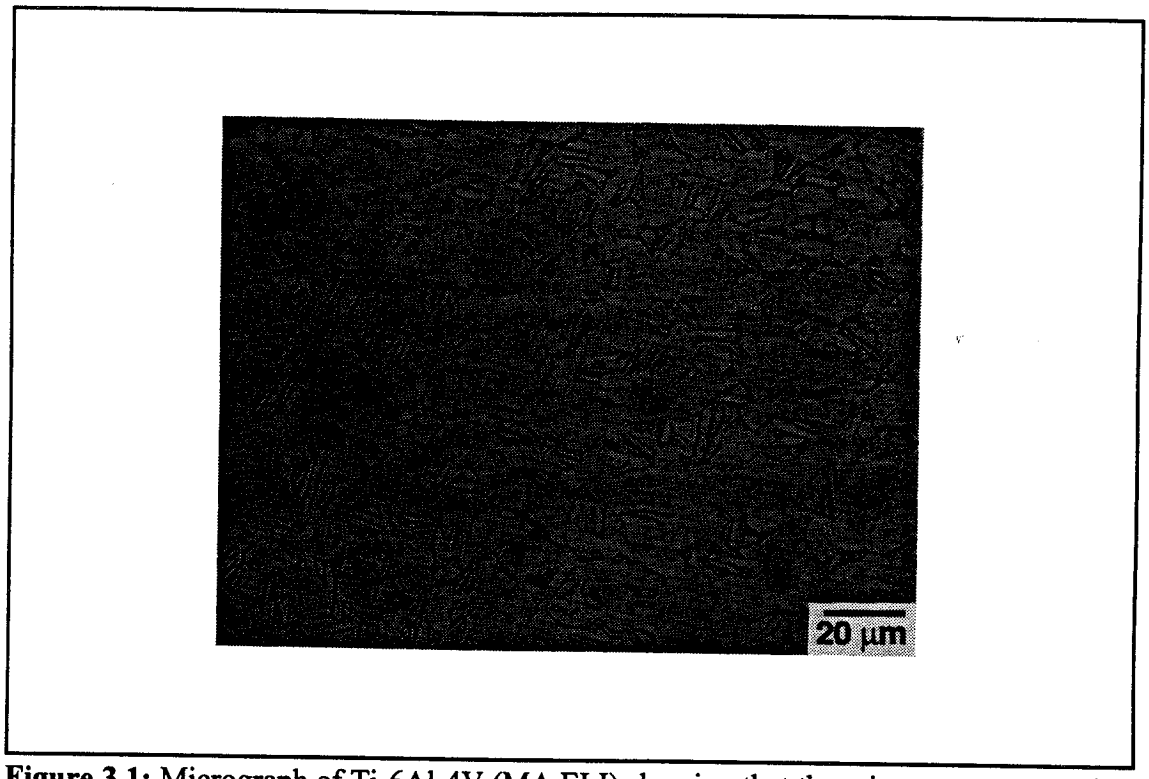

Figure 3.1: Micrograph of Ti-6Al-4V (MA,ELI) showing that the microstructure consists of equiaxed α with retained β.

Microconsole controller and 50 kN load cell was used to conduct all monotonic load and FCP rate tests. The test machine was interfaced with Fracture Technology Associates (FTA) PC-based software to control all test conditions and acquire data. Specimens were ultrasonically cleaned in acetone for at least five minutes before testing to remove machining debris.

All experiments utilized fracture mechanics methods applied to the compact tension (CT) specimen shown in Figure 3.2, machined in the L-T orientation. Holes were tapped into the specimen to accommodate a plexiglass environmental cell and knife edges, as seen in Figure 3.3. The specimens were mounted in the load train via clevises, and the applied stress intensity was calculated from measured load and crack length using a standard elastic

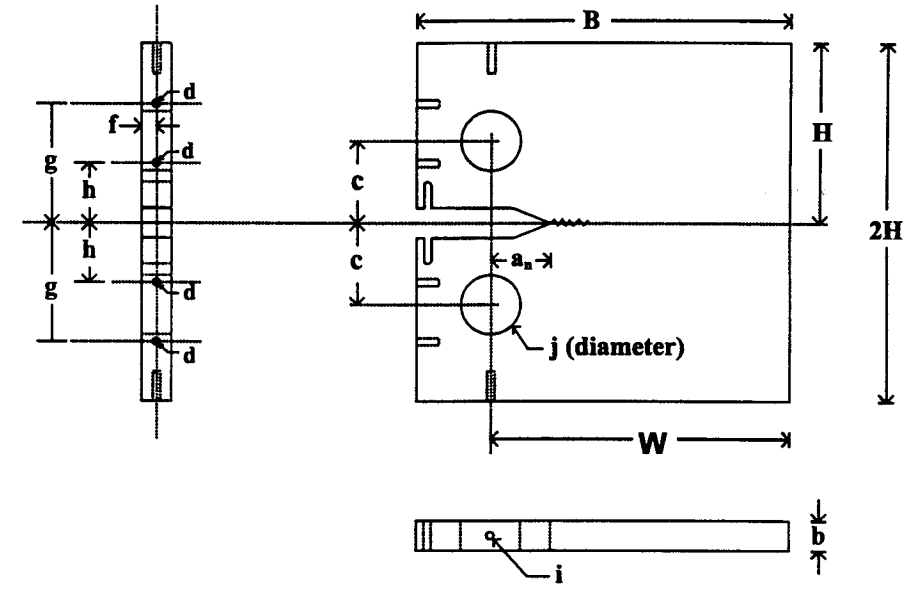

Notch Detail

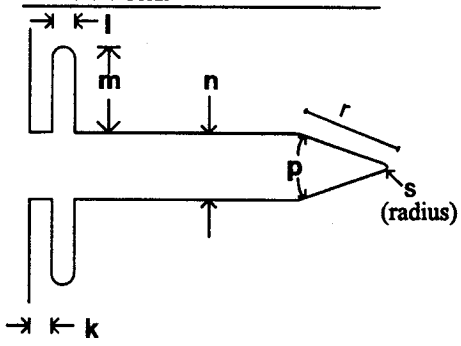

angle	deg	tol.
p	30	± 1

Dim.	(mm)	tol. (mm)
H	38.1	± 0.15
W	63.5	± 0.15
b	6.4	± 0.03
a_n	12.4	± 0.15
B	79.4	± 0.15
c	17.5	± 0.15
f	3.2	± 0.15
g	25.4	± 0.15
h	12.7	± 0.15
k	2.0	± 0.15
l	3.2	± 0.15
m	6.4	± 0.15
n	4.3	± 0.15
r	8.3	± 0.15
s	0.13	± 0.13

hole	spec.	size	depth (mm)	tol. (mm)
d	tapped	2-56	3.8	
l	tapped	4-40	2.5	
j	smooth	12.7 mm	through thickness	± 0.15

Figure 3.2: Schematic showing dimensions of the compact tension specimen utilized in EAC experiments.

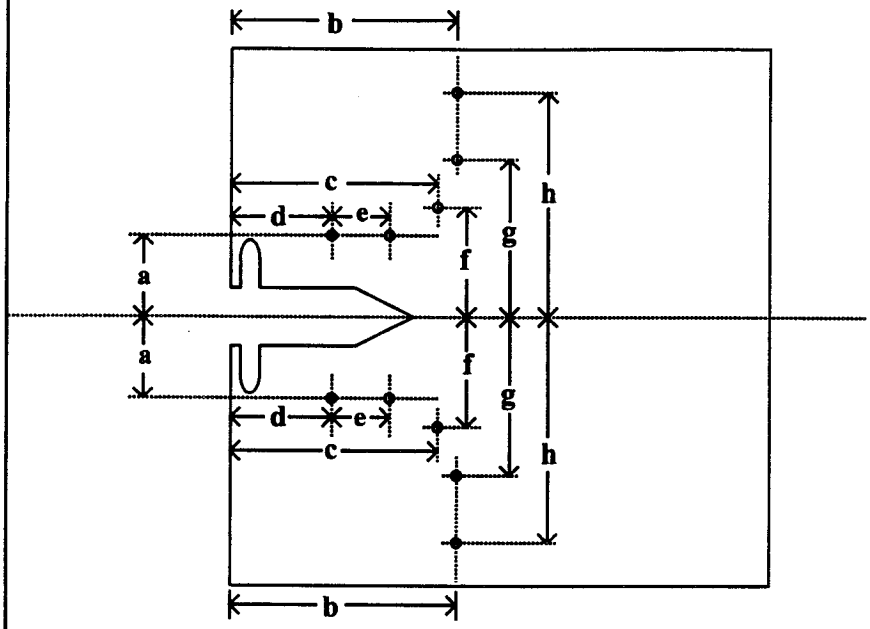

	Dim. (mm)	Tol. (mm)		Dim. (mm)	Tol. (mm)
a	4.69	±0.15	e	10.2	±0.15
b	41	±0.15	f	9.26	±0.15
c	38.6	±0.15	g	21	±0.15
d	17	±0.15	h	33.1	±0.15

Note: All holes are size 2-56.

Figure 3.3: Schematic showing locations of holes in the CT specimen to accommodate a plexiglass environmental cell.

solution[1]:

$$K = \frac{P}{b\sqrt{W}} f\left(\frac{a}{W}\right) \qquad (3.1)$$

$$f\left(\frac{a}{W}\right) = \frac{2+\frac{a}{w}}{\left(1-\frac{a}{W}\right)^{\frac{3}{2}}}\left[0.886+4.64\left(\frac{a}{W}\right)-13.32\left(\frac{a}{w}\right)^2+14.72\left(\frac{a}{W}\right)^3-5.6\left(\frac{a}{W}\right)^4\right] \qquad (3.2)$$

where a is crack length, W is specimen width, b is specimen thickness, and P is applied load. In order to insure that the specimen was predominantly elastic at all applied loads, the following condition was satisfied, in accordance with ASTM standards[1]:

$$(W - a) \geq \frac{4}{\pi}\left(\frac{K_{max}}{\sigma_{YS}}\right)^2 \qquad (3.3)$$

3.2.2 Crack Length Measurement Methods

3.2.2.1 Compliance

The elastic compliance method was used to determine crack length during all fatigue experiments. The relationship between compliance and crack length is expressed in terms of the dimensionless quantities (EvB)/P and a/W, where E is the elastic modulus, and v is the displacement in the loading direction between measurement points, located to give the crack mouth opening displacement (CMOD in Figure 3.2). The following polynomial expression was used to determine crack length:[1]

$$\frac{a}{w} = 1.00098 - 4.66951u_x + 18.4601u_x^2 - 236.825u_x^3 + 1214.88u_x^4 - 2143.5701u_x^5 \qquad (3.4)$$

$$u_x = \left(\left[\frac{BE\nu}{P} \right]^{\frac{1}{2}} + 1 \right)^{-1} \qquad (3.5)$$

3.2.2.2 Direct Current Potential Drop (DCPD)

The DCPD method was used to measure crack length during all monotonic load experiments. Total crack length was determined from DCPD measurements using the following equation:[1]

$$\frac{a}{w} = -0.5051 + 0.8857\left(\frac{V}{V_o}\right) - 0.1398\left(\frac{V}{V_o}\right)^2 + 0.0002398\left(\frac{V}{V_o}\right)^3 \qquad (3.6)$$

where V is the measured potential for a crack length and V_o is a reference potential defined for (a/W) = 0.241. Visual measurements of the initial crack length (notch + fatigue precrack) and the measured potential at crack initiation yielded V_o for each specimen and applied current through Equation 3.6.

3.2.2.3 Visual

Visual crack length measurements were made from markings on the fracture surface produced by changes in applied test conditions and viewed after specimens were fractured. Measurements were made using Image-Pro Plus image analysis software connected to a video camera with a 10x magnifying lens. The image analysis software was calibrated using the specimen thickness, measured with a micrometer. Visual crack length measurements were entered into the analysis software, along with the corresponding value of either the dimensionless quantity (EvB)/P, or the potential drop. Visual measurements were used to

correct the crack lengths calculated by Equations 3.4 and 3.6.

For all six specimens used in the study, post-test crack length measurements observed at transitions in fracture surface appearance were compared to the uncorrected values given by the compliance or DCPD method, as shown in Figure 3.4. The crack lengths determined by both methods are within ± 10% of actual crack lengths for all cases. A straight line was fit to the data using least squares regression. The slope of the line was 0.9964 ± 0.0486 using a 95% confidence interval, thus the slope of the line was statistically equal to 1.0.

3.2.3 Monotonic Loading

Experiments to determine K_{TH}, the threshold stress intensity for environmental crack initiation, as a function of load line displacement rate were performed at several constant CMOD rates. FTA software was utilized to control the CMOD rate, measured by a clip gage, and crack length was calculated using DCPD measurements. The specimens used for monotonic load experiments were fatigue precracked in a 3.5% NaCl solution at a fixed electrode potential of -500 mV_{SCE} from (a/W) of 0.2 to 0.5 at a constant ΔK of 15 MPa$\sqrt{m}$, R of 0.1 and frequency of 5 Hz, except for one specimen which was precracked to an (a/W) of 0.68 in moist air.

In all monotonic load experiments conducted to determine K_{TH}, a 3.5% NaCl solution at a fixed electrode potential of -500 mV_{SCE} was used. A single test was performed in moist air to determine the plane strain crack initiation fracture toughness, J_{IC}.

3.2.4 Fatigue Testing

Fatigue crack propagation was produced in stress intensity control, with load measured to provide active feedback control and CMOD measured to provide crack length

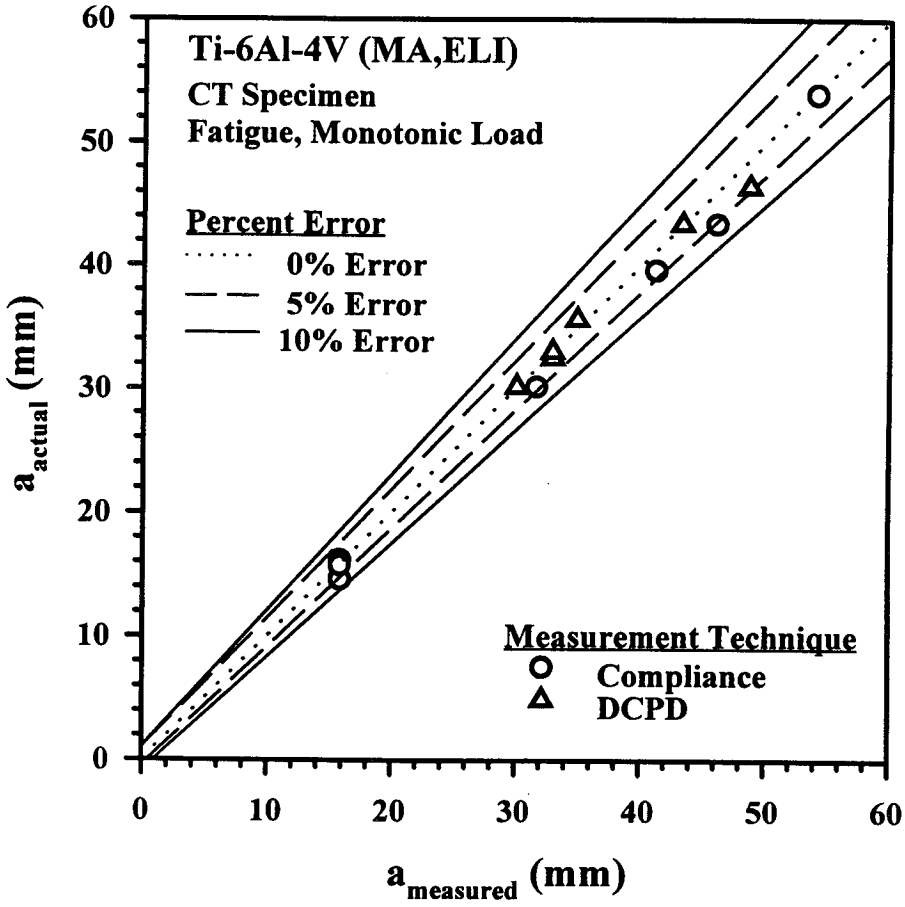

Figure 3.4: Comparison of post-test crack length measurements, a_{actual}, with uncorrected compliance and DCPD values, $a_{measured}$.

for stress intensity calculations. Experiments were conducted using FTA compliance based software, which provides measurement of da/dN - ΔK, closure stress intensities, ΔK_{eff}, and da/dN - ΔK_{eff} according to standardized test procedures.[1] The FTA software utilizes the secant method to calculate da/dN. Stress intensity was always varied sinusoidally with time in a fatigue experiment.

3.2.4.1 Fatigue Precracking

All fatigue specimens were fatigue precracked under a constant ΔK (15 MPa$\sqrt{m}$ and R of 0.1) from (a/W) of 0.2 to 0.25. The precrack ΔK was equal to or less than the first applied ΔK after the precrack, or the final K_{max} obtained during precracking did not exceed the initial K_{max} for which test data were obtained. All specimens were precracked in the test environment, either moist air or a 3.5% NaCl solution (-500 mV_{SCE}).

3.2.4.2 K Gradient Procedure

The K gradient method was utilized to generate da/dN versus ΔK data. K_{max} was defined as:

$$K_{max} = K_{maxo}\, e^{[C\,(a - a_o)]} \qquad (3.7)$$

where K_{max} is the maximum stress intensity corresponding to crack length a, K_{maxo} is the initial maximum stress intensity at a_o, a_o is the initial crack length, and C is a constant taken as $\pm$ 0.06 mm^{-1}. The specimen dimensions, precracking, K gradient procedures, and the method used to determine da/dN comply with ASTM Standard E647-91[1]. Fatigue experiments were conducted at constant R; K_{max} and ΔK varied during the experiments.

Several tests were also conducted holding ΔK, R, and the frequency constant. These

tests were conducted to determine changes in crack closure loads as a function of crack length and time at constant ΔK levels. Tests were also conducted with ΔK and R constant, but frequency was varied after a set increment of crack growth, in order to determine the precise variation of da/dN with frequency.

3.3 Environment

A plexiglass environmental cell was used to fully immerse the crack tip in an aerated solution of 3.5 weight percent NaCl. A rubber gasket was used to seal the top and bottom portions of the cell to each face of the CT specimen. The cell top and bottom were connected with a flexible latex sheet to contain the solution. This design was utilized so that the cell would not interfere with CT compliance by introducing friction forces.

The CT specimen was maintained at a fixed electrode potential of -500 mV_{SCE} with a potentiostat, platinum wire mesh counter electrode, and two Ag/AgCl reference electrodes located along the crack path on each side of the specimen. The counter electrode was isolated from the cell and positioned in a separate 2 liter reservoir. Electrode potential, and the difference from one side of the specimen to the other, were monitored throughout each experiment with two Ag/AgCl reference electrodes. Generally, the difference was less than 20 mV_{SCE}. The solution was circulated continuously through the cell and the specimen notch at 0.5 ml/sec from a 2 liter reservoir. This apparatus, illustrated in Figure 3.5, was designed to maintain constant solution environment conditions for test times of up to one month.

3.4 Crack Closure Measurements

FTA software was utilized to monitor crack closure levels during fatigue precracking

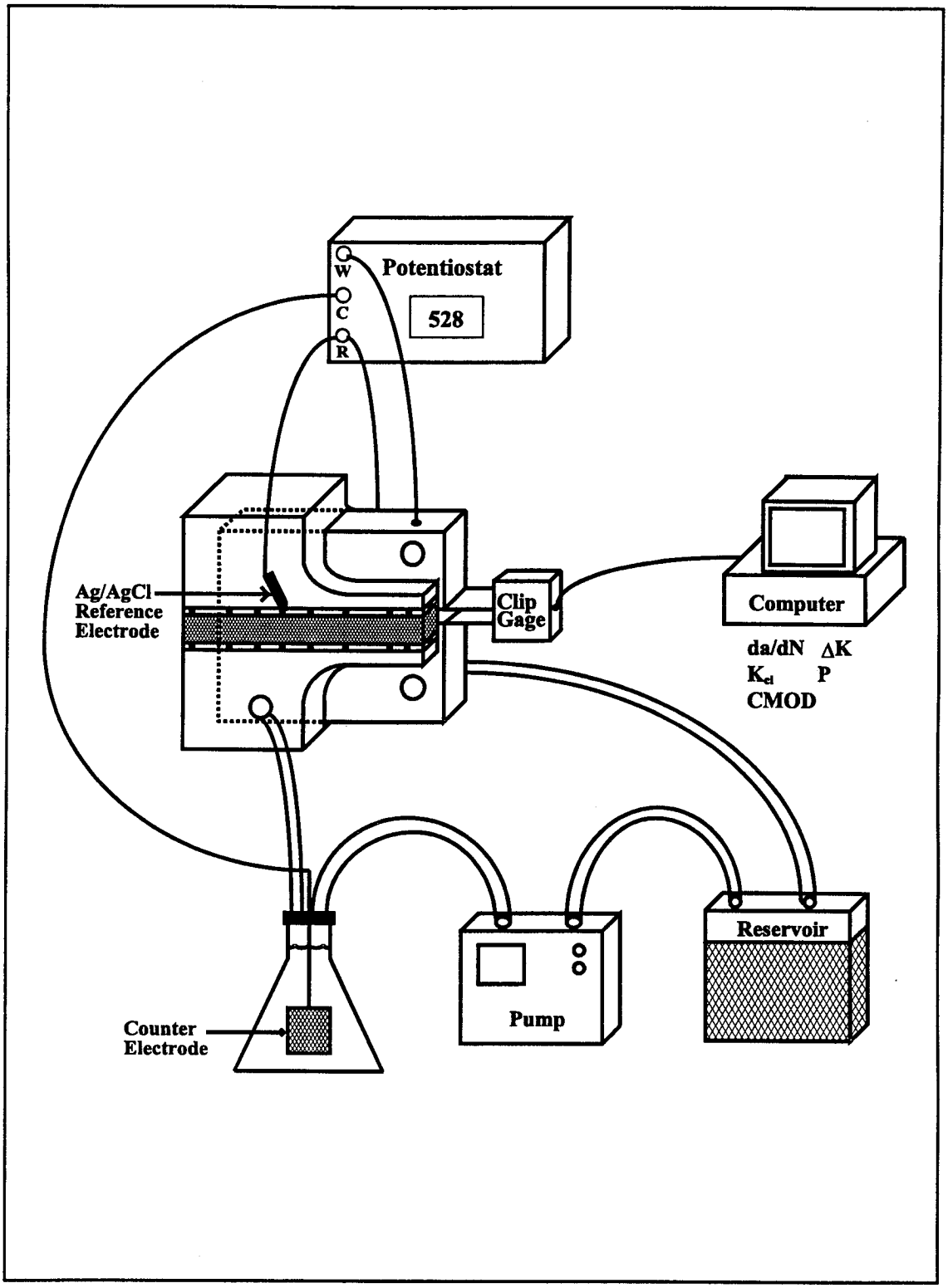

Figure 3.5: Schematic of environmental setup used in all EAC experiments (W = working electrode, C = counter electrode, R = reference electrode).

and fatigue experiments. The software employs the elastic compliance technique to enable both crack length and crack closure measurement.[28] The procedure involves collecting 400 evenly spaced load-displacement (P-v) data pairs during both the loading and unloading portions of each fatigue cycle. A least squares fit of P-v data is then performed on segments of data with a range of 10% of maximum load and which overlap by 5%, as illustrated in Figure 3.6. Segment 1 ranges from 98 to 88% of maximum load, segment 2 from 93 to 83% of maximum load , segment 3 from 88 to 78%, and so forth. Each slope is compared with the slope of the linear region of the load-displacement curve, and the percent change in slope is computed. The first slope segment corresponding to a percent change in slope greater than either 1, 2, 4, 8, or 16% from the linear region of the curve is identified. Load levels corresponding to a slope offset of 1, 2, 4, 8, or 16% are computed (Figure 3.7) and used to calculate K_{cl} and ΔK_{eff}. The closure level corresponding to a 2% slope offset was utilized to calculate ΔK_{eff} during all fatigue experiments.[28]

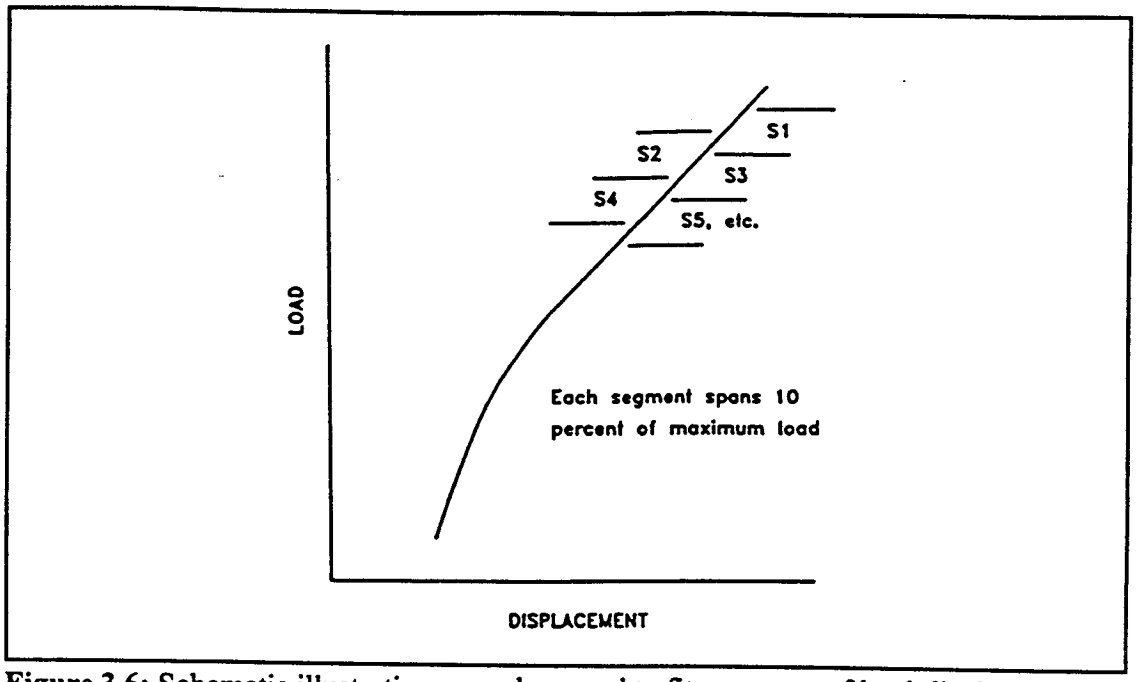

Figure 3.6: Schematic illustrating procedure used to fit segments of load-displacement data to a straight line. After Donald.[28]

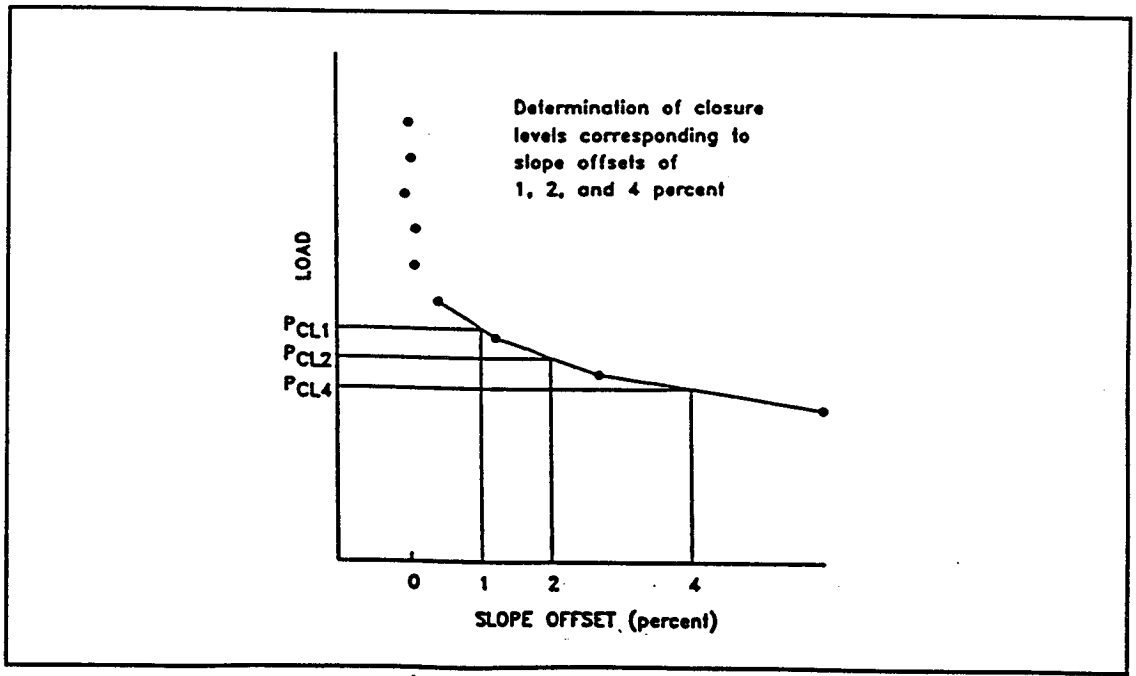

Figure 3.7: Schematic illustrating method used to compute P_{cl} using offsets of 1, 2, 4, 8, and 16%. After Donald.[28]

Chapter 4: Experimental Results

This chapter will present the results of the experiments conducted on Ti-6Al-4V (MA,ELI) in order to generate data to test the computer models. The results are compared to the environmental FCP behavior of standard grade Ti-6Al-4V (MA).

4.1 Monotonic Loading

4.1.1 Fracture Toughness

The plane strain fracture toughness, K_{IC}, for Ti-6Al-4V (MA,ELI) in moist air is required to assess the extent of NaCl embrittlement. However, since the CT specimens used did not meet the size requirement found in ASTM E399-90[29], K_{IC} could not be directly determined. Instead, an elastic-plastic analysis was utilized and J_{IC} was experimentally determined. The equations used to calculate $J_{elastic}$ and $J_{plastic}$ are given in ASTM Standard E1152-87.[30] The "plastic" area under the experimental load versus load-line displacement plot was calculated by subtracting the "elastic" area from the "total" area using an unloading compliance line calculated from the DCPD crack length measurement. In all of the tests, $J_{plastic}$ was less than 10% of J_{total}.

An experiment was conducted in moist air at a constant CMOD rate of 4.7×10^{-5} mm/sec. Figure 4.1 shows the resulting load and DCPD data as a function of CMOD. Crack initiation was defined at the first resolvable increase in the DCPD signal above a mildly increasing background. In accordance with ASTM E813-90[31], J_{IC} was determined as 49.7 kJ/m^2. Plane strain conditions were assumed at crack initiation, and K_{JIC} was calculated using:

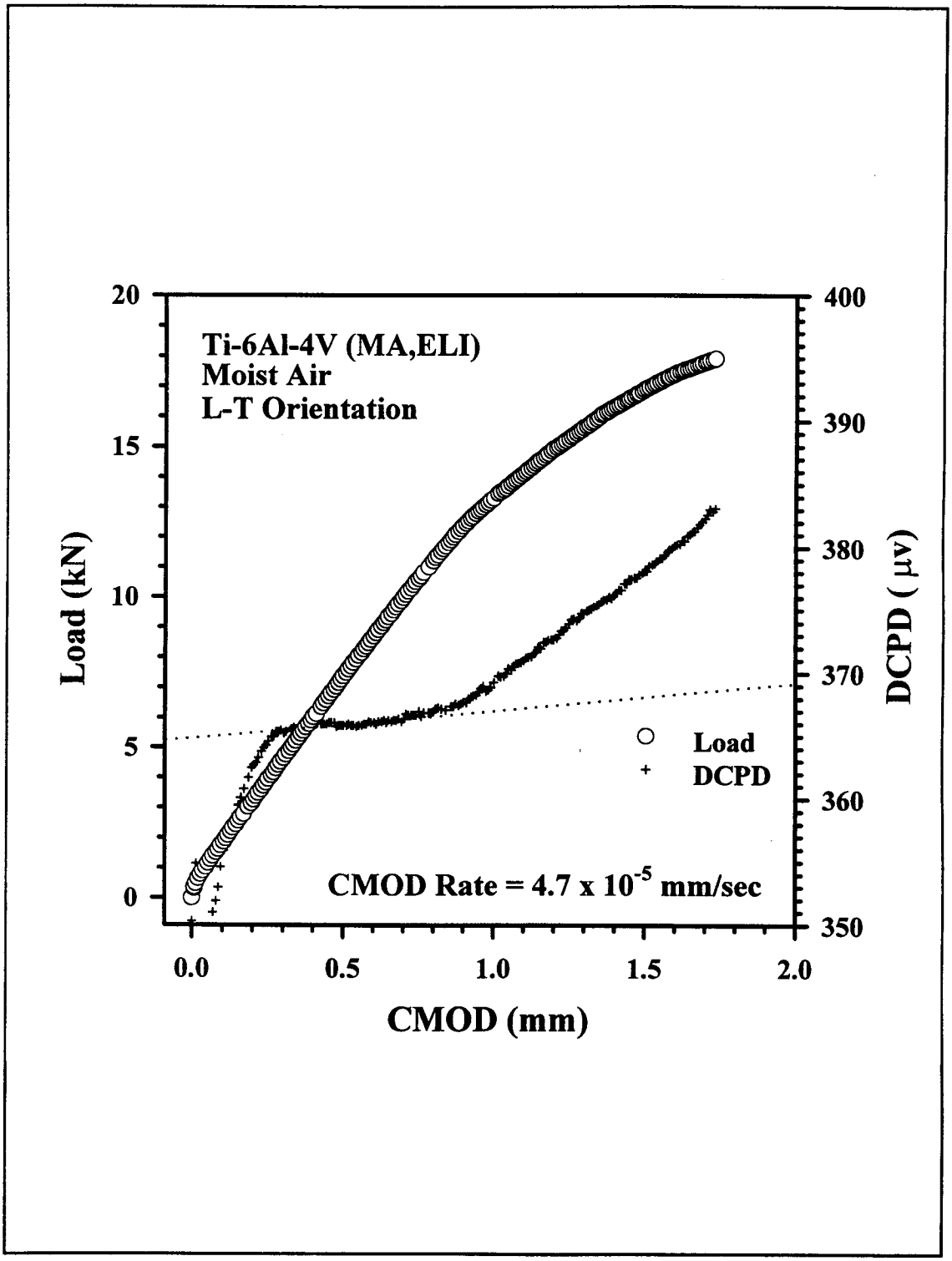

Figure 4.1: Load and DCPD versus CMOD for monotonic loading of Ti-6Al-4V (MA,ELI) in moist air for a CMOD rate of 4.7 x 10^{-5} mm/sec. The dashed line was used to determine the DCPD signal which corresponds to the onset of crack growth.

$$K_{JIC} = \sqrt{\frac{J_{IC}\ E}{(1-\nu^2)}} \qquad (4.1)$$

where ν is Poisson's Ratio (0.33) and E is 110 GPa.[32] K_{JIC} equals 78 MPa$\sqrt{m}$. K_{IC} should be between 65 and 75 MPa$\sqrt{m}$ for mill-annealed Ti-6Al-4V.[9] The ELI grade is generally tougher, consistent with the measured value of 78 MPa$\sqrt{m}$.

4.1.2 Stress Corrosion Cracking Behavior

The first issue addressed to understand the complex environmental fatigue behavior of Ti-6Al-4V in NaCl was stress corrosion cracking. Dawson and Pelloux[33] observed SCC in mill-annealed Ti-6Al-4V, and reported a K_{ISCC} value of 23 MPa$\sqrt{m}$ in 3.5% NaCl at a free corrosion potential.

In order to determine the SCC susceptibility of the mill-annealed, extra low interstitial Ti-6Al-4V used in this study, constant CMOD rate experiments were conducted. Figure 4.2 is a plot of applied load versus CMOD for an experiment conducted in 3.5% NaCl (-500 mV_{SCE}) at a constant CMOD rate of 3 x 10^{-5} mm/sec. K_{TH} was defined as the point on the P-ν plot where the data first deviated from linearity. (NaCl deposits formed on the DCPD wires and interfered with crack growth detection from electrical potential.) K_{TH} was calculated from the J integral at crack initiation.

For the results shown in Figure 4.2, where the CMOD rate was 3 x 10^{-5} mm/sec, (V_{LL} $\approx$ 2.3 x 10^{-5} mm/sec *), K_{TH} was calculated as 55 MPa$\sqrt{m}$. A second experiment was

---

*Load line displacement (V_{LL}) is estimated from CMOD using a geometric relationship.[34]

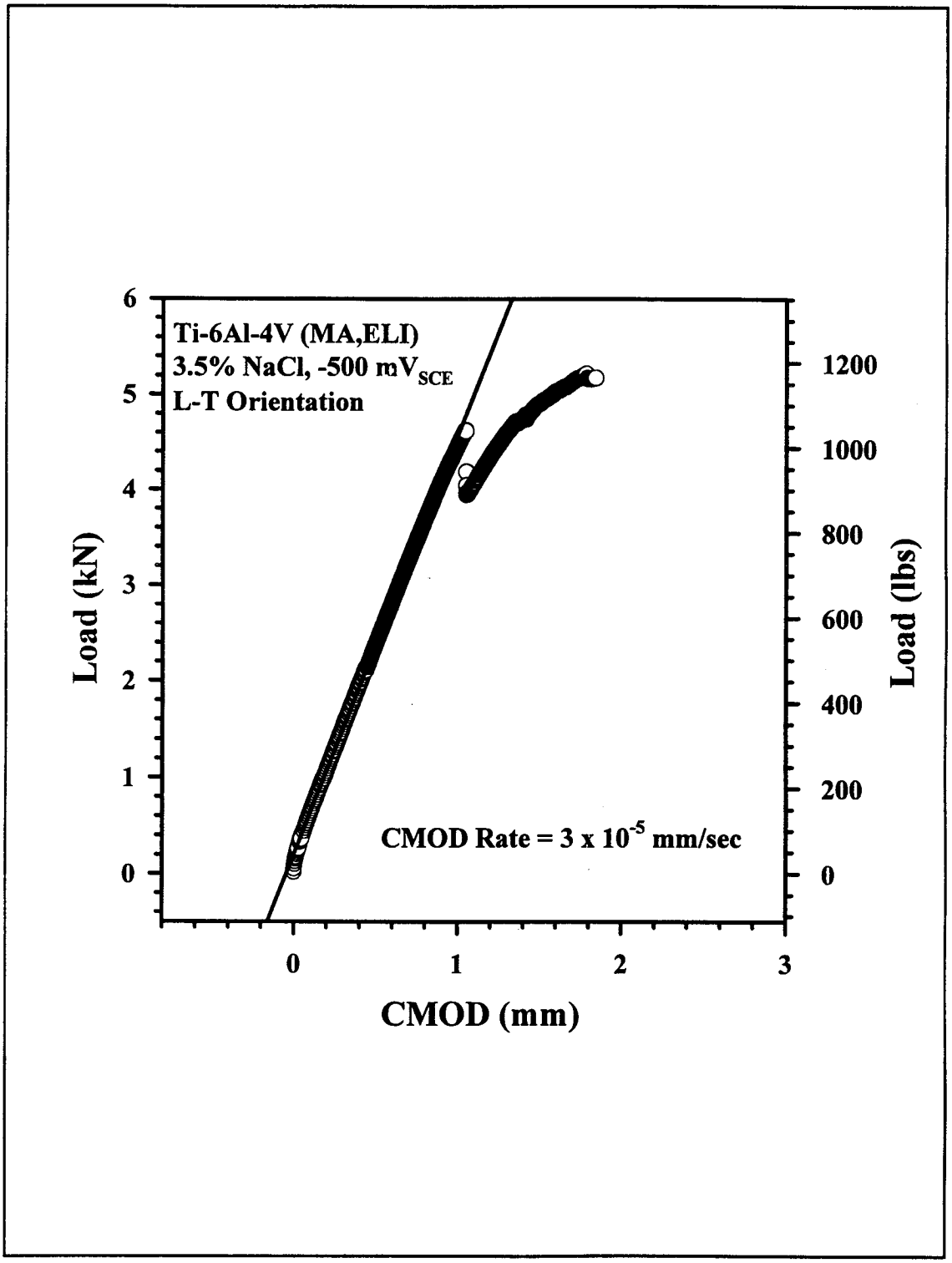

Figure 4.2: Load versus CMOD for monotonic loading of Ti-6Al-4V (MA,ELI) in 3.5% NaCl at a fixed electrode potential of -500 mV_{SCE} for a CMOD rate of 3 x 10^{-5} mm/sec. The solid line represents a linear relationship between load and CMOD.

conducted under the same conditions, except CMOD rate was increased to 4.7 x 10^{-5} mm/sec ($V_{LL} \approx 3.4 \times 10^{-5}$ mm/sec). Measured load versus CMOD data are shown in Figure 4.3, and K_{TH} was calculated as 48 MPa$\sqrt{m}$.

A final experiment was conducted where load on precracked Ti-6Al-4V (MA,ELI) was increased monotonically in 65 minutes to a level corresponding to a stress intensity of 40 MPa$\sqrt{m}$. This corresponds to a V_{LL} of approximately 9.2 x 10^{-5} mm/sec. Since cracking was not observed, the load was held constant for 137 hours at this level. The specimen was at a fixed electrode potential of -500 mV_{SCE} for the first 55 hours, and then switched to free corrosion for the remainder of the experiment. The open circuit, or free corrosion potential was measured as approximately -240 mV_{SCE}. The resulting load versus CMOD plot is shown in Figure 4.4. The crack did not grow during this test, since the load remained constant. A load drop of 0.11 kN would have been noticeable and corresponded to 0.22 mm of crack growth.

The stress intensity values calculated for crack initiation in the Ti-6Al-4V (MA,ELI)/ NaCl system are much higher than K_{ISCC} reported by Dawson and Pelloux[33] for mill-annealed Ti-6Al-4V. The major difference between the alloy studied by Dawson and Pelloux, and the alloy used during this research, is the purity of the ELI condition. This increased value for K_{TH} indicates an increased resistance to SCC.

K_{TH} depends on load-line displacement rate, as evidenced by these two experiments. Moskovitz and Pelloux[35] reported a dependence of K_{TH} on loading rate for an $\alpha + \beta$ alloy, Ti-6Al-6V-2Sn (MA), in 3.5% NaCl. Figure 4.5 is a plot of K_{TH} versus stress intensity rate (dK/dt) for single edge notch (SEN) specimens (Δ, $\square$). Also shown are the results ($\circ$)

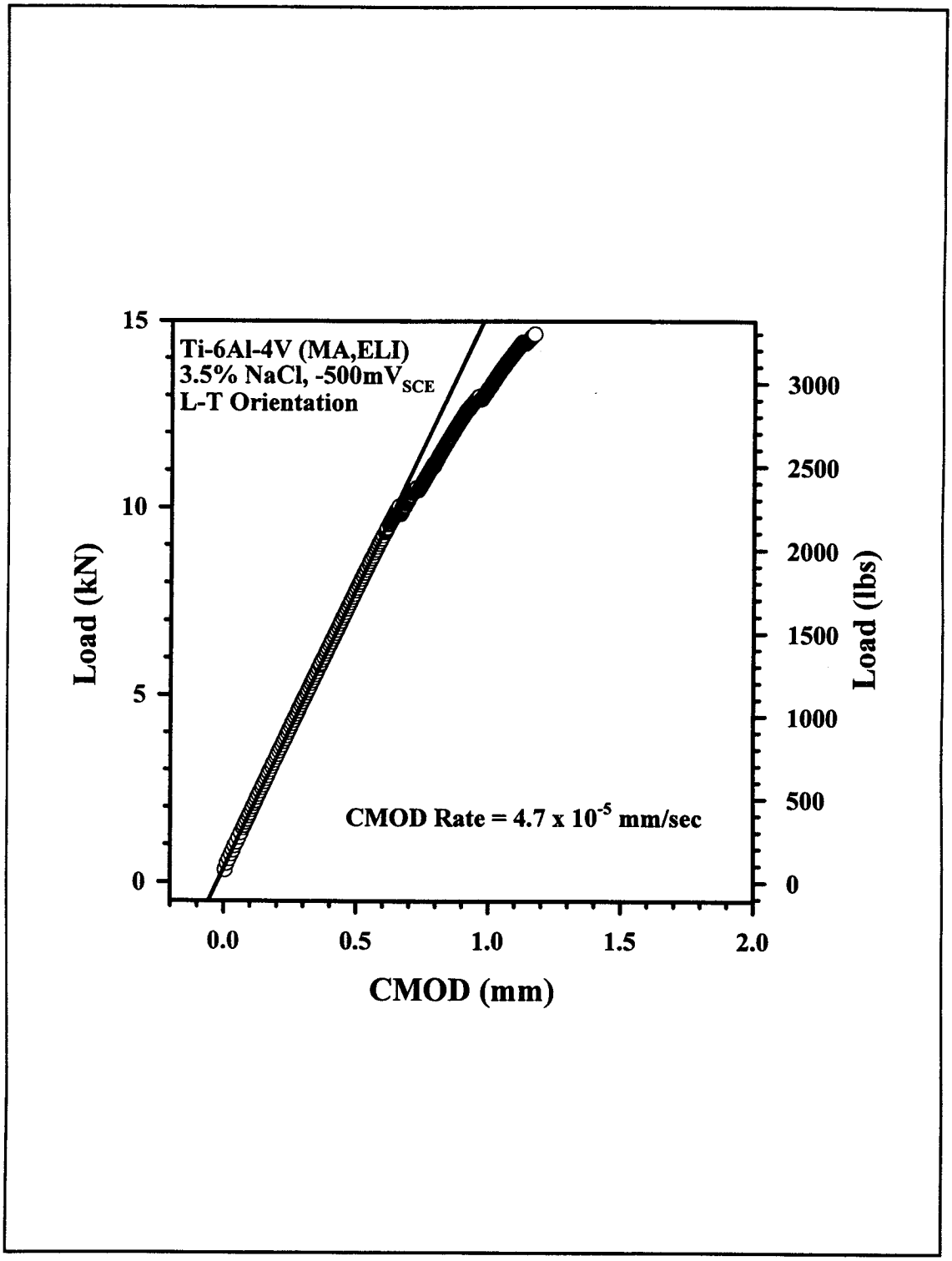

Figure 4.3: Load versus CMOD for monotonic loading of Ti-6Al-4V (MA,ELI) in 3.5% NaCl at a fixed electrode potential of -500 mV_{SCE} for a CMOD rate of 4.7 x 10^{-5} mm/sec. The solid line represents a linear relationship between load and CMOD.

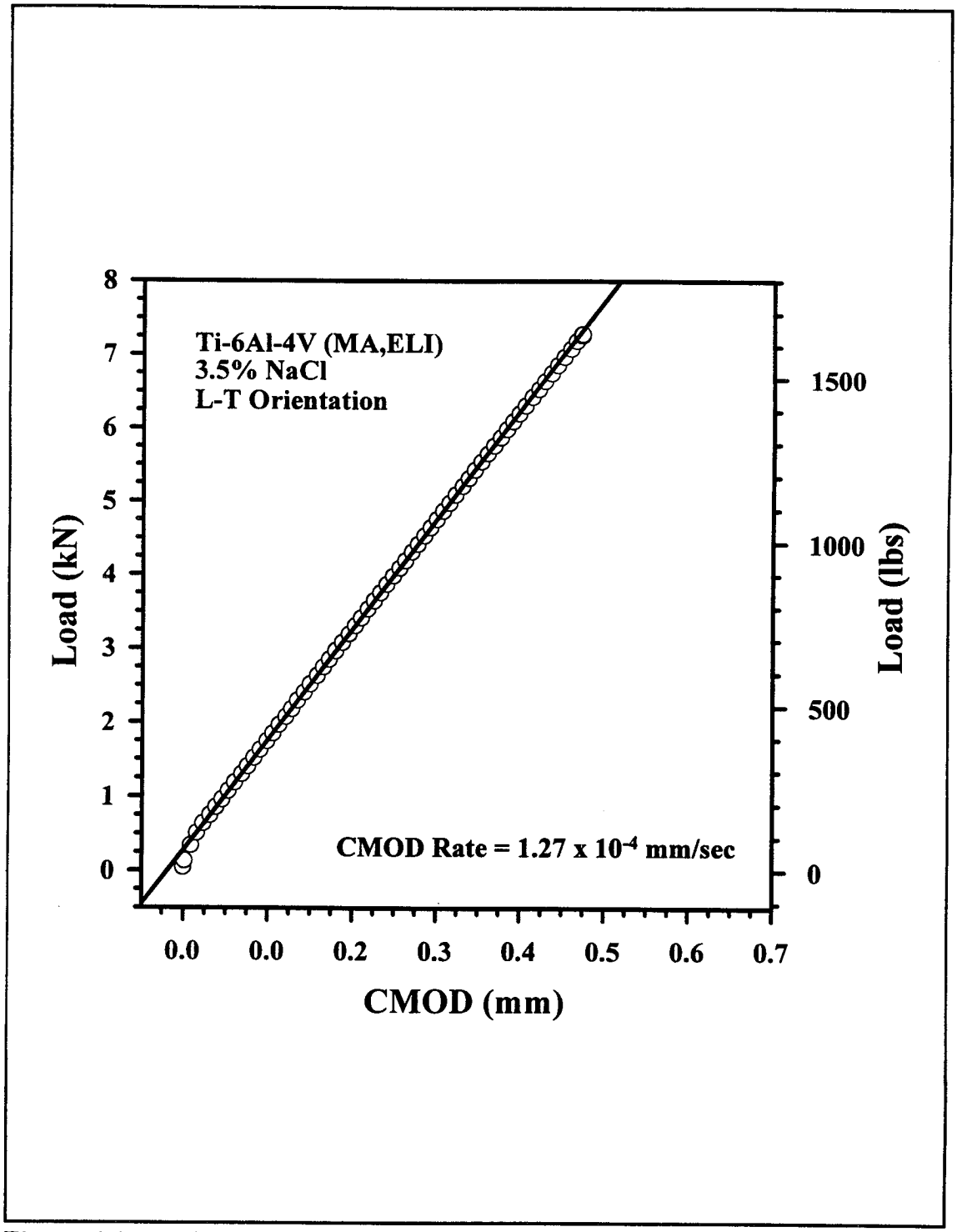

Figure 4.4: Load versus CMOD for Ti-6Al-4V (MA,ELI) in 3.5% NaCl. Load was monotonically increased to a stress level of 40 MPa$\sqrt{m}$ in 65 minutes, and then held constant for 137 hours. The CT specimen was at a fixed electrode potential of -500 mV_{SCE} for 55 hours and then switched to free corrosion.

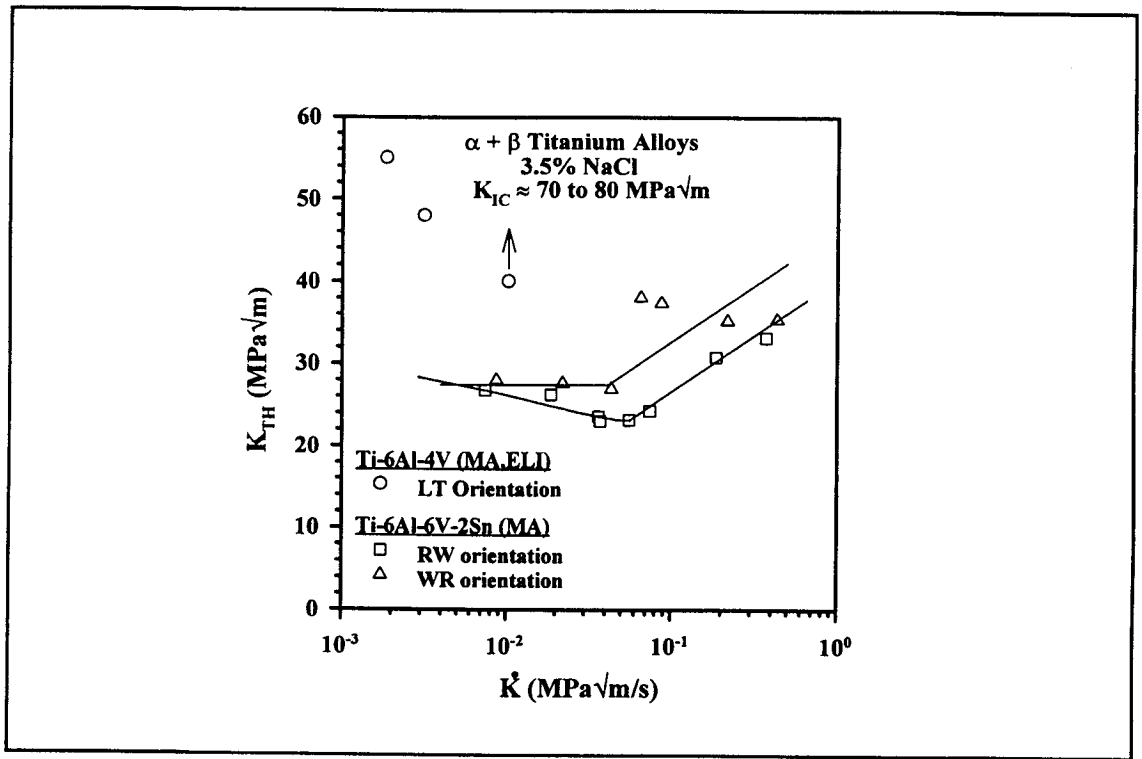

Figure 4.5: Dependence of K_{TH} on loading rate for Ti-6Al-6V-2Sn (MA) and Ti-6Al-4V (MA,ELI) in 3.5% NaCl. Data for Ti-6Al-6V-2Sn after Moskovitz and Pelloux.[35]

for the experiments seen in Figures 4.2 through 4.4. K_{TH} was plotted versus stress intensity rate because strain rates control the value of K_{TH}, and stress intensity rate controls the strain rate. In order to calculate the stress intensity rates for the Ti-6Al-6V-2Sn data, the change in load with respect to time (dP/dt) was calculated for each K_{TH} value. This dP/dt was then substituted for load in the stress intensity expression for a SEN specimen, so that stress intensity rate could be calculated instead of stress intensity.

Environment assisted cracking (EAC) occurs in the Ti-6Al-4V (MA,ELI) system, as seen by a comparison of the data shown in Figures 4.1 and 4.3. The experiments were conducted under identical loading conditions; only the environment was changed from moist air to 3.5% NaCl (-500 mV_{SCE}). Unlike the data in Figure 4.1, the data in Figure 4.2 (and to

a lesser extent in Figure 4.3) exhibit decreases in load at constant CMOD. These load drops of 0.2 to 0.4 kN correspond to "bursts" of crack growth. Since the only difference between the two experiments is environment, EAC likely occurred, albeit at a very high K level.

ELI grade Ti-6Al-4V (MA) exhibits a $(da/dt)_{environment}$ that is less than 10^{-5} mm/sec. Figure 4.4 presented the results of an experiment conducted in 3.5% NaCl (-500 mV_{SCE}) where the stress intensity was held constant at 40 MPa$\sqrt{m}$ for 137 hours. A load drop of 0.11 kN would have been noticeable, and corresponded to 0.22 mm of crack growth. As seen in Figure 4.4, the load did not drop by a resolvable amount. However, assuming a maximum crack extension of 0.22 mm during this experiment, the corresponding $(da/dt)_{environment}$ is 4.5×10^{-7} mm/sec. The environment enhanced time-based crack growth rate for Ti-6Al-4V is accordingly less than this very low value.

Since the K_{TH} values determined for Ti-6Al-4V (MA,ELI) are much higher than literature data for K_{ISCC}, SCC does not significantly contribute to time or R dependent environmental fatigue for the range of stress intensities used in this study (5 to 45 MPa$\sqrt{m}$).

4.2 Environment Enhanced Fatigue Crack Growth

4.2.1 Literature Background

4.2.1.1 Effect of Environment on da/dN

FCP in Ti-6Al-4V is generally strongly environment sensitive, with multiple da/dN-ΔK power law transitions reported for moist air and aqueous chloride solution. [33,36-39] ELI grade Ti-6Al-4V (MA) displays a complex, multiple slope behavior in both moist air and a 1.0% NaCl solution (-500 mV_{SCE}), as seen in Figures 4.6 and 4.7. A 1.0% NaCl solution

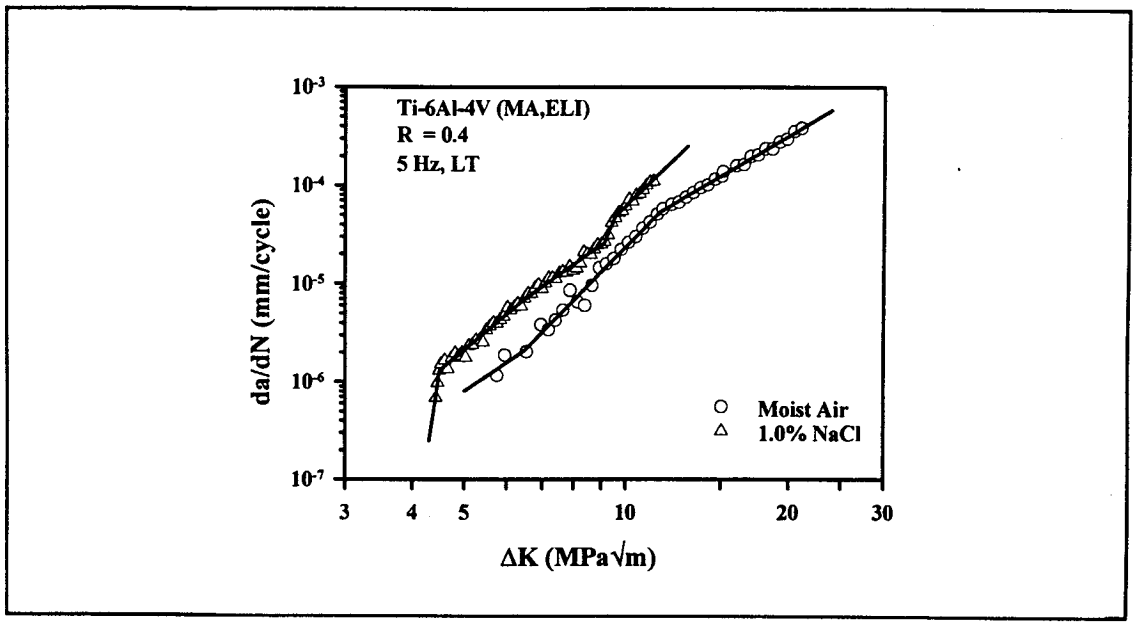

Figure 4.6: Comparison of da/dN versus ΔK for Ti-6Al-4V (MA,ELI) in moist air and a 1.0% NaCl solution (R = 0.4 and f = 5 Hz). The solid lines represent power law trends in the data. After Gangloff and Kim.[9]

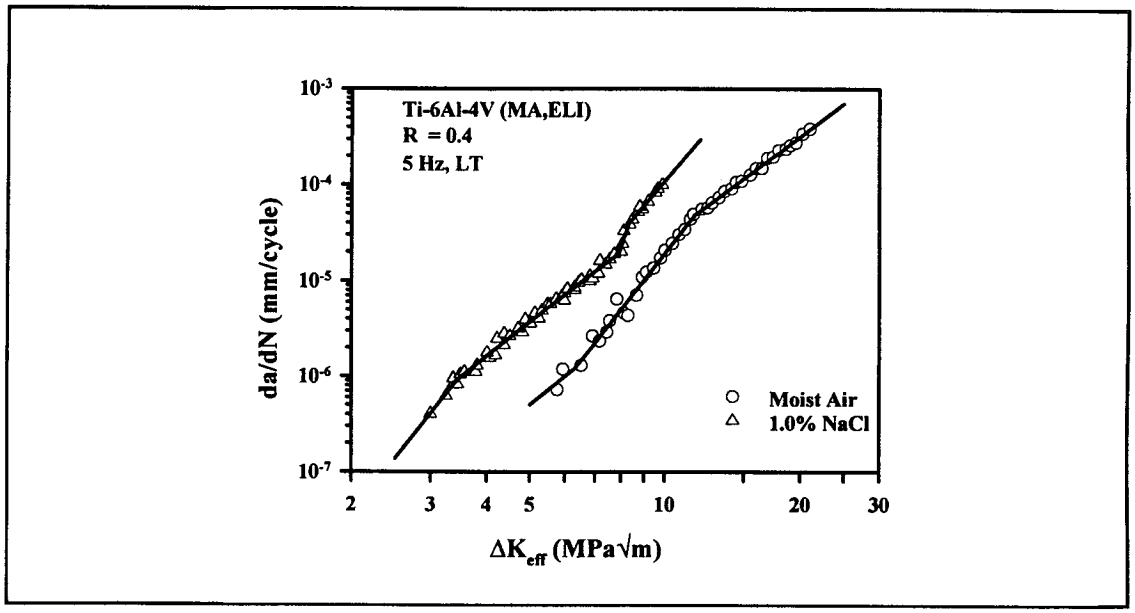

Figure 4.7: Comparison of da/dN versus ΔK_{eff} for Ti-6Al-4V (MA,ELI) in moist air and a 1.0% NaCl solution (R = 0.4 and f = 5 Hz). The solid lines represent power law trends in the data. After Gangloff and Kim.[9]

(-500 mV_{SCE}) is detrimental and enhances fatigue crack growth rates relative to FCP in moist air, as seen in Figure 4.8. The NaCl environment increased FCP rates by an average factor of 2.5 for an R of 0.1, by 2.0 for an R of 0.4, and by 2.2 for an R of 0.7. The data were taken from a study of this same heat of Ti-6Al-4V (ELI) by Gangloff and Kim.[9]

4.2.1.2 Effect of Stress Ratio on da/dN

The effect of stress ratio on FCP in Ti-6Al-4V(MA,ELI) in moist air and a 1.0% NaCl solution (-500 mV_{SCE}) is demonstrated in Figures 4.9 and 4.10. These data are replotted from Figure 4.8. As R increases from 0.1 to 0.7, da/dN increases at a constant ΔK in both environments.

4.2.1.3 Effect of Sinusoidal Frequency on da/dN

The effect of frequency on FCP in titanium alloys is strongly environment sensitive. Three different forms of frequency dependence were identified by Dawson and Pelloux[33] for the mill-annealed $\alpha + \beta$ alloys Ti-6Al-6V-2Sn and Ti-6Al-4V, as schematically illustrated in Figure 4.11.

"Type 1" is a frequency independent behavior, and was observed by Dawson and Pelloux[33] for FCP in inert environments, moist air, and aqueous solutions containing a corrosion inhibitor, Na_2SO_4. For "Type 2" behavior, da/dN increases with decreasing frequency for all ΔK. Dawson and Pelloux observed this behavior for titanium alloys in distilled water and methanol-HCl solutions. "Type 3" behavior is unique to $\alpha + \beta$ titanium alloys in aqueous solutions containing the halide ions Cl^- and Br^-. For "Type 3" behavior, da/dN increases as f decreases at high ΔK values, but da/dN decreases as f decreases at low ΔK values. "Type 3" behavior was later observed by Dawson[40] for Ti-6Al-6V-2Sn in

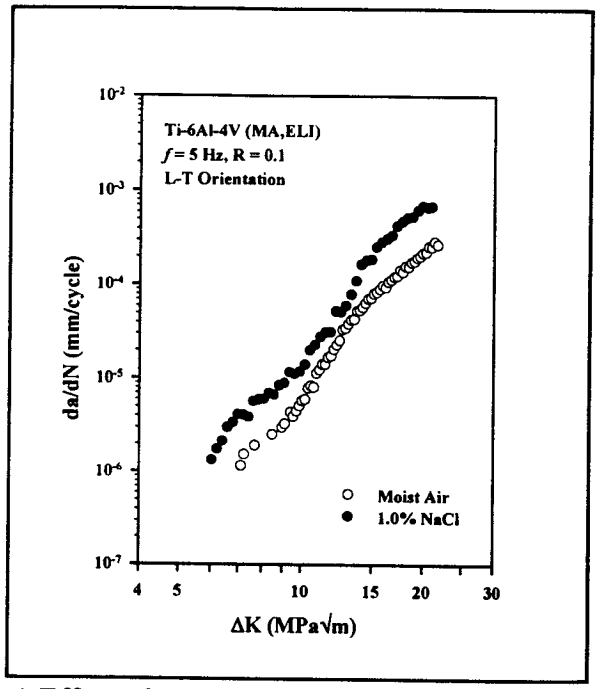

a) Effect of environment for R = 0.1

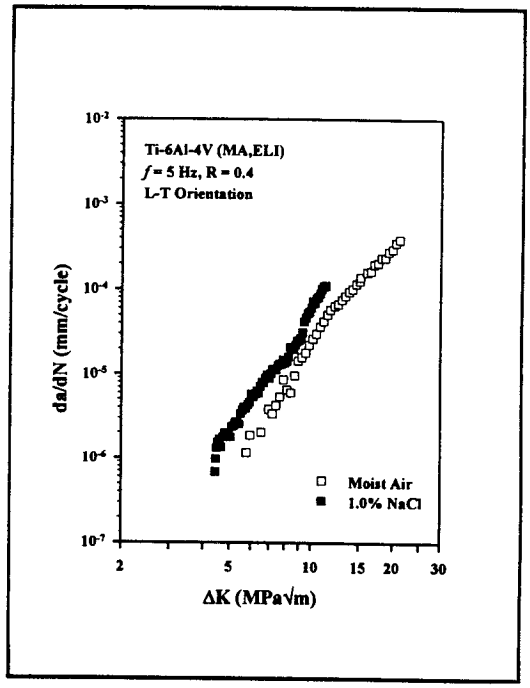

b) Effect of environment for R = 0.4

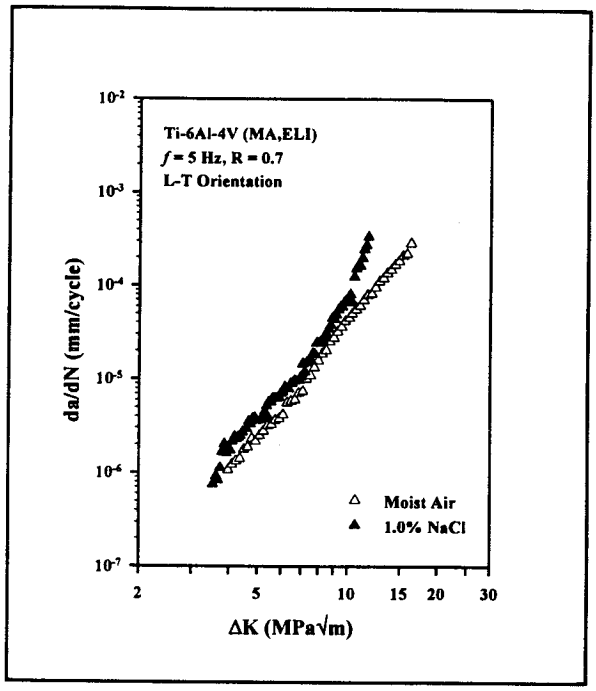

c) Effect of environment for R = 0.7

Figure 4.8: Effect of environment on fatigue crack growth in Ti-6Al-4V (MA, ELI) at stress ratios of 0.1, 0.4, and 0.7. After Gangloff and Kim.[9]

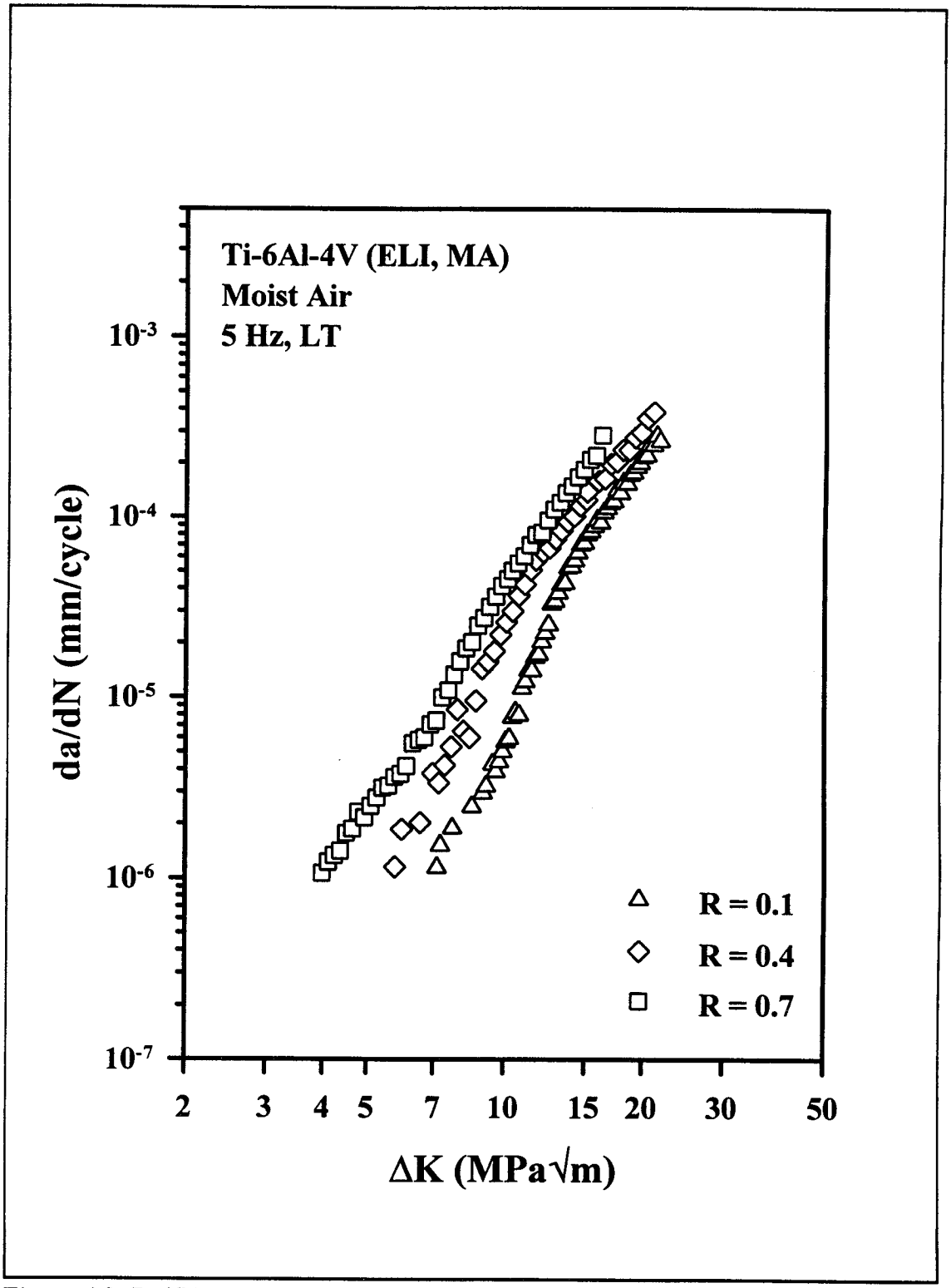

Figure 4.9: Da/dN versus ΔK for Ti-6Al-4V (MA,ELI) in moist air at stress ratios of 0.1, 0.4, and 0.7. After Gangloff and Kim.[9]

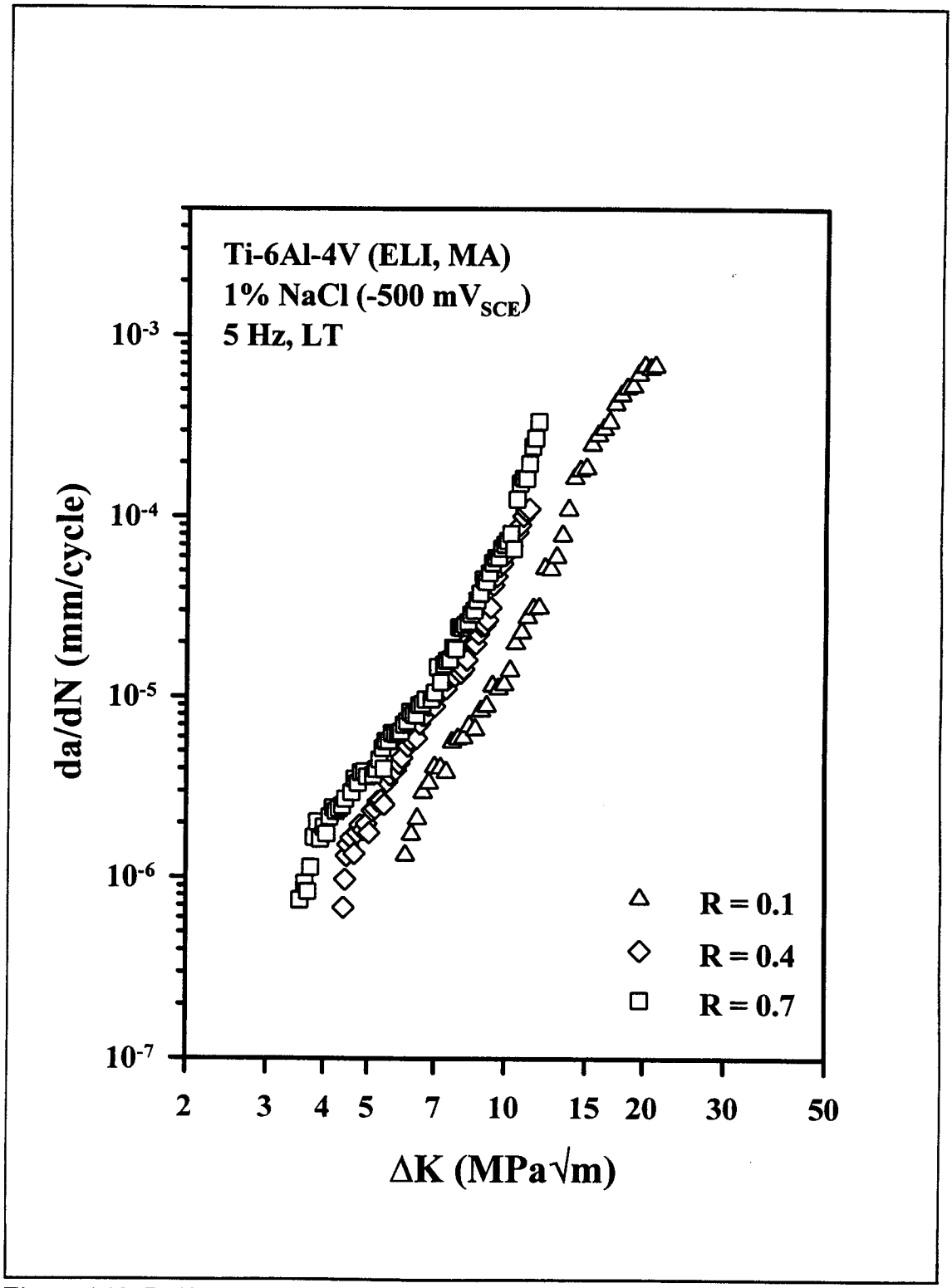

Figure 4.10: Da/dN versus ΔK for Ti-6Al-4V (MA,ELI) in 1.0% NaCl (-500 mV$_{SCE}$) at stress ratios of 0.1, 0.4, and 0.7. After Gangloff and Kim.[9]

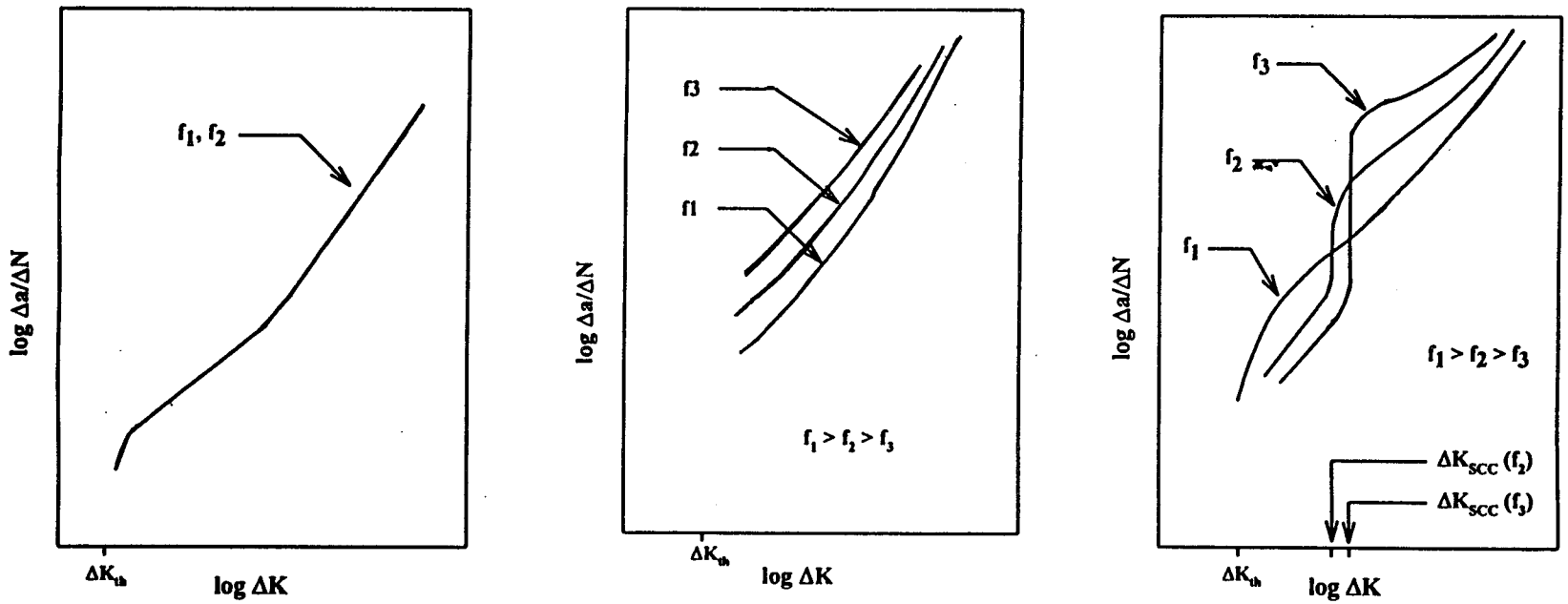

a) Type 1
Frequency independent
Examples: Vacuum, Argon, Air

b) Type 2
Δa/ΔN increases for decreasing frequency
Examples: Methanol, DMSO

c) Type 3
Reversal of frequency effect above and below ΔK_{SCC}
Examples: Aqueous NaCl and KBr solutions

Figure 4.11: Schematic depicting the effect of frequency on FCP in titanium alloys in various environments. After Dawson and Pelloux.[33]

methanol-water solutions, and by Yoder *et. al.*[41] for beta annealed and mill annealed Ti-6Al-4V in 3.5% NaCl solutions. Figure 4.12 shows this behavior for Ti-6Al-4V(MA) in 3.5% NaCl for R = 0.1. Note that these data do not extend to particularly low growth rates.

"Type 3" behavior has been called the frequency "crossover" effect by Dawson and Pelloux.[33] The "crossover" is a change in the ordering of da/dN at a transition ΔK value associated with the onset of "cyclic" SCC. Below the transition ΔK levels, labeled ΔK_{SCC} in Figure 4.11, da/dN decreases with decreasing frequency, perhaps due to passive film formation at the crack tip. Above ΔK_{SCC}, da/dN is perhaps controlled by hydrogen embrittlement; da/dN increases as frequency decreases and more time is allowed for hydrogen embrittlement to occur.

Dawson and Pelloux[33] reported that the threshold for "cyclic" SCC (ΔK_{SCC}) is lower than K_{ISCC} and increases as frequency decreases, as shown in Figure 4.13. As frequency decreases, ΔK_{SCC} should approach $(1-R)K_{ISCC}$, since this corresponds to K_{max} equalling K_{ISCC}. As seen in Figure 4.13, this behavior is observed for standard grade Ti-6Al-4V (MA) in NaCl.

Figure 4.14 demonstrates the effect of frequency for beta annealed (BA) Ti-6Al-4V in a 3.5% NaCl solution for R of 0.1 and ΔK values between 16 and 59 MPa$\sqrt{m}$. The data are consistent with the frequency crossover effect. Notice in Figure 4.13 that if a constant value of ΔK is selected, such that ΔK is less than $(1-R)K_{ISCC}$ (for K_{ISCC} = 23 MPa$\sqrt{m}$), a critical frequency exists at which this ΔK value is equal to ΔK_{SCC}. For example, if a ΔK value of 11 MPa$\sqrt{m}$ is selected, then the critical frequency is 10 Hz; at this frequency, the selected ΔK is equal to ΔK_{SCC}. For frequencies less than this critical frequency, the selected

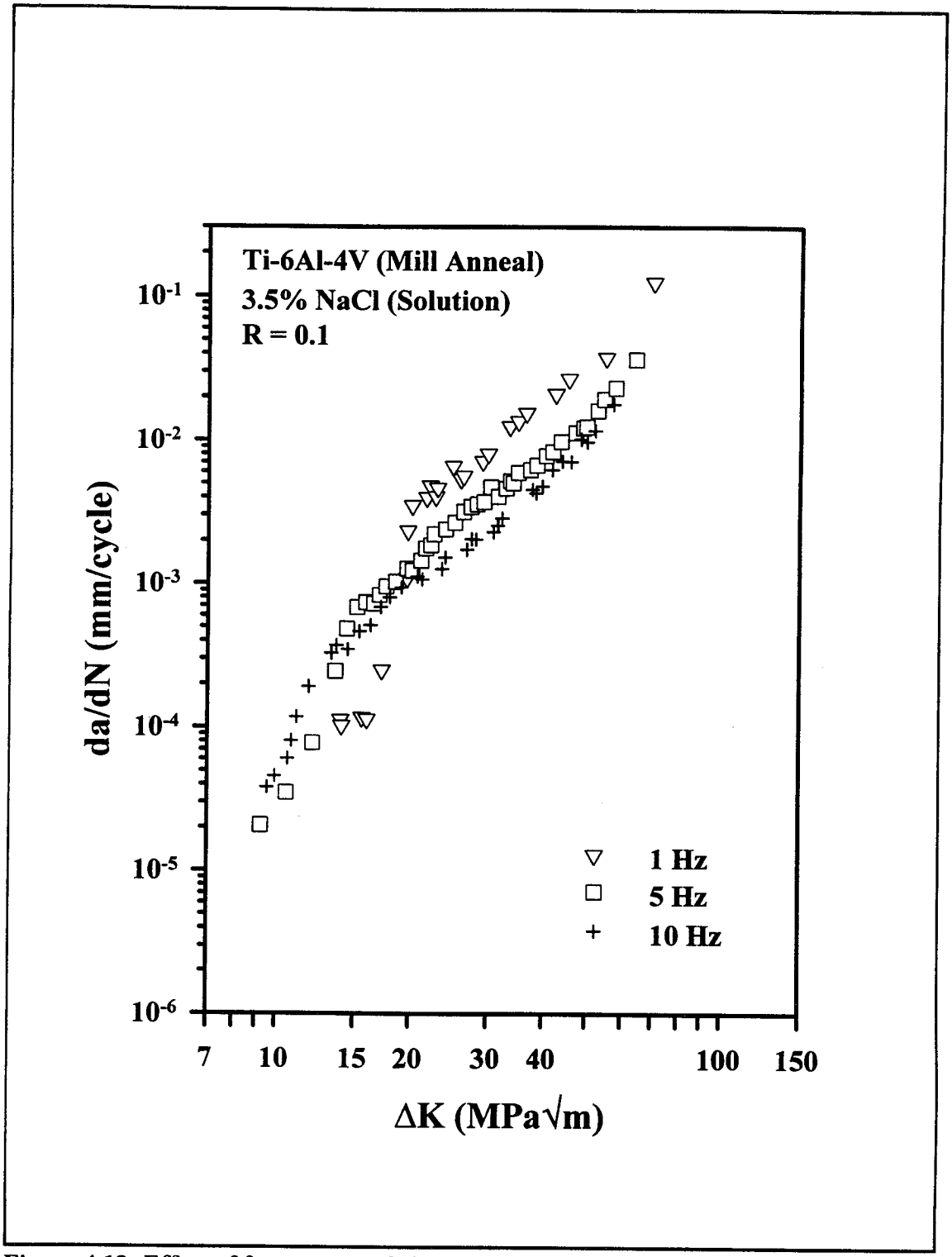

Figure 4.12: Effect of frequency on fatigue crack growth in Ti-6Al-4V (MA) in 3.5% NaCl. After Dawson and Pelloux.[33]

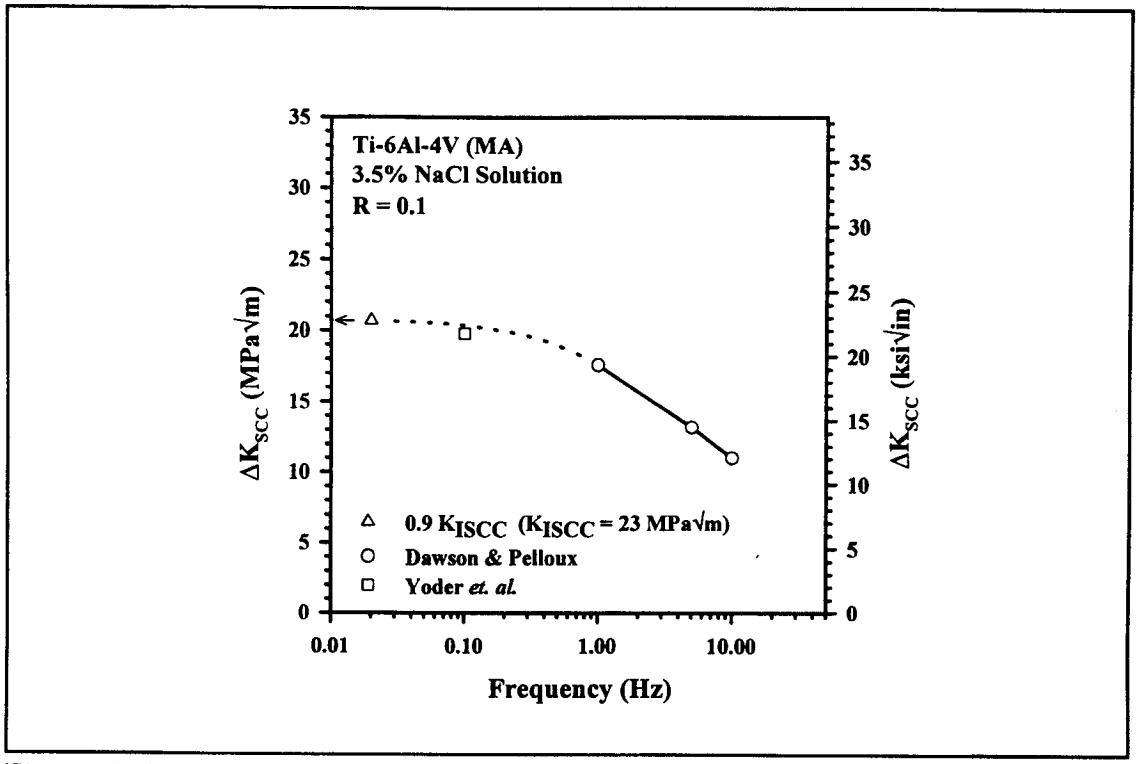

Figure 4.13: ΔK_{SCC} versus frequency for Ti-6Al-4V (MA) in 3.5% NaCl solution. After Dawson and Pelloux[33] and Yoder *et. al.*[41]

ΔK value is below ΔK_{SCC}, for frequencies above this critical value, ΔK is above ΔK_{SCC}. Figure 4.14 indicates a maximum da/dN for each ΔK value except 59 MPa$\sqrt{m}$. These maximum values occur at the critical frequency where ΔK is equal to ΔK_{SCC}. Figure 4.15 is a plot of ΔK_{SCC} versus frequency for the data presented in Figure 4.14. Figure 4.16 illustrates this concept of a critical frequency. For frequencies less than f_{crit}, at a fixed ΔK^*, da/dN decreases as frequency decreases since ΔK^* is below ΔK_{SCC}. For frequencies above f_{crit}, da/dN decreases as frequency increases since ΔK^* is above ΔK_{SCC}.

The Wei and Landes[23] linear superposition model appears to correctly describe the effect of frequency on da/dN for mill annealed titanium alloys in aqueous chloride solutions for FCP above K_{ISCC}.[42-43] The model does not, however, accurately account for corrosion

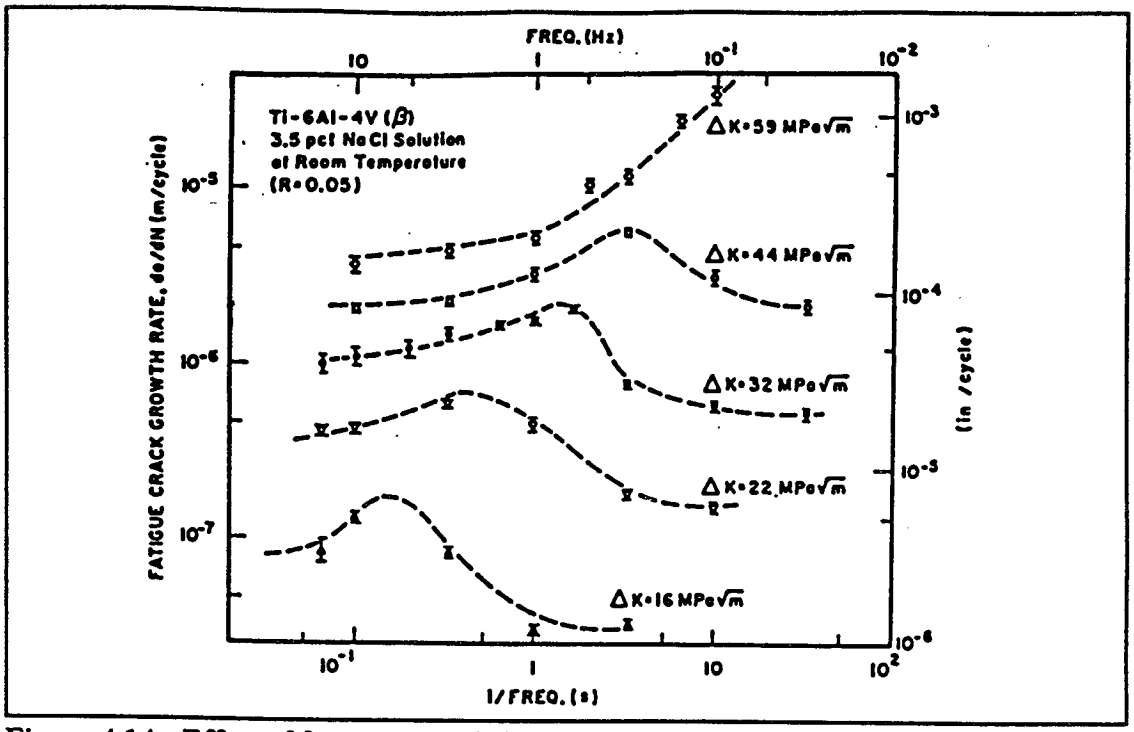

Figure 4.14: Effect of frequency on fatigue crack growth in Ti-6Al-4V (BA) in a 3.5% NaCl solution for R = 0.1. After Chiou and Wei.[44]

fatigue crack growth below K_{ISCC}. Bucci[42] attributed this difficulty to "extrapolation" of cyclic SCC below K_{ISCC}. Meyn[43] and Speidel *et. al.*[39] regard corrosion fatigue below K_{ISCC} as "true corrosion fatigue," a process distinct from cyclic SCC above K_{ISCC}. The assumption made by Meyn[43] and Speidel *et. al.*[39] implies that the threshold for cyclic SCC is the static load K_{ISCC}, an assumption not supported by the results published by Dawson and Pelloux[33], who found that ΔK_{SCC} was frequency dependent.

4.2.2 Results for Ti-6Al-4V (MA,ELI)

In order to determine the effect of frequency on EFCP in Ti-6Al-4V (MA,ELI), two separate K-gradient experiments were conducted at a R of 0.1, and frequencies of 1 and 40 Hz. The experiments were conducted in a 3.5% NaCl solution, at a fixed electrode potential of -500 mV_{SCE}. Unfortunately, the experiment for a frequency of 1 Hz was invalid since the

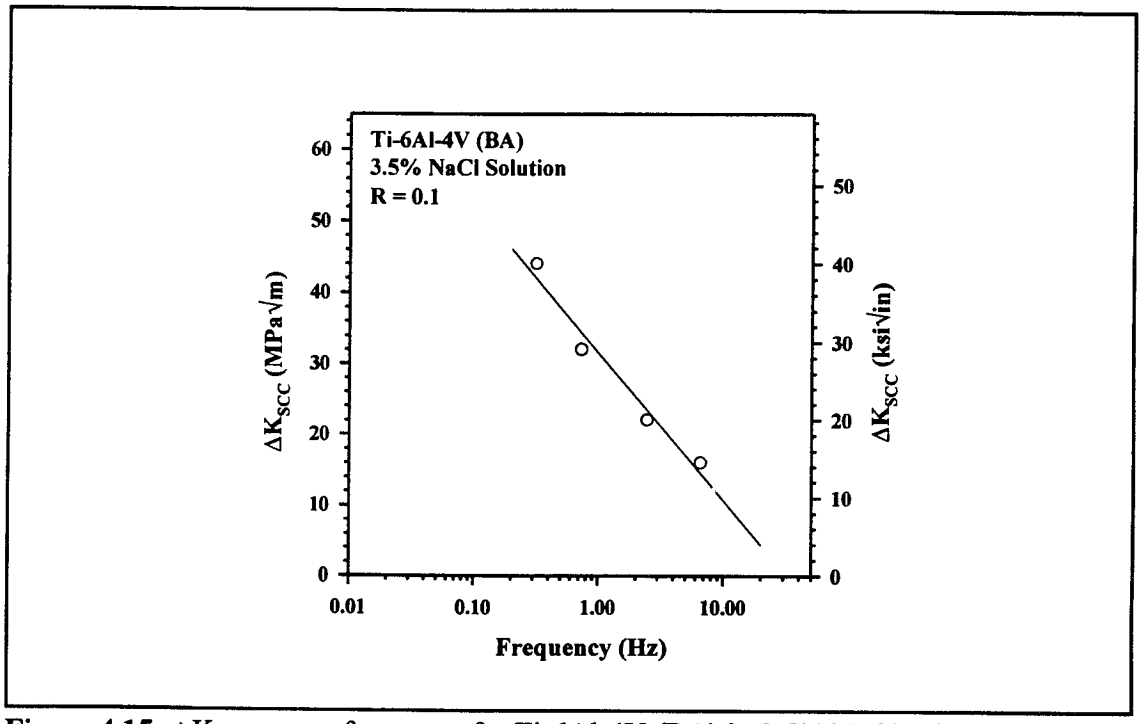

Figure 4.15: ΔK_{SCC} versus frequency for Ti-6Al-4V (BA) in 3.5% NaCl using results from Chiou and Wei.[44]

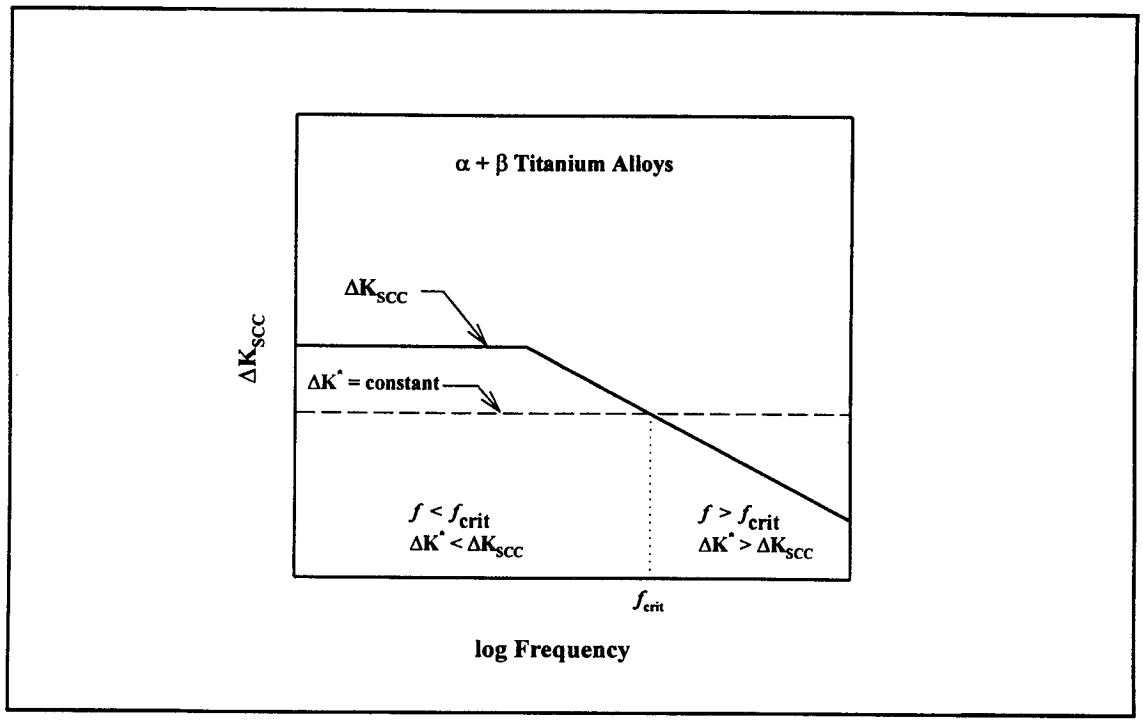

Figure 4.16: Schematic illustrating ΔK_{SCC} as a function of f, and the concept of a critical frequency, f_{crit}, where $\Delta K = \Delta K_{SCC}$.

effective modulus calculated at the end of the test varied by more than 10% from the actual value for Ti-6Al-4V.** Gangloff and Kim[9] generated data for the same heat of Ti-6Al-4V at a frequency of 5 Hz and R of 0.1 in an earlier study for a slightly different environment, a 1.0% NaCl solution at a fixed electrode potential of -500 mV_{SCE}. Figure 4.17 shows the results for the 40 Hz test conducted in aqueous chloride, as well as the results generated by Gangloff and Kim.[9] Also shown are the results of a K gradient test conducted in moist air ($R = 0.1, f = 5$ Hz) and two tests conducted at a constant ΔK of 15 MPa$\sqrt{m}$, frequency of 5 Hz, and R of 0.1. One test was conducted in moist air (●) and one in a 3.5% NaCl solution at -500 mV_{SCE}(▲).

In order to determine the precise effect of frequency on da/dN, an experiment was conducted in 3.5% NaCl (-500 mV_{SCE}). ΔK was held constant throughout the test, either at 12.5 MPa$\sqrt{m}$ or at 25 MPa$\sqrt{m}$, while R was constant at 0.1. The ΔK values were selected so that one was above and one was below K_{ISCC} of 23 MPa$\sqrt{m}$ reported for Ti-6Al-4V (MA) in 3.5% NaCl.[17] If the ELI grade Ti-6Al-4V (MA) behaves similarly to the standard grade Ti-6Al-4V (MA), the alloy should exhibit the frequency "crossover" effect. The frequency was changed after an increment of crack growth and da/dN was determined by linear regression of a versus N. For both ΔK levels, experiments were conducted for a range of frequencies between 0.03 and 10 Hz. By determining da/dN for a constant ΔK, small changes in da/dN due to frequency can be resolved. Figure 4.18 summarizes crack length as a function of cycle number for this experiment. Figure 4.19 is an expanded plot of a

---

**This 1 Hz experiment required six weeks to complete, and illustrates the long times and complexities involved in conducting a corrosion fatigue experiment.

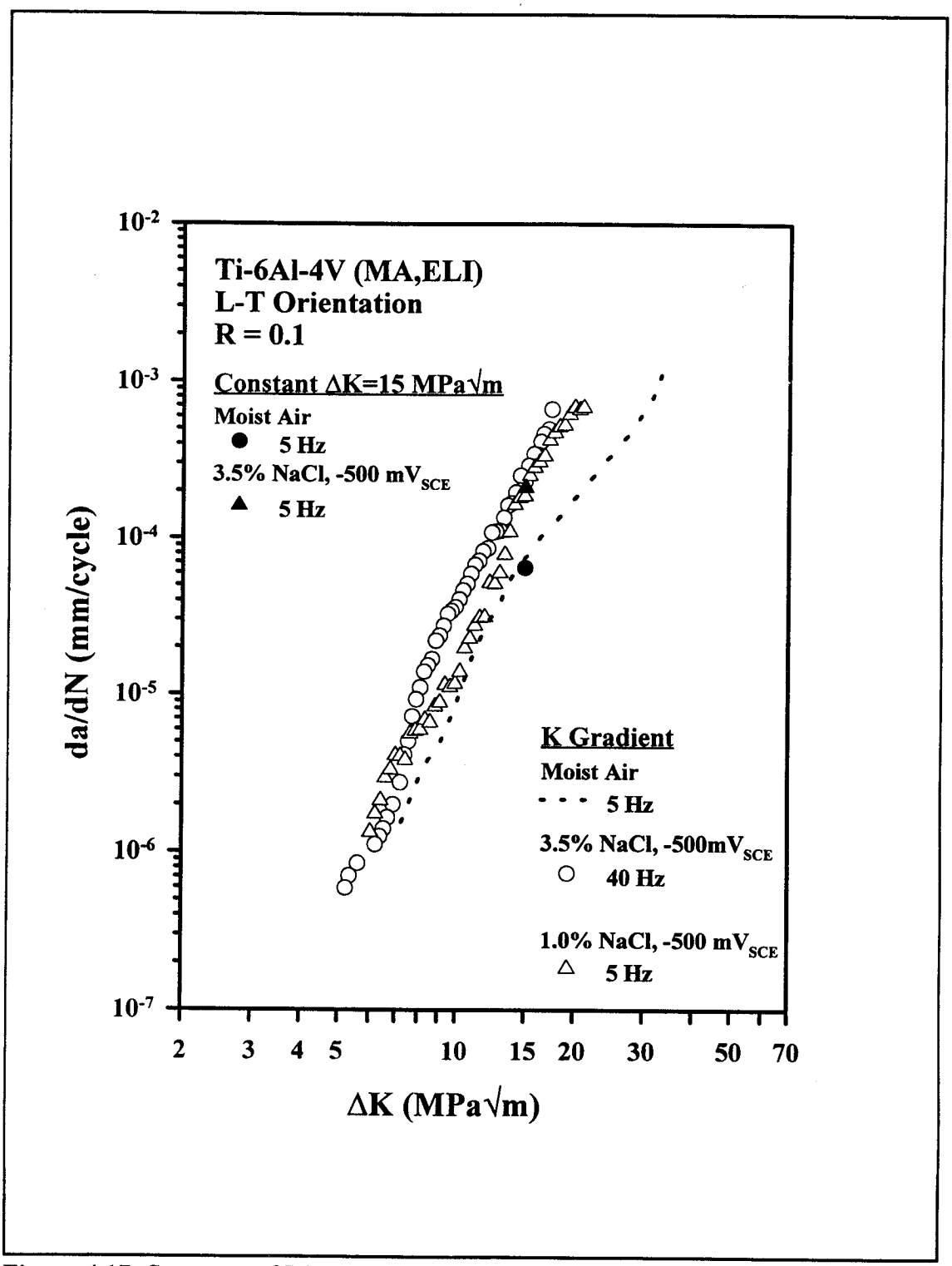

Figure 4.17: Summary of FCP results for Ti-6Al-4V (MA,ELI) in moist air and aqueous chloride solution for frequencies of 5 and 40 Hz.

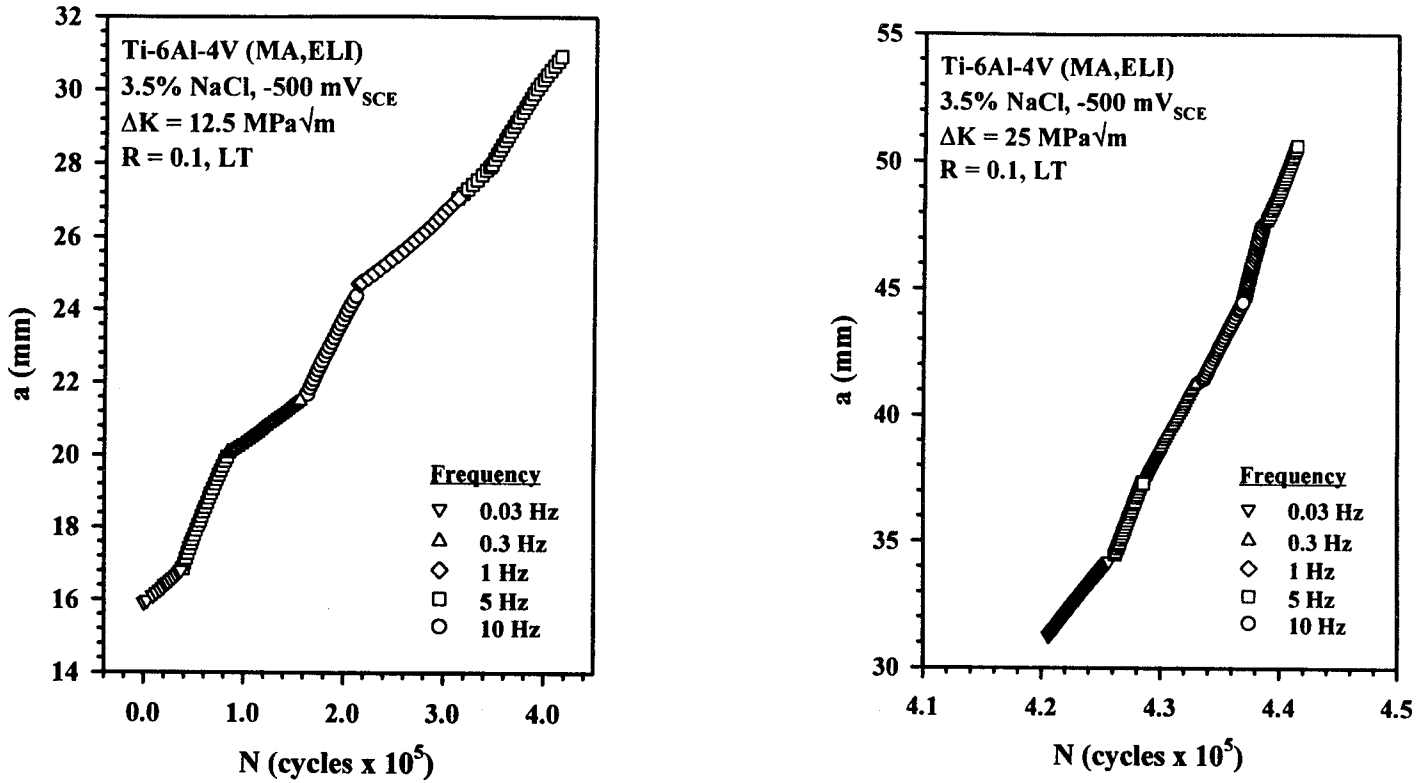

Figure 4.18: Crack length versus cycle number for Ti-6Al-4V (MA,ELI) in 3.5% NaCl at a fixed electrode potential of -500 mV_{SCE}. Frequency was varied after an increment of crack growth for a) $\Delta K = 12.5$ MPa$\sqrt{m}$ and b) $\Delta K = 25$ MPa$\sqrt{m}$ for R = 0.1.

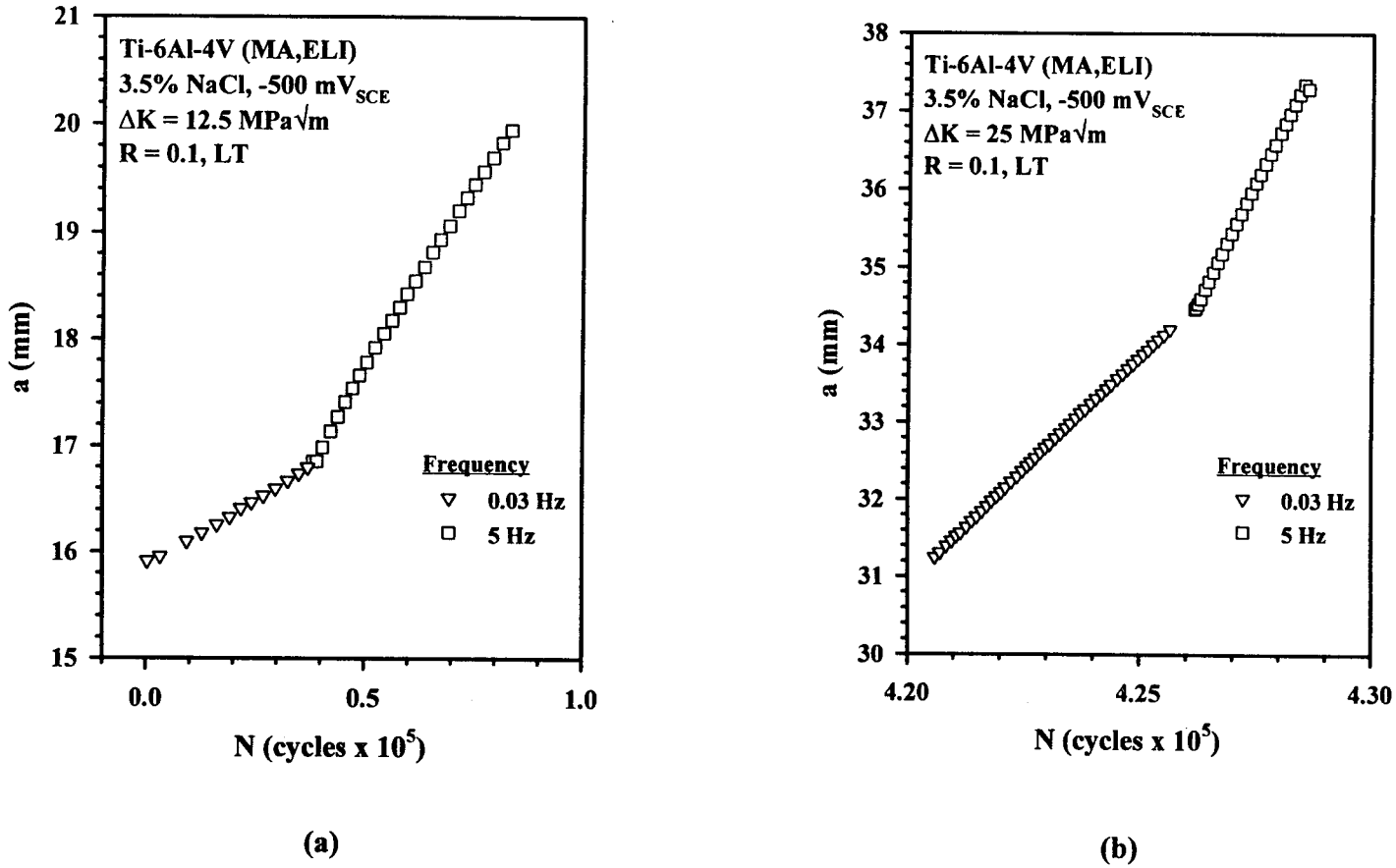

Figure 4.19: Crack length versus cycle number for Ti-6Al-4V (MA,ELI) in 3.5% NaCl at a fixed electrode potential of -500 mV_{SCE} for frequencies of 0.03 and 5 Hz, R = 0.1, and ΔK values of a) 12.5 and b) 25 MPa√m.

versus N for the first two frequencies utilized during both ΔK levels. As seen in Figures 4.18 and 4.19, crack length was generally linear with respect to N. There were also no transients observed when the frequency was varied. The data seen in Figure 4.19 for the first two frequencies where data were collected clearly show that at both ΔK values, as frequency increases da/dN increases.

Figure 4.20 is a plot of da/dN as a function of frequency for the two ΔK values, as well as data for the same constant ΔK values and a frequency of 40 Hz taken from Figure 4.17. The data point for $\Delta K = 25$ MPa$\sqrt{m}$ and a frequency of 40 Hz was extrapolated from Figure 4.17 using a Paris Equation. At the low ΔK value of 12.5 MPa$\sqrt{m}$, da/dN is proportional to $f^{0.18}$; at the high ΔK level of 25 MPa$\sqrt{m}$, da/dN is proportional to $f^{0.10}$. The slope of the line fit through the data for $\Delta K = 12.5$ MPa$\sqrt{m}$ is 0.18 ± 0.163 based on a 95% confidence interval, while the slope of the line fit through the data for $\Delta K = 25$ MPa$\sqrt{m}$ is 0.10 ± 0.174 based on a 95% confidence interval. The data for a frequency of 40 hz were not included in the calculation. The two slopes are statistically equal, and are consistent with zero slope (f independent) based on these confidence intervals. Frequency has a mild effect on da/dN for ΔK less than 25 MPa$\sqrt{m}$; the alloy does not exhibit the frequency "crossover" effect, and in fact, da/dN increases monotonically with increasing frequency. These data better define the frequency dependence of EFCP rates for $\alpha + \beta$ titanium alloys in the important low-ΔK regime, compared to the limited data in Figure 4.12.

The data seen in Figure 4.20 do not exhibit the frequency "crossover" effect. This can be attributed to the high K_{TH} value and the increased resistance to SCC. The increased resistance to SCC leads to a high value for ΔK_{SCC} that is greater than 25 MPa$\sqrt{m}$ for all of

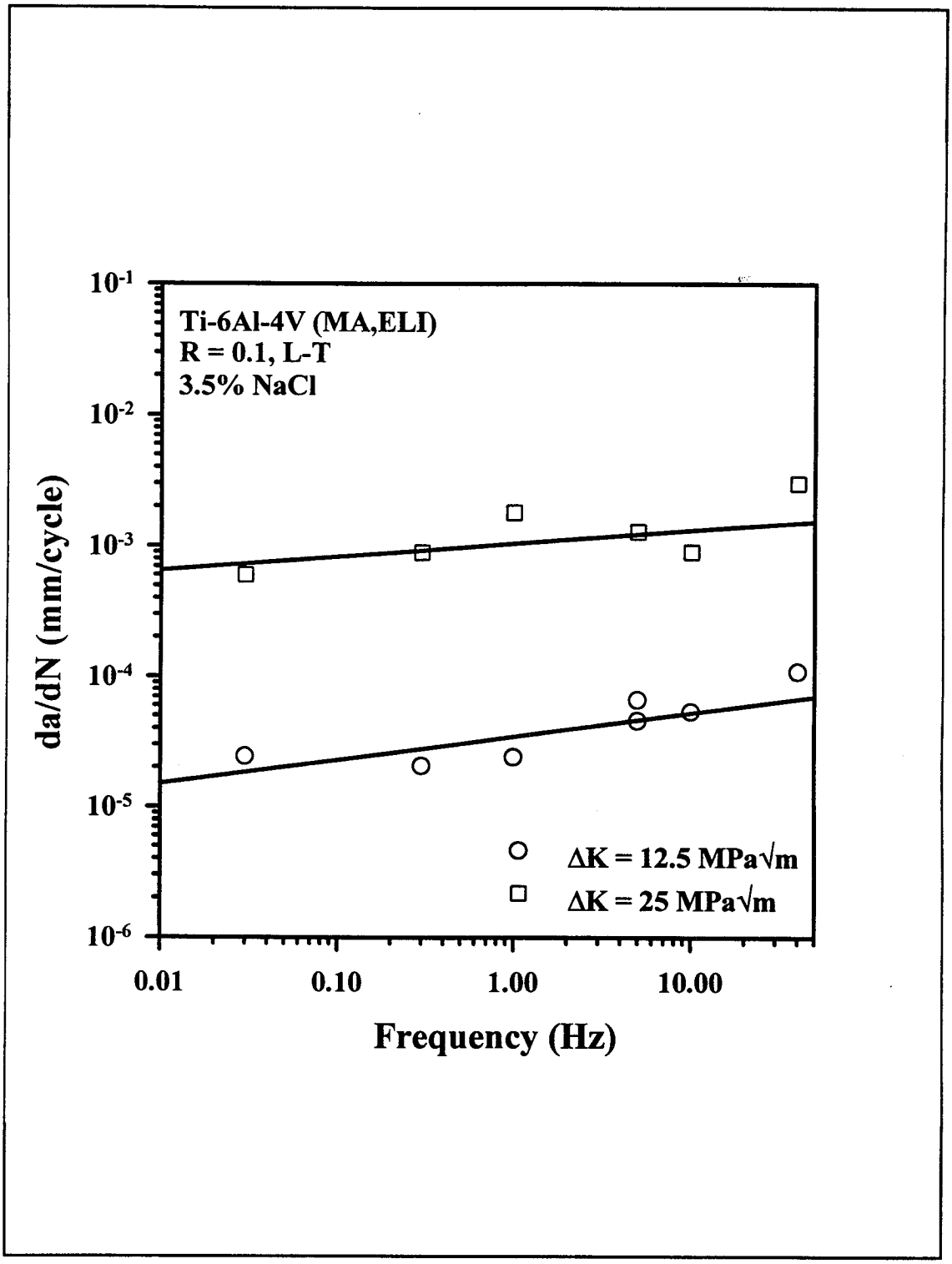

Figure 4.20: Da/dN as a function of frequency in Ti-6Al-4V (MA,ELI) in a 3.5% NaCl solution at a fixed electrode potential of -500 mV_{SCE} at R = 0.1 and ΔK values of 12.5 and 25 MPa√m.

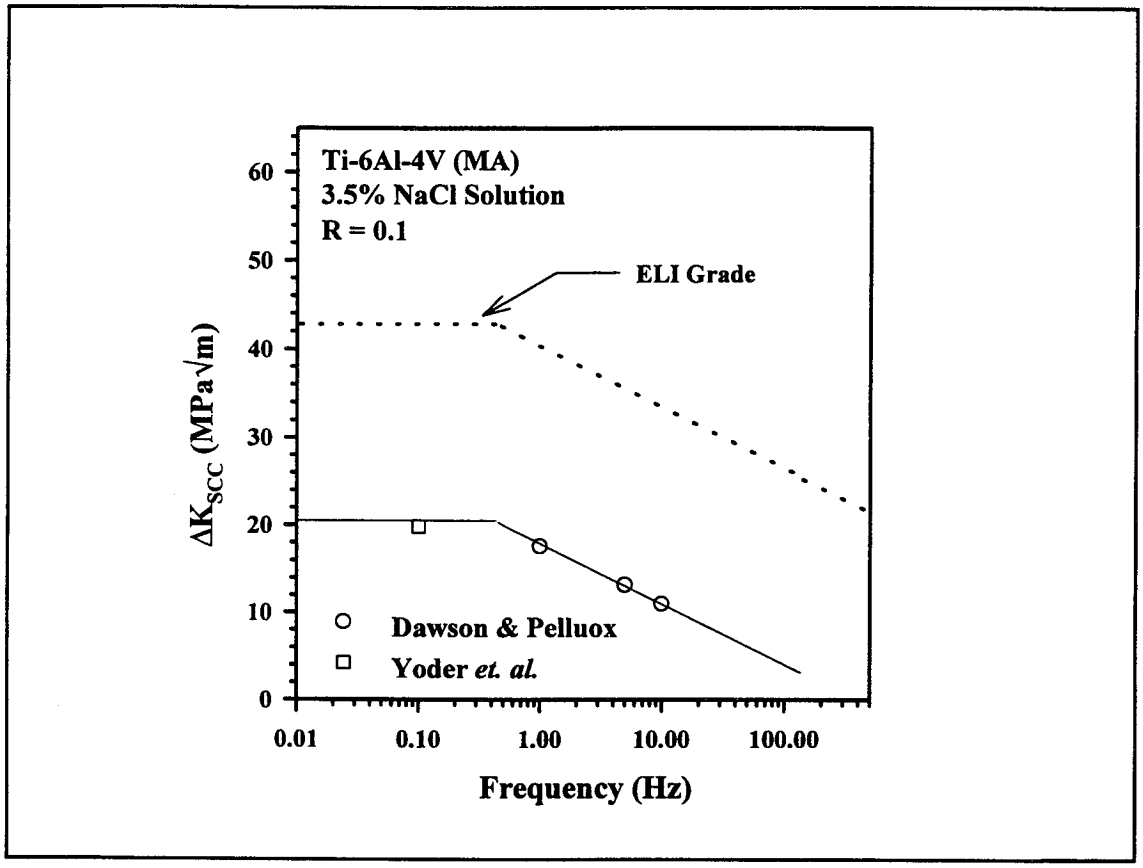

Figure 4.21: Expected trend in ΔK_{SCC} for Ti-6Al-4V (MA,ELI) in a 3.5% NaCl solution at R = 0.1.

the frequencies tested. Figure 4.21 shows ΔK_{SCC} as a function of frequency using results from Dawson and Pelloux[33] and Yoder *et. al.*[41] These results are consistent with a K_{ISCC} value of 23 MPa$\sqrt{m}$. The results for the ELI grade were scaled so that at low frequencies, ΔK_{SCC} would approach (1-R) K_{TH} for a K_{TH} value of 48 MPa$\sqrt{m}$ (From Figure 4.5) and R of 0.1. Based on these results, a ΔK of 25 MPa$\sqrt{m}$ would equal ΔK_{SCC} at a frequency of 200 Hz; five times higher than the fastest frequency where data were collected, 40 Hz. Since this frequency was never attained, cyclic SCC did not occur during the variable frequency test; ΔK values of 12.5 and 25 MPa$\sqrt{m}$ were always below ΔK_{SCC}, and da/dN was directly proportional to $f^{0.10 \text{ to } 0.18}$.

Shown in Figure 4.22 are the data for ELI grade Ti-6Al-4V (MA) (●,■) and Ti-6Al-4V (BA) (▽,△) at ΔK values of 16 and 22 MPa√m taken from the literature.[44] The data for the ELI grade were scaled, using a Paris Equation, from ΔK values of 12.5 and 25 MPa√m to those employed by the literature.[44] As seen in the Figure, the ELI grade exhibits da/dN which are higher than the beta-annealed Ti-6Al-4V in NaCl. Also, the ELI clearly does not exhibit the frequency crossover effect, while the beta-annealed alloy does.

4.3 Crack Closure Phenomena

Crack closure levels were recorded during all fatigue experiments. P_{cl}, the crack closure load, was calculated at the first deviation in slope of the load-displacement data, defined at an offset of 2% from linearity.[30] In order to determine the accuracy of the FTA software in determining closure levels, K_{cl} was measured as a function of crack length in moist air and a 3.5% NaCl solution (-500 mV_{SCE}) for a constant ΔK of 15 MPa√m, R of 0.1, and f of 5 Hz. Figure 4.23 is a plot of K_{cl} versus crack length, and Figure 4.24 is a plot of K_{cl}/K_{max} versus crack length for air and chloride. In each environment, the values of K_{cl}/K_{max} were 0.3 and essentially constant with increasing crack length. A model by Newman predicts that plasticity induced closure is important for R less than 0.4.[45] For example, the predicted value of K_{cl}/K_{max} is 0.3 for a R of 0.1, and 0.45 for a R of 0.4 for the titanium alloy used during this study. Figures 4.23 and 4.24 establish that neither abnormal surface roughness nor corrosion debris from NaCl exposure promote crack closure above the level typical of plasticity induced closure.

Figure 4.25 is a plot of K_{cl}/K_{max} versus ΔK for the fatigue test conducted in the 3.5%

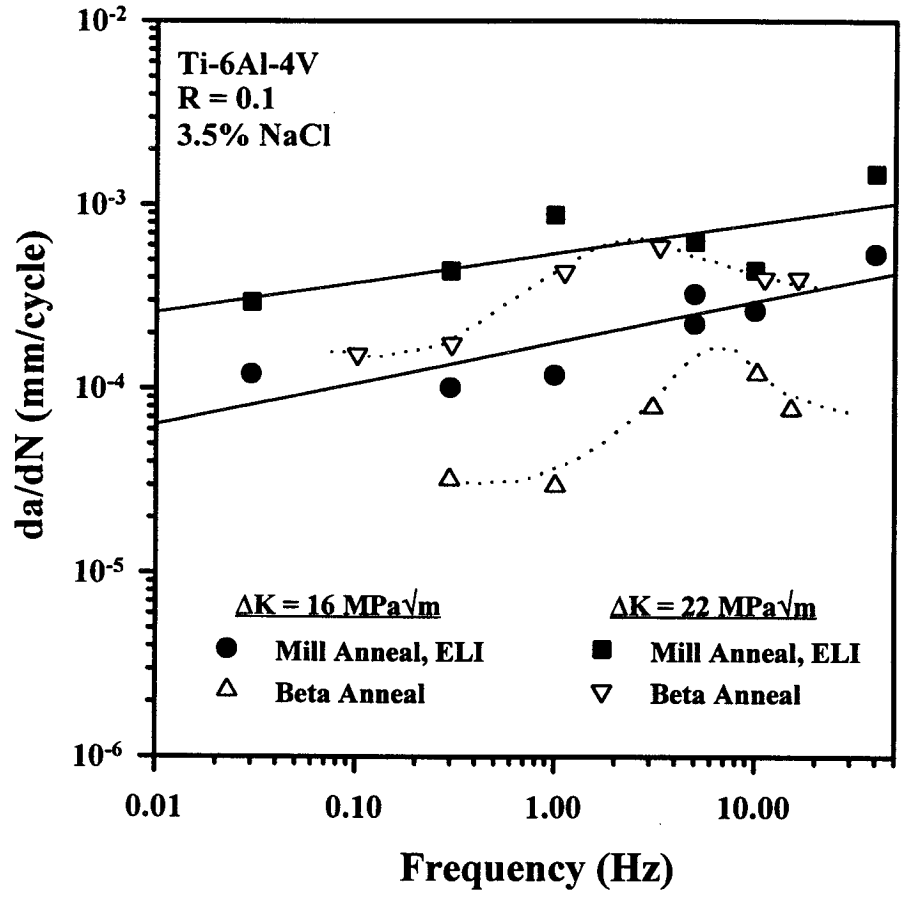

Figure 4.22: Da/dN as a function of frequency in ELI grade Ti-6Al-4V (MA) and Ti-6Al-4V (BA) in 3.5% NaCl for ΔK values of 16 and 22 MPa$\sqrt{m}$ and R = 0.1.

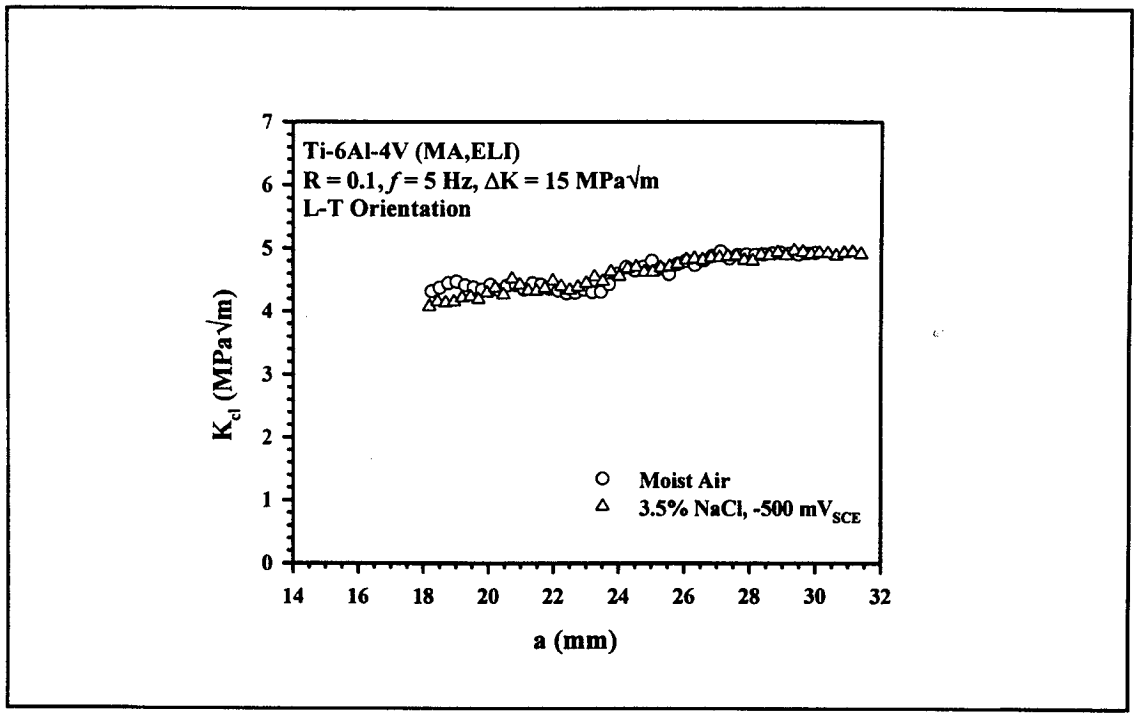

Figure 4.23: K_{cl} versus crack length for Ti-6Al-4V (MA,ELI) in moist air and a 3.5% NaCl solution for a constant ΔK of 15 MPa$\sqrt{m}$, R of 0.1, and frequency of 5 Hz.

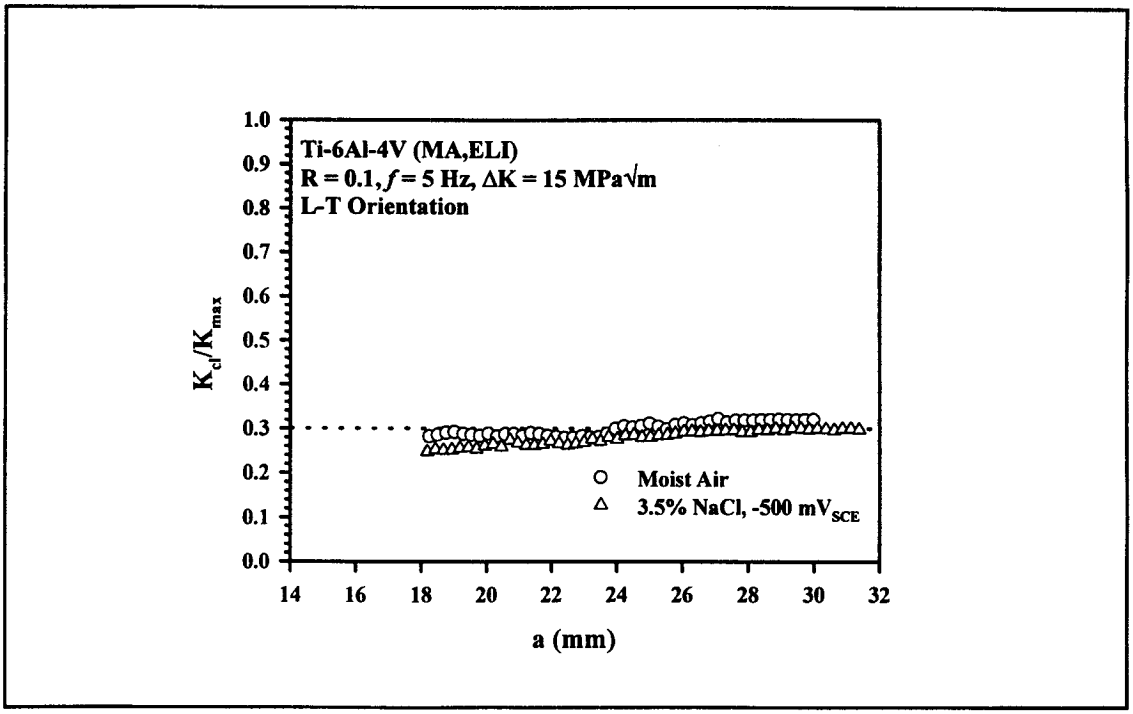

Figure 4.24: K_{cl}/K_{max} versus crack length for Ti-6Al-4V (MA,ELI) in moist air and a 3.5% NaCl solution for a constant ΔK of 15 MPa$\sqrt{m}$, R of 0.1, and frequency of 5 Hz.

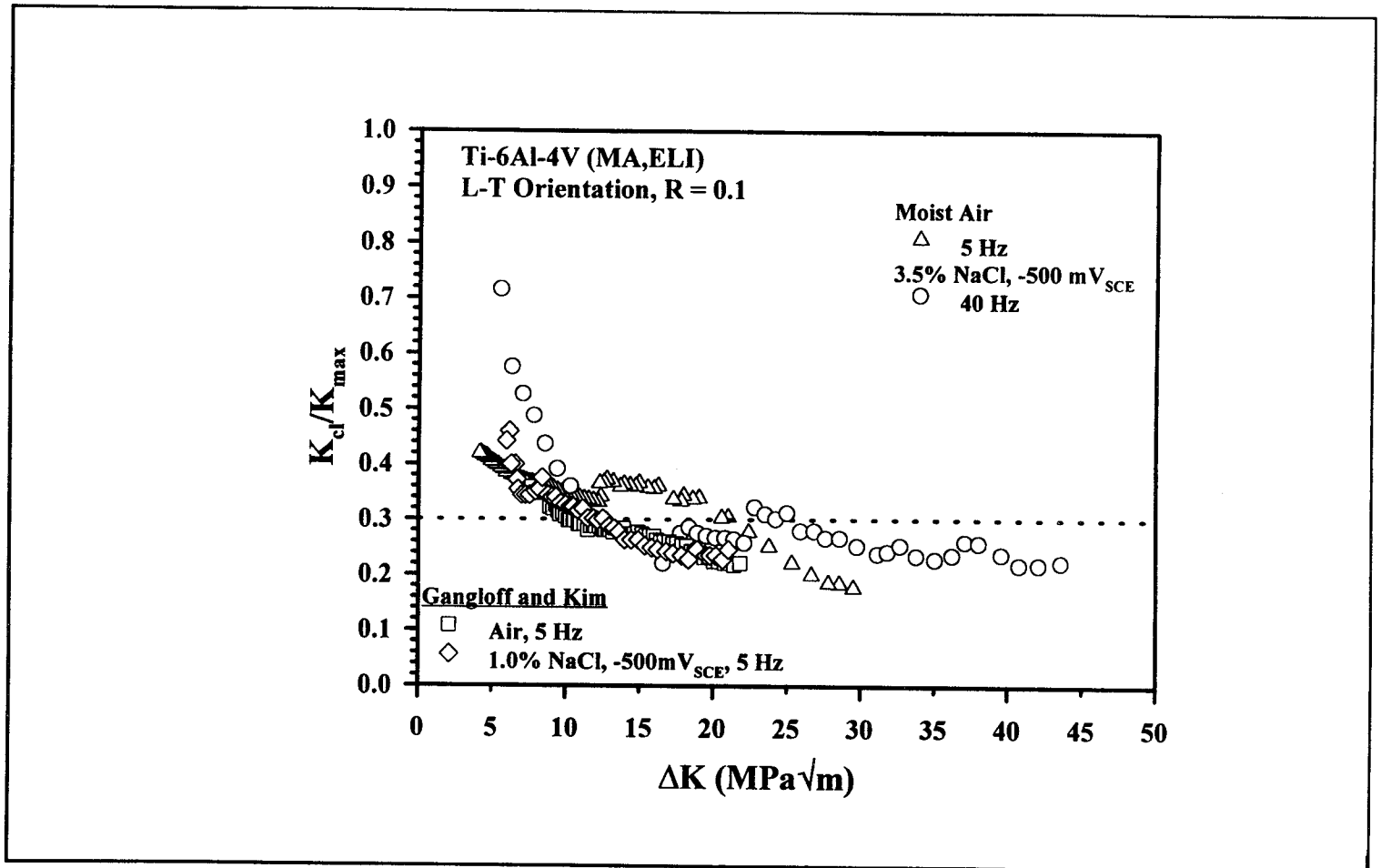

Figure 4.25 K_{cl}/K_{max} versus ΔK for Ti-6Al-4V (MA,ELI) in moist air, a 3.5% NaCl solution (-500 mV_{SCE}), and a 1.0% NaCl solution (-500 mV_{SCE}) for various frequencies and a R of 0.1. The dashed line represents the value expected using the model by Newman[45] for plasticity induced closure.

NaCl solution at a fixed electrode potential of -500 mV_{SCE} for a frequency of 40 Hz, as well as the test conducted in moist air at a frequency of 5 Hz. Also shown in the figure are the results reported by Gangloff and Kim[9] for Ti-6Al-4V (MA,ELI) in moist air and 1.0% NaCl (-500 mV_{SCE}) for a frequency of 5 Hz. For ΔK values between 10 MPa$\sqrt{m}$ and 25 MPa$\sqrt{m}$, the values of K_{cl}/K_{max} center around 0.3 for all of the experiments. These levels are consistent with plasticity induced closure, as predicted by Newman.[45] The model does not, however, explain the rise in closure levels at ΔK levels below 10 MPa$\sqrt{m}$, particularly for the NaCl case. Notice that the difference between the replicate tests in moist air (Δ and $\square$) is larger than the effect of environment.

Closure levels were recorded during the Ti-6Al-4V (MA,ELI) EFCP experiment conducted in aqueous chloride where ΔK was held constant and frequency was varied. Figure 4.26 is a plot of K_{cl}/K_{max} versus crack length for this variable frequency test. As shown in the figure, frequency and test time have little effect on closure levels at both ΔK levels. For a ΔK level of 25 MPa$\sqrt{m}$, K_{cl}/K_{max} was 0.3 (Figure 4.26b) for all frequencies , with the possible exception of the initial low frequency segment. This level is in excellent agreement with the data in Figure 4.24 and is consistent with plasticity induced closure, as predicted by Newman.[45] For a ΔK level of 12.5 MPa$\sqrt{m}$, K_{cl}/K_{max} was 0.38 (Figure 4.26a), slightly higher than that expected for plasticity induced closure. The high levels of K_{cl}/K_{max} seen at the lower ΔK levels in Figure 4.25 and Figure 4.26a could be due to roughness or oxide induced closure. Both of these closure phenomena are time dependent, and important in the near threshold regime where there is a small crack tip opening displacement. The data in Figure 4.20, however, suggest that time does not affect closure levels.

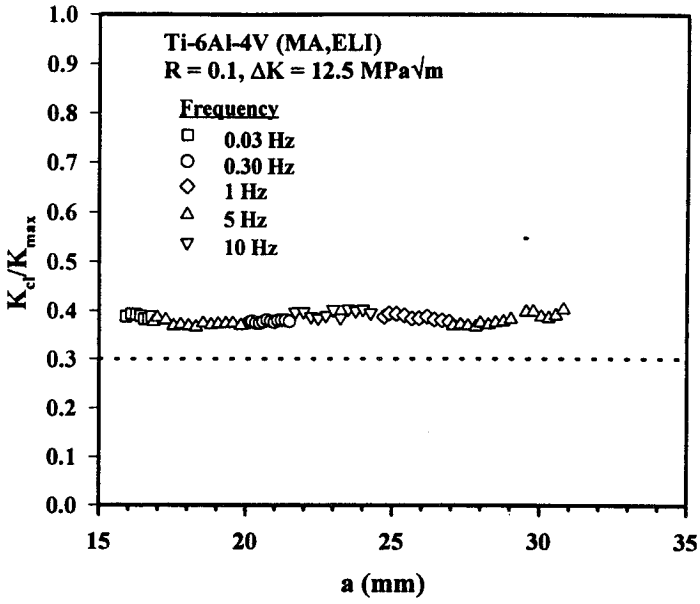

(a)

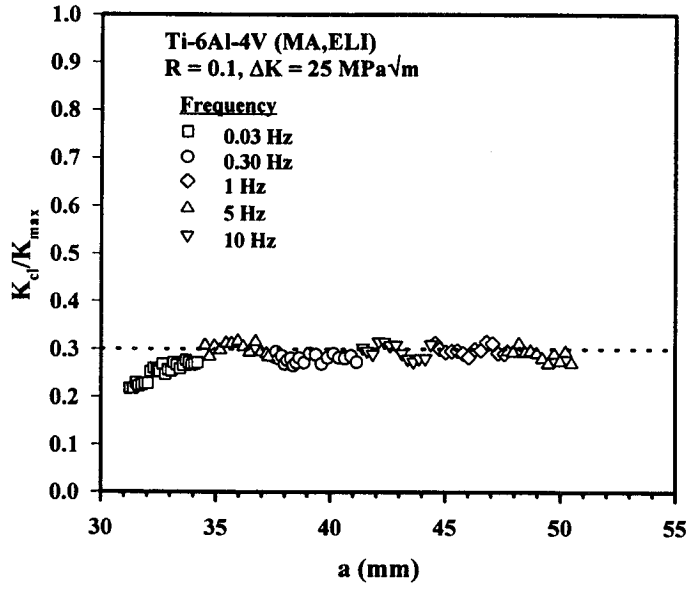

(b)

Figure 4.26: K_{cl}/K_{max} for Ti-6Al-4V (MA,ELI) in 3.5% NaCl at a fixed electrode potential of -500 mV_{SCE} for variable frequency, R of 0.1, and a) ΔK = 12.5 MPa$\sqrt{m}$ and b) ΔK = 25 MPa$\sqrt{m}$.

Chapter 5: Application of Computer Models

This chapter discusses the applications of the linear superposition and the interpolative models to environmental FCP data for standard and ELI grade Ti-6Al-4V (MA). Specific results are presented coupled with a discussion of the capabilities of each model.

5.1 Linear Superposition Model

The Wei and Landes linear superposition model was applied to Ti-6Al-4V (MA) in a 3.5% NaCl solution, using data from Dawson and Pelloux,[33] and the computer program UVAFAS.EXE. The model was not applied to ELI grade Ti-6Al-4V due to the high K_{TH} and near f independence of da/dN exhibited by this alloy. In order to apply the linear superposition model, inert environment mechanical fatigue data and SCC velocity data were required. Fatigue data for Ti-6Al-4V (MA) in dehumidified and purified argon served as the inert environment mechanical fatigue component,[46] while $(da/dt)_{environment}$ data for Ti-6Al-4V (MA) in a 0.6M KCl (4.3% KCl) solution at -500 mV versus a standard hydrogen electrode (SHE) served as the SCC velocity data.[39] The crack velocity data are for a different environment than the 3.5% NaCl environment utilized by Dawson and Pelloux,[33] but should be adequate since, when dealing with SCC of $\alpha + \beta$ titanium alloys in aqueous solutions, the anion (Cl^-) is dominantly detrimental, while the cation (K^+ or Na^+) does not have a large effect. According to Blackburn *et. al.*, cations less noble than titanium, such as Na^+ and K^+, have no effect on SCC behavior.[47]

Figure 5.1 summarizes the fatigue data for Ti-6Al-4V (MA) in a variety of environments. The data for dehumidified and TSP purified argon (o) were fit to the Forman

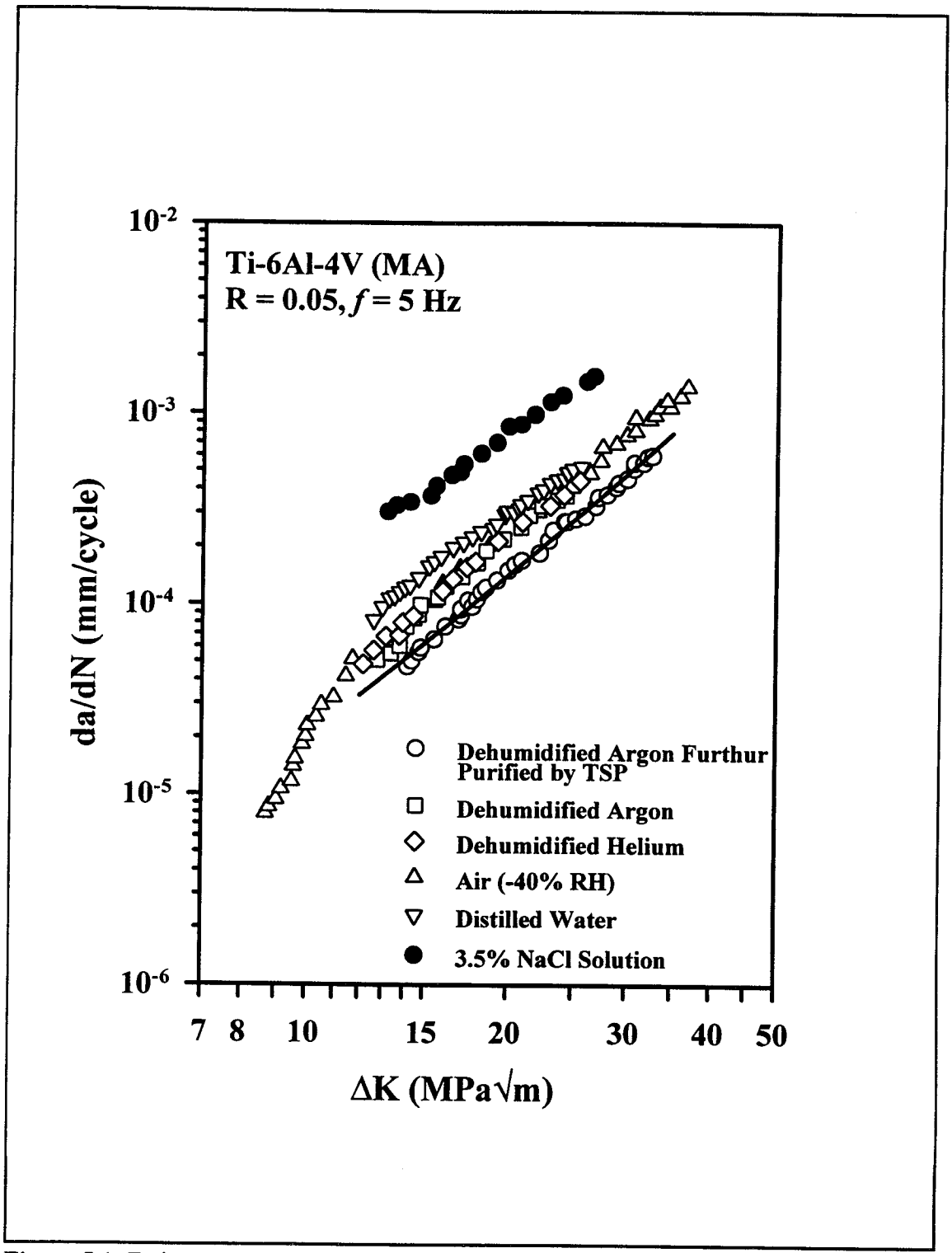

Figure 5.1: Fatigue crack growth behavior of Ti-6Al-4V (MA) in various environments for a frequency of 5 Hz and R of 0.05. After Shih and Wei.[46]

Equation with closure (Equation 2.2); the parameter α was 2.5, while S_{max}/σ_o was 0.3. The constant p was entered as 0.25, while q was 0.75, based on NASA FLAGRO materials files. ΔK_{th} was calculated using an expression determined by Speidel[48] for a wide variety of materials in vacuum, including Ti-6Al-4V. The equation is:

$$\Delta K_{th} = 2.7 \; X \; 10^{-5} \; E \qquad \textbf{(5.1)}$$

where E is the elastic modulus given in MPa, and ΔK_{th} is in MPa$\sqrt{m}$. The elastic modulus was taken as 110 MPa[33], corresponding to a ΔK_{th} of 3.0 MPa$\sqrt{m}$. K_C was entered as 78 MPa$\sqrt{m}$ based on results presented in Section 4.1.1. The constants C and n were fit, C was determined to be 9.9×10^{-8}, while n was determined as 2.6. The coefficient of determination was 0.9941. The fitted equation is shown in Figure 5.1 as a solid line. Da/dN was in units of mm/cycle, while ΔK was in units of MPa$\sqrt{m}$.

Figure 5.2 shows the stress corrosion crack velocity data input to the superposition model. The data were fit to a Sigmoidal Equation of the form:

$$\frac{da}{dt} = e^{B} \left(\frac{K}{K_{TH}} \right)^{P} \left[\ln \left(\frac{K}{K_{TH}} \right) \right]^{Q} \left[\ln \left(\frac{K_C}{K} \right) \right]^{D} \qquad \textbf{(5.2)}$$

where K_{TH} is the threshold for stress corrosion cracking and K_C is the fracture toughness. K_{TH} was entered as 23 MPa$\sqrt{m}$[33], while K_C was 78 MPa$\sqrt{m}$. For the -500 mV_{SHE} (-259 mV_{SCE}) case, B was 1.068, P was -8.738, Q was 1.482, and D was determined to be -4.735. The coefficient of determination of the fitted equation, shown in Figure 6.2 as a solid line, was 0.9919. Da/dt was in units on mm/cycle, while K was in units of MPa$\sqrt{m}$.

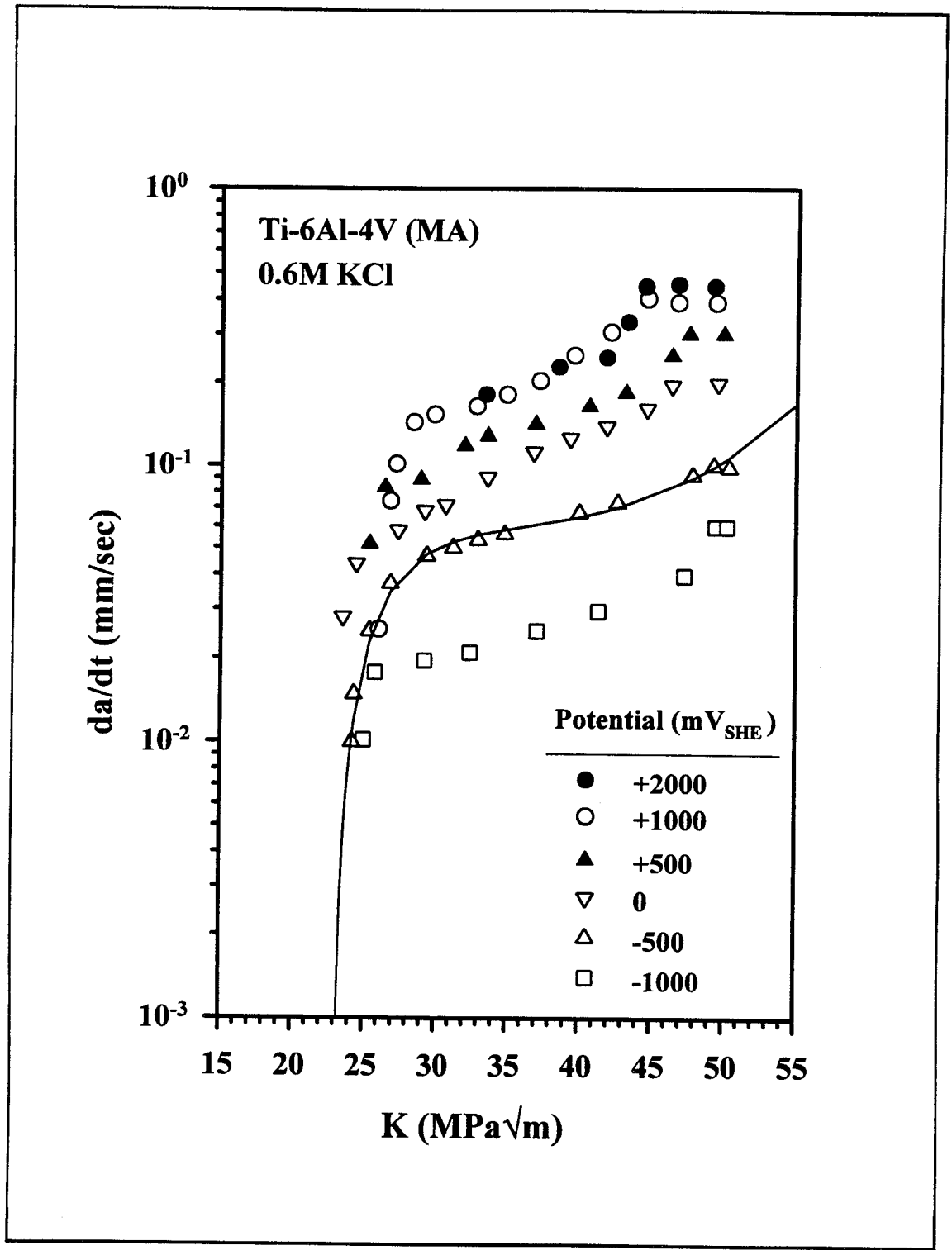

Figure 5.2: Stress corrosion crack velocity data for Ti-6Al-4V (MA) in a 0.6M KCl solution as a function of electrode potential. After Speidel *et. al.*[40]

EFCP rates were predicted using the linear superposition model in UVAFAS.EXE for Ti-6Al-4V in a 3.5% NaCl solution (at a free corrosion potential), R of 0.1, and frequencies of 1, 5, and 10 Hz. Figure 5.3 compares predictions with experimental EFCP rate data taken from a study by Dawson and Pelloux.[33] The SCC data used were for -259 mV_{SCE}; this is similar to the free corrosion potential (-239 mV_{SCE}) measured for ELI Ti-6Al-4V during the CMOD experiment discussed in Chapter 4, and is assumed relevant to the Dawson and Pelloux experiments with standard grade Ti-6Al-4V.

As seen in Figure 5.3, the linear superposition model reasonably predicts the effect of frequency for ΔK values where K_{max} is above K_{ISCC} (23 MPa$\sqrt{m}$). Below this threshold, linear superposition substantially underpredicts EFCP rates. The partial accuracy of the model can be attributed to the frequency "crossover" effect and "cyclic" SCC. Above the ΔK value where K_{max} is equal to K_{ISCC}, ΔK is always above ΔK_{SCC}. Above ΔK_{SCC}, da/dN increases as frequency decreases, a result reasonably predicted by linear superposition. Below the ΔK values where K_{max} is equal to K_{ISCC}, da/dN decreases with decreasing frequency; this trend is opposite that expected by linear superposition. Bucci[42] applied the superposition model to Ti-8Al-1Mo-1V (MA), in 3.5% NaCl and found similar results.

The linear superposition model was utilized to predict the effect of frequency on da/dN for Ti-6Al-4V (MA)/NaCl at a constant ΔK of 25 MPa$\sqrt{m}$ and R of 0.1. The same inert environment mechanical fatigue data and SCC velocity data for Ti-6Al-4V were utilized, as well as the same equation constants for the Forman and Sigmoidal Equations. Da/dN was predicted over a range of frequencies and compared to the data from Dawson and Pelloux.[33] Figure 5.4 is a plot of linear superposition predictions compared to experimental

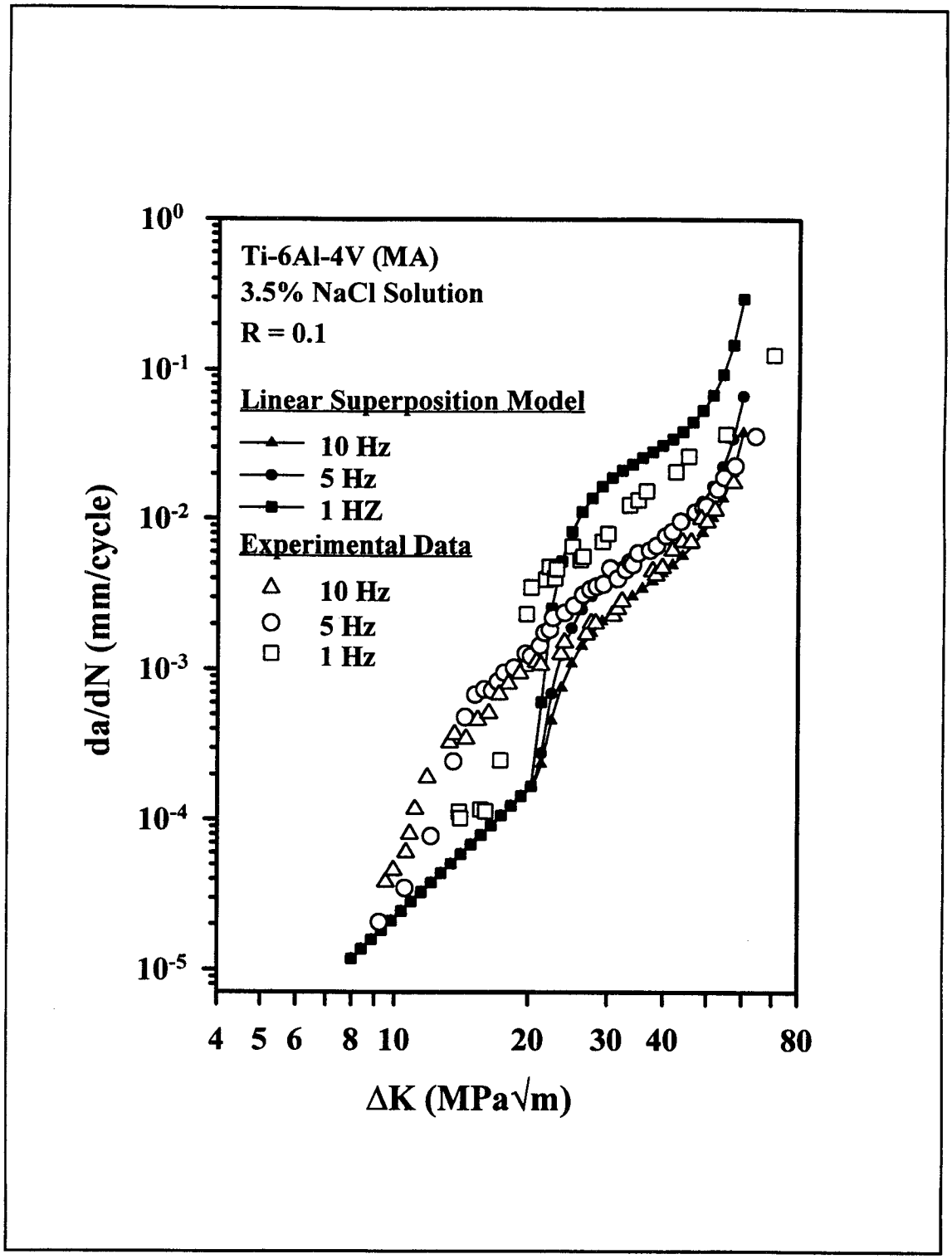

Figure 5.3: Linear superposition predictions for Ti-6Al-4V (MA,ELI) in a 3.5% NaCl solution, R of 0.1, and frequencies of 1, 5, and 10 Hz.

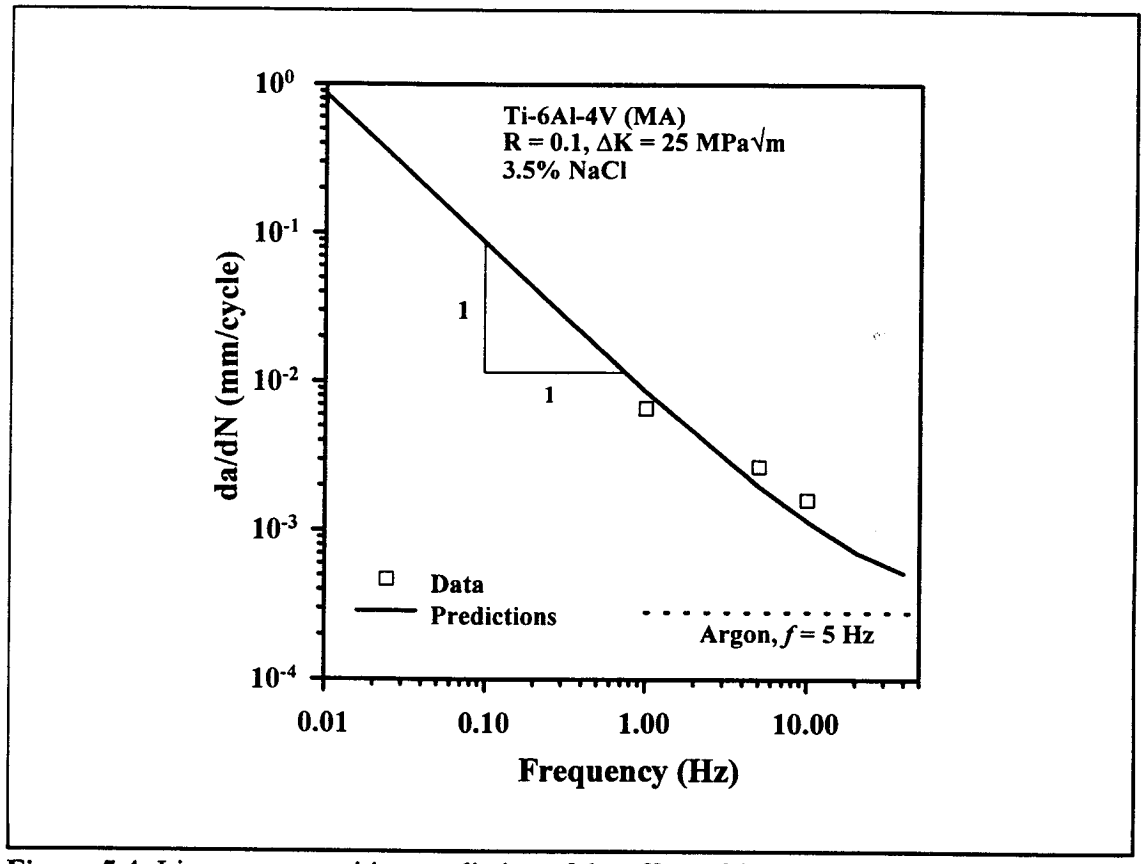

Figure 5.4: Linear superposition prediction of the effect of frequency on FCP in Ti-6Al-4V (MA) in a 3.5% NaCl solution for R = 0.1 and $\Delta K = 25$ MPa$\sqrt{m}$.

data, which shows that the model is accurate for frequencies greater than 1 Hz. The Dawson and Pelloux study did not, however, consider the important case of EFCP at lower frequencies, nor the important effects of electrode potential. Linear superposition is, of course, not accurate for the ELI grade of Ti-6Al-4V. The interpolative model is tested next.

5.2 Interpolative Model

5.2.1 Standard Grade Ti-6Al-4V (MA)

The interpolative model implemented in UVAFAS was tested using data from Dawson and Pelloux for Ti-6Al-4V(MA) in a 3.5% NaCl solution[33]; conditions were

constant except for f, thus all of the equation parameters were expressed as a function of frequency. To test the model, data for frequencies of 1 and 10 Hz were fit to the Forman Equation with and without closure, the SINH Equation, and the Sigmoidal Equation.

Since two data sets were used, the equation parameters were related to two loading variables, frequency and either the hold time or the stress ratio, even though τ equalled zero and R was constant. Using interpolation constants determined from these two relationships, equation parameters were interpolated to describe EFCP rates at a frequency of 5 Hz and a range of ΔK values. In all of the tests, K_C was entered as 135 MPa$\sqrt{m}$. The values of ΔK_{th} were 12.0 MPa$\sqrt{m}$ for 1 Hz and 8.0 MPa$\sqrt{m}$ for 10 Hz; ΔK_{th} was interpolated for 5 Hz. These values for K_C and ΔK_{th} were optimized using the cubic approximations (Section 2.2.3) applied to NaCl FCP rate data. The parameter α was 2.5, while S_{max}/σ_o was 0.3. For all of the data discussed in this section, the units for da/dN are mm/cycle, while the units for ΔK are MPa$\sqrt{m}$. The equation parameters determined by the model can only be used with these units.

All of the equation parameters were interpolated using the logarithmic form of the frequency dependence. When the interpolative model was originally developed using the data from Dawson and Pelloux[33], this frequency dependence was the only form available. The form was selected because it was known that "cyclic" stress corrosion cracking occurs in standard grade Ti-6Al-4V, and that da/dN increases as frequency decreases for ΔK values above Δ_{KSCC}. The logarithmic form of the frequency dependence predicts this trend in da/dN. For ΔK values below ΔK_{SCC}, da/dN decreases as frequency decreases; this trend is opposite that expected using the logarithmic frequency dependence, thus the model will overpredict

da/dN rates as frequency decreases, and the model will be conservative. This is assuming that the coefficients in the interpolation functions are positive. A negative coefficient would yield the opposite trend.

The values of ΔK_{th} were optimized using the cubic approximation. Note that the data in Figure 4.12, however, do not extend to low growth rates. Typically, ΔK_{th} is defined for growth rates less than 10^{-7} mm/sec; the Dawson and Pelloux[33] data only extend to 10^{-5} mm/sec. This is two orders of magnitude faster than that associated with threshold behavior, thus the ΔK_{th} values calculated by the cubic approximation are not accurate. According to the cubic approximation, ΔK_{th} is being reached at crack growth rates between 10^{-5} and 10^{-4} mm/sec, which is incorrect. This inaccuracy in the values of ΔK_{th} means that the model cannot be used to interpolate trends in fatigue behavior in the near threshold regime, the model can only be used to predict trends in fatigue behavior for ΔK values within the establishing data base. The current analysis was limited in this regard. Input ΔK_{th} parameters, are in fact, more likely to equal ΔK_{SCC}. This problem is corrected if more data in the near threshold regime are fit to the cubic approximation.

The first equation tested was the Forman Equation with closure. Three cases were studied, (1) fitting C and n, with p entered as 0.25 and q as 0.75, (2) fitting C and n, with p and q entered as 2.0, and (3) fitting C, n, p, and q. The values of p and q of 0.25 and 0.75 were taken from the NASA FLAGRO material files for Ti-6Al-4V (MA). The case of p = q = 2.0 was recommended by Newman[49] for use when values are not definable from wide range da/dN-ΔK data. The values determined for the equation parameters, as well as the resulting interpolation functions are given in Appendix B for all of the crack growth rate

equations used to model the Dawson and Pelloux data. Results are shown graphically in Figure 5.5 , Figure 5.6, and Figure 5.7.

The Forman Equation without closure was tested. Again, three cases were studied, (1) fitting C and n with p entered as 0.25 and q as 0.75, (2) fitting C and n with p and q entered as 2.0, and (3) fitting C, n, p, and q. In all three cases, m was 1.0. Results are shown in Figure 5.8 , Figure 5.9, and in Figure 5.10.

The Hyperbolic Sine Equation was tested fitting the parameters C_2, C_3, and C_4 while the parameter C_1 was 0.5. The case of $C_1 = 0.5$ was recommended by Haritos.[21] Results are shown in Figure 5.11. Finally, the Sigmoidal Equation was tested, yielding the results seen in Figure 5.12.

In order to determine the accuracy of each model, the coefficient of determination (r^2) was calculated for each of the interpolated equations for $f = 5$ Hz shown in Figures 5.5 through 5.12. These values are summarized in Table 5.1. The Forman Equation (with and without closure) yielded the best results when fitting all four parameters; results were slightly less accurate when fitting C and n with $p = q = 2.0$. The inclusion of crack closure terms did not improve the fits. The least accurate results occurred when using the Forman Equation with C and n fit, $p = 0.25$, and $q = 0.75$. This is expected since these values of p and q were determined using data for moist air.[6] The Sigmoidal Equation and the Hyperbolic Sine Equation both displayed accuracy similar to the Forman Equation with C, n, p, and q fit.

As seen by the results presented in Figures 5.5 through 5.12 and Table 5.1, the logarithmic form of the frequency dependence was able to accurately interpolate trends in

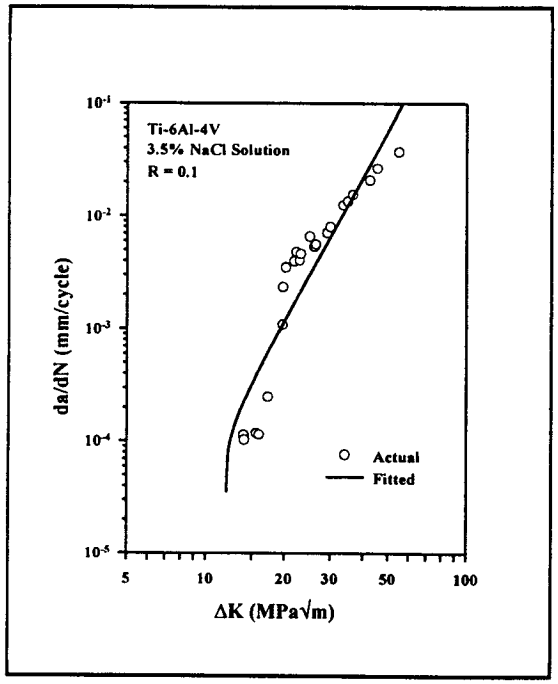

a) Actual and fitted data for $f = 1$ Hz.

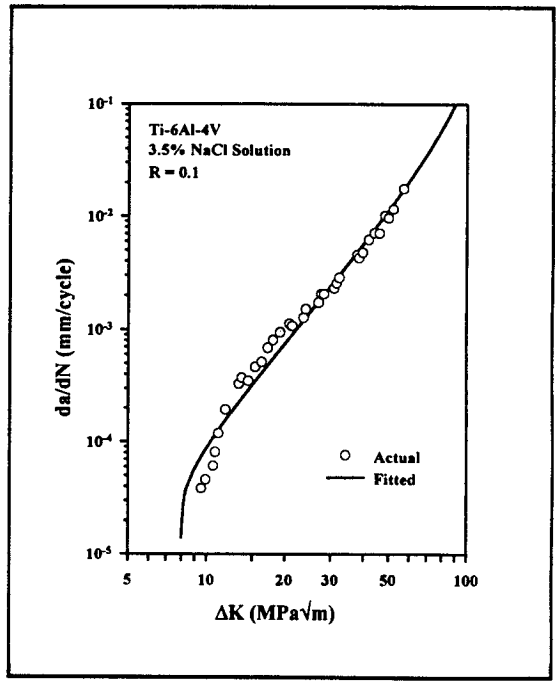

b) Actual and fitted data for $f = 10$ Hz.

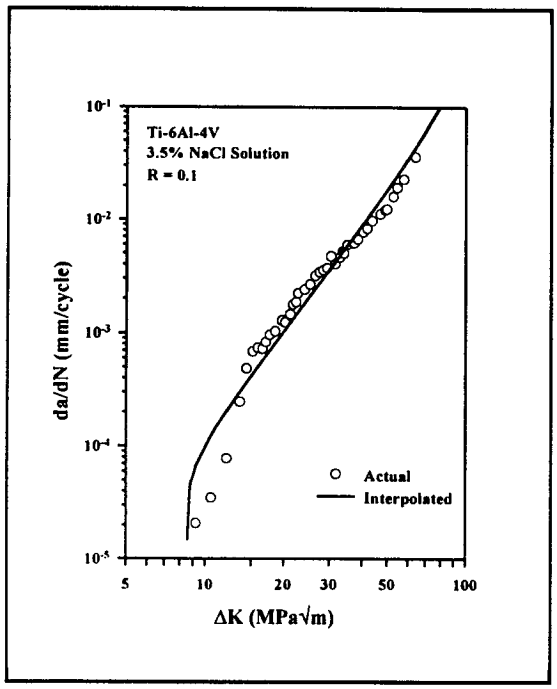

c) Actual and interpolated data for $f = 5$ Hz.

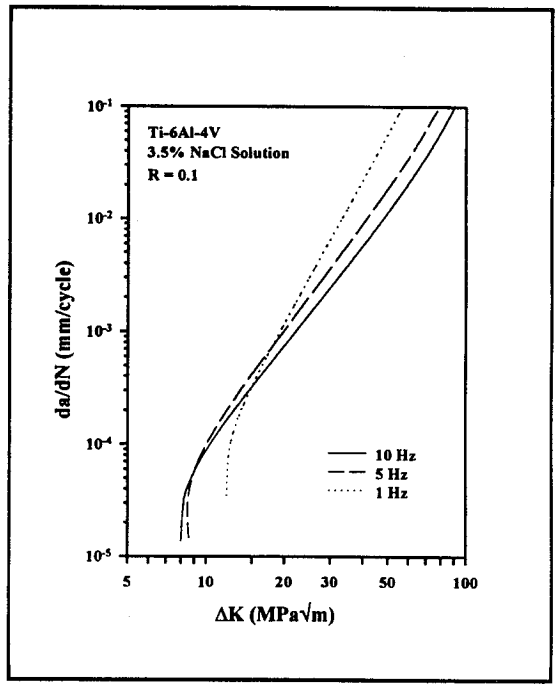

d) Effect of frequency on da/dN.

Figure 5.5: Interpolation results for Ti-6Al-4V (MA) in a 3.5% NaCl solution and R of 0.1 using the Forman Equation with closure (C, n fit, p = 0.25, q = 0.75).

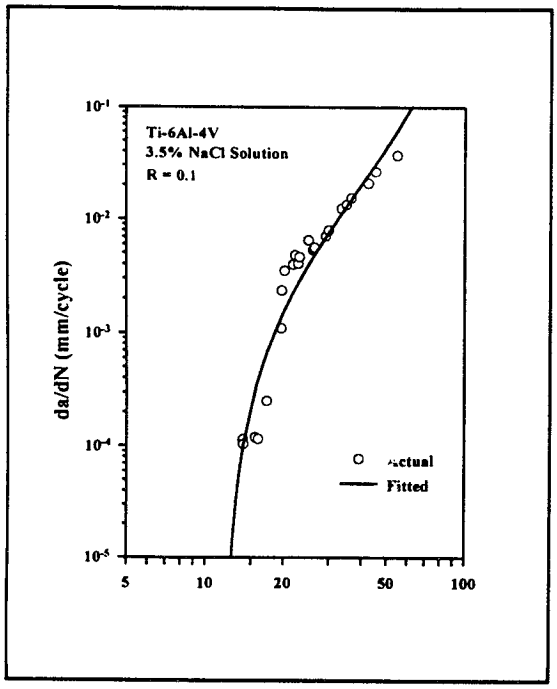

a) Actual and fitted data for $f = 1$ Hz.

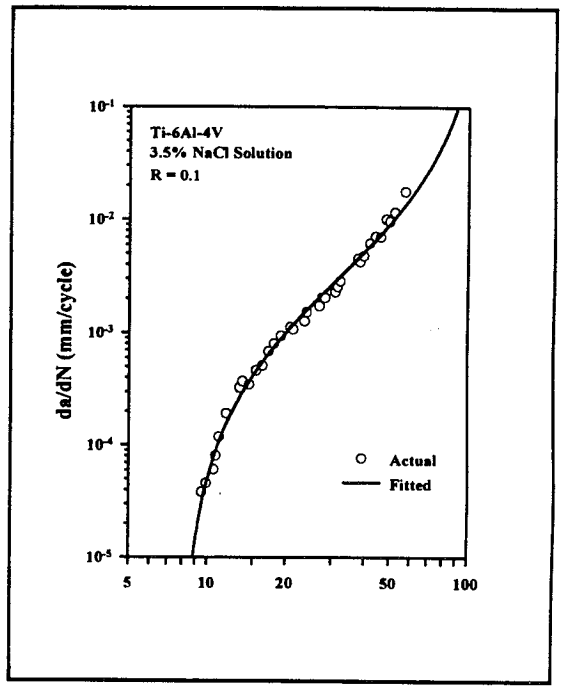

b) Actual and fitted data for $f = 10$ Hz.

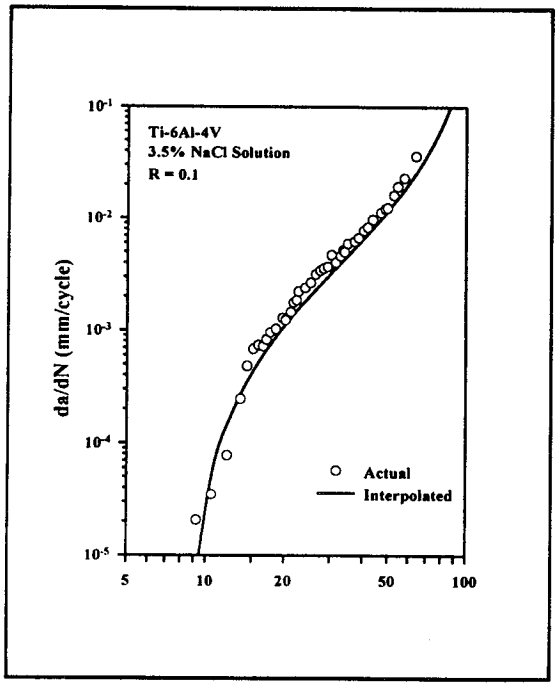

c) Actual and interpolated data for $f = 5$ Hz.

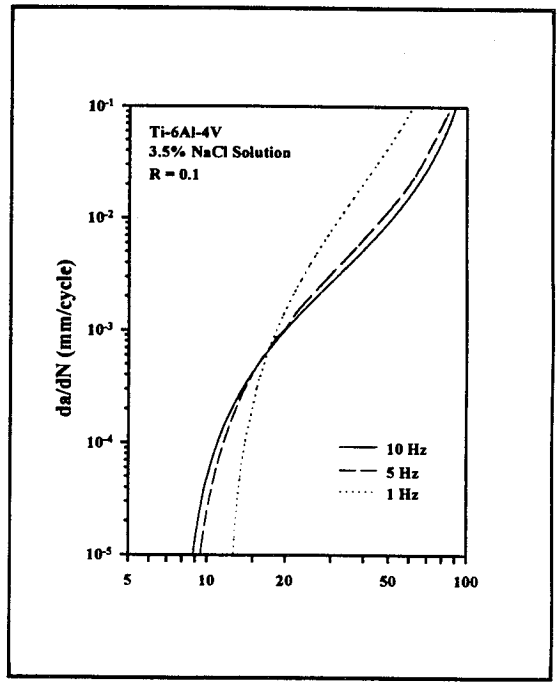

d) Effect of frequency on da/dN.

Figure 5.6: Interpolation results for Ti-6Al-4V (MA) in a 3.5% NaCl solution and R of 0.1 using the Forman Equation with closure (C, n fit, p = q = 2.0).

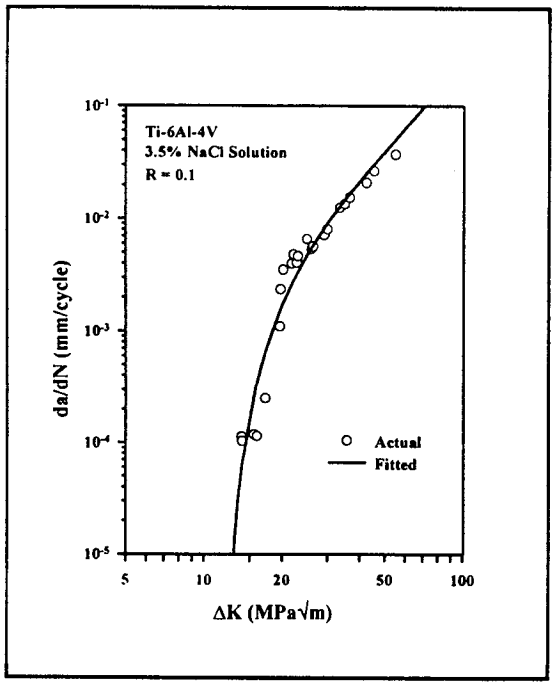

a) Actual and fitted data for $f = 1$ Hz.

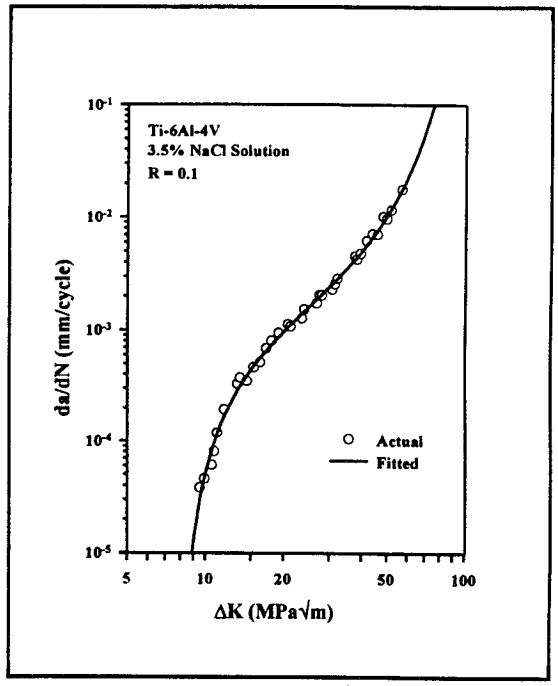

b) Actual and fitted data for $f = 10$ Hz.

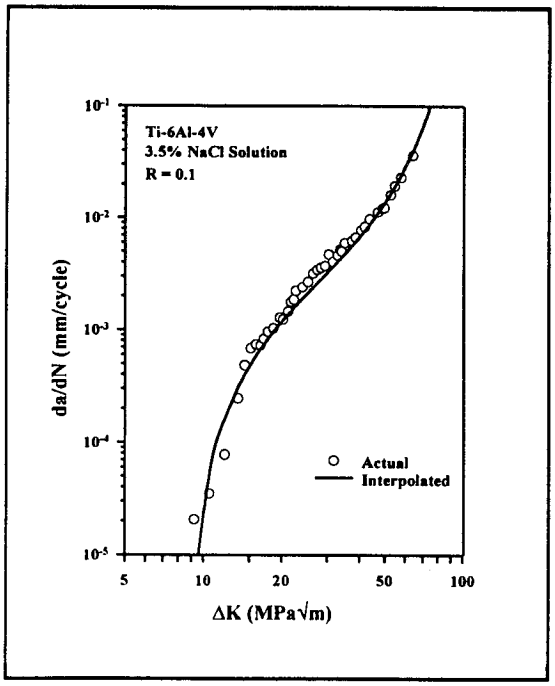

c) Actual and interpolated data for $f = 5$ Hz.

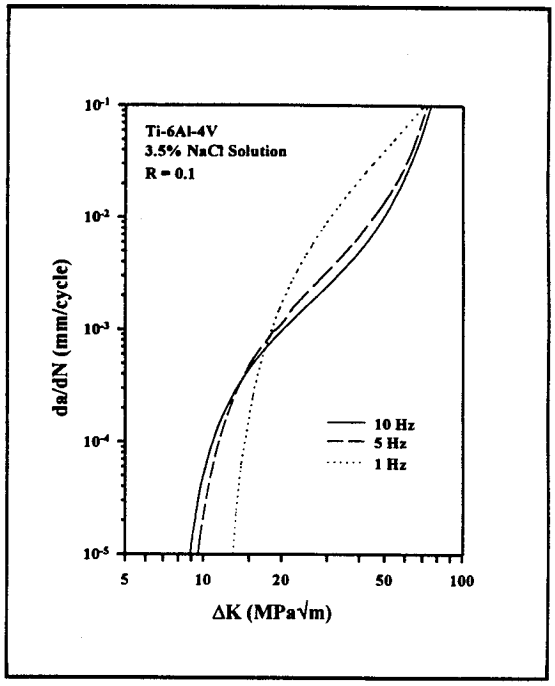

d) Effect of frequency on da/dN.

Figure 5.7: Interpolation results for Ti-6Al-4V (MA) in a 3.5% NaCl solution and R of 0.1 using the Forman Equation with closure (C, n, p, q fit).

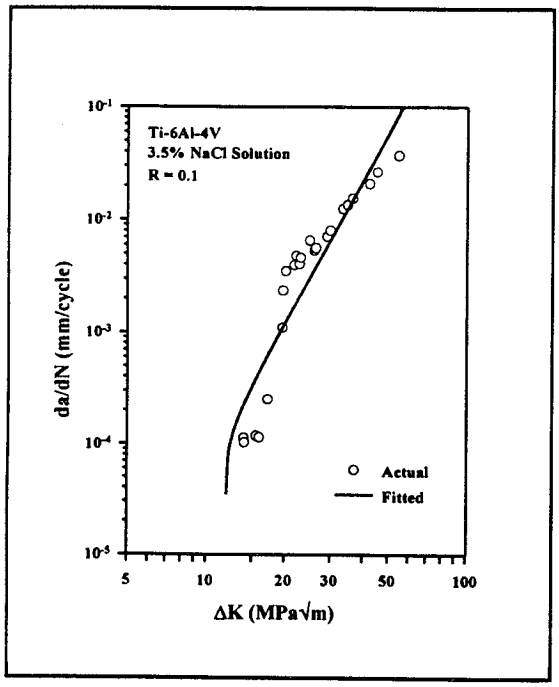

a) Actual and fitted data for f = 1 Hz.

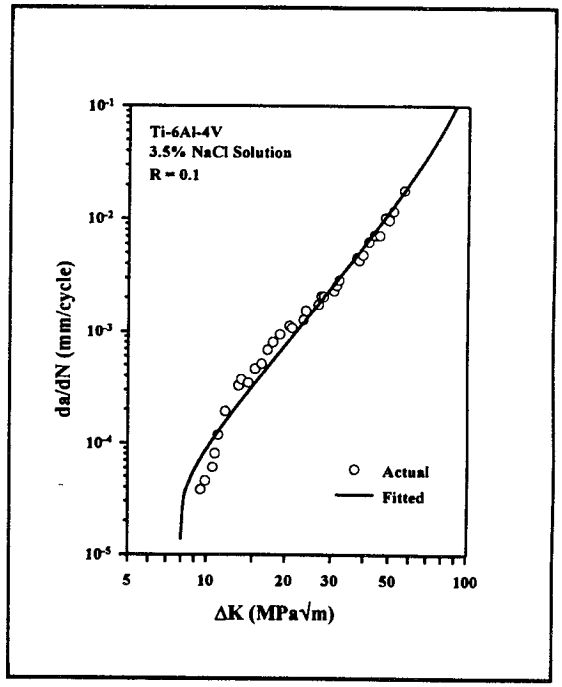

b) Actual and fitted data for f = 10 Hz.

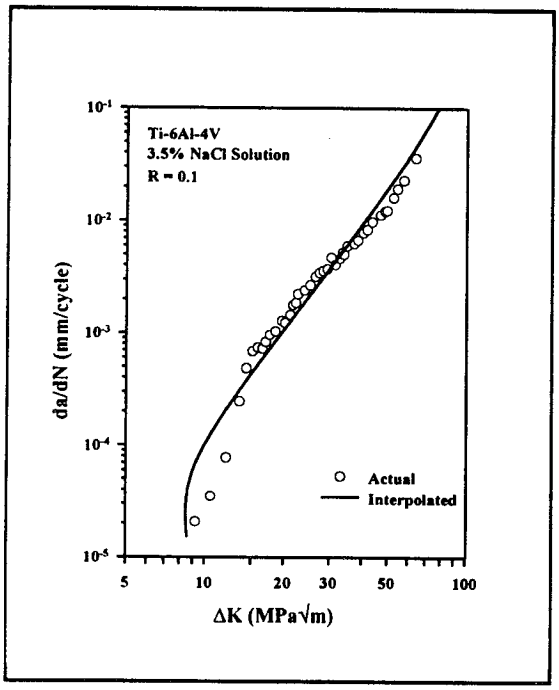

c) Actual and interpolated data for f = 5 Hz.

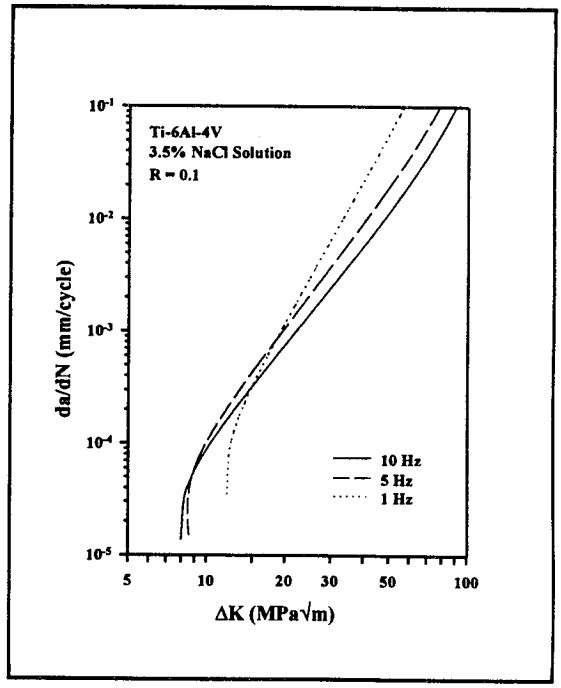

d) Effect of frequency on da/dN.

Figure 5.8: Interpolation results for Ti-6Al-4V (MA) in a 3.5% NaCl solution and R of 0.1 using the Forman Equation without closure (C, n fit, p = 0.25, q = 0.75).

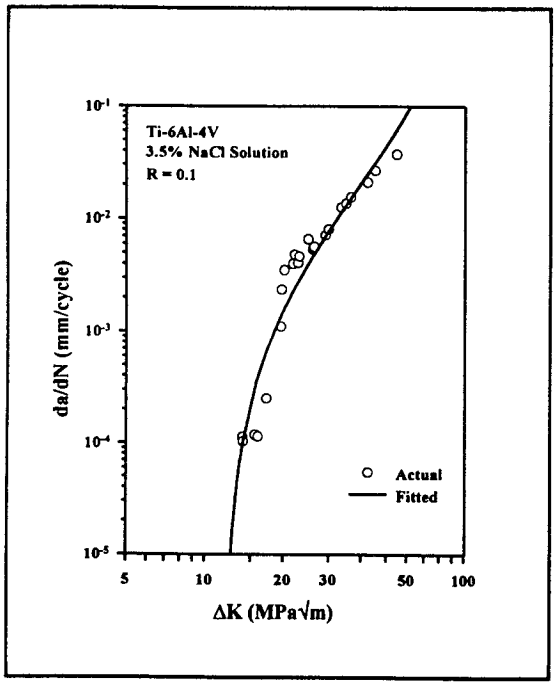

b) Actual and fitted data for $f = 1$ Hz.

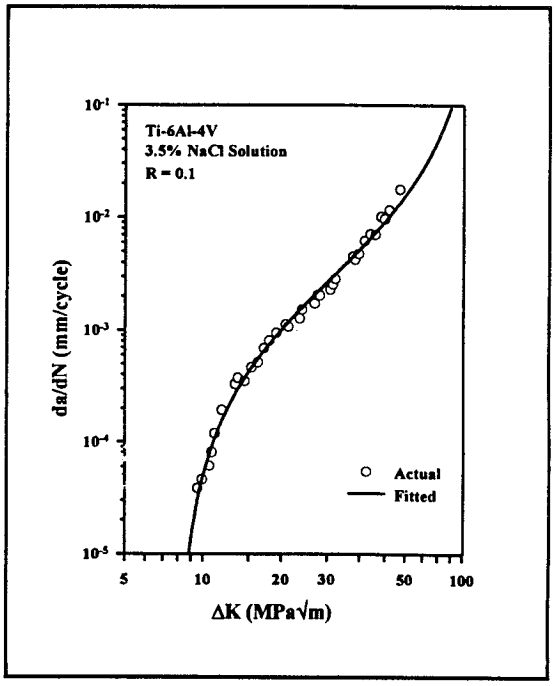

b) Actual and fitted data for $f = 10$ Hz.

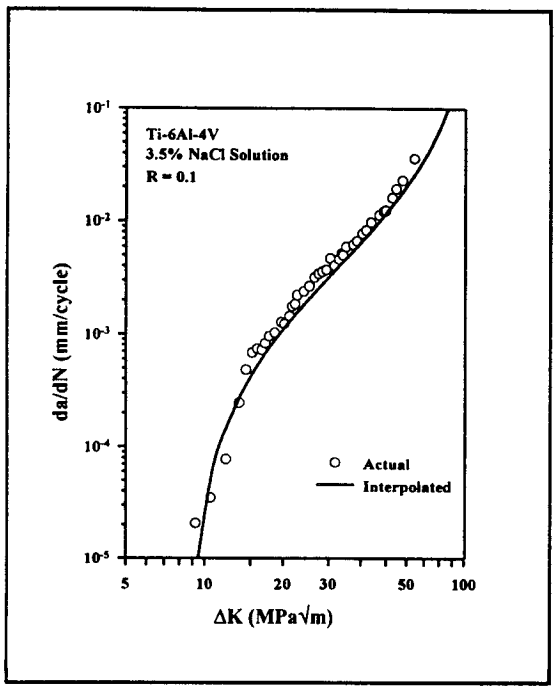

c) Actual and interpolated data for $f = 5$ Hz.

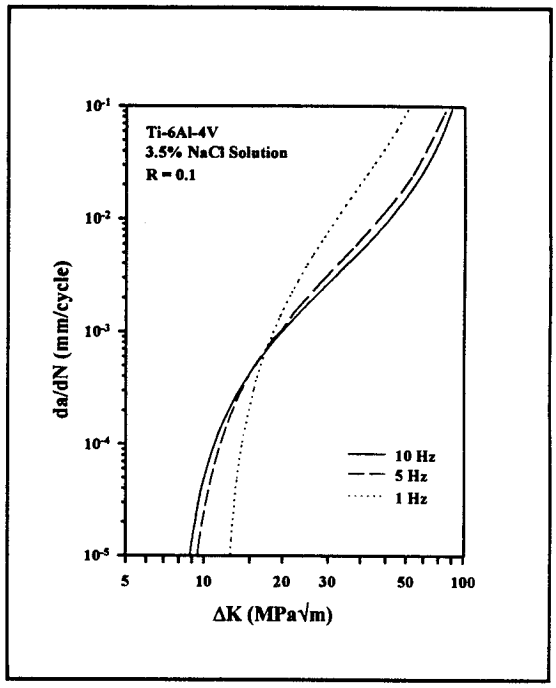

d) Effect of frequency on da/dN.

Figure 5.9: Interpolation results for Ti-6Al-4V (MA) in a 3.5% NaCl solution and R of 0.1 using the Forman Equation without closure (C, n fit, p = q = 2.0).

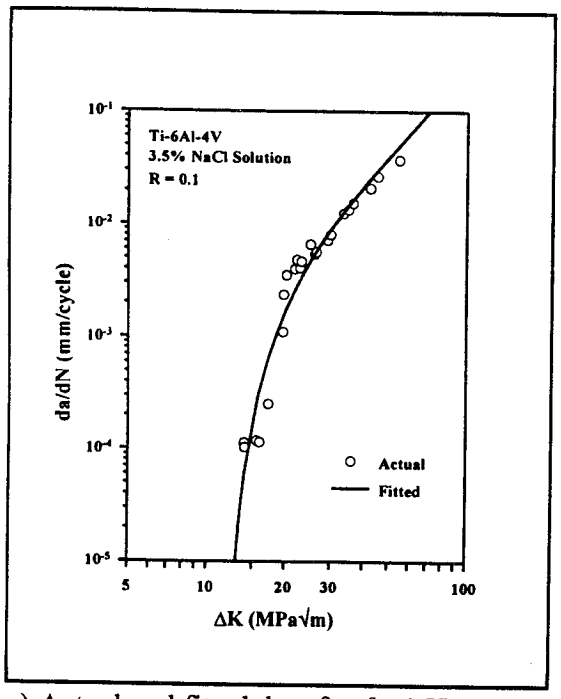

a) Actual and fitted data for f = 1 Hz.

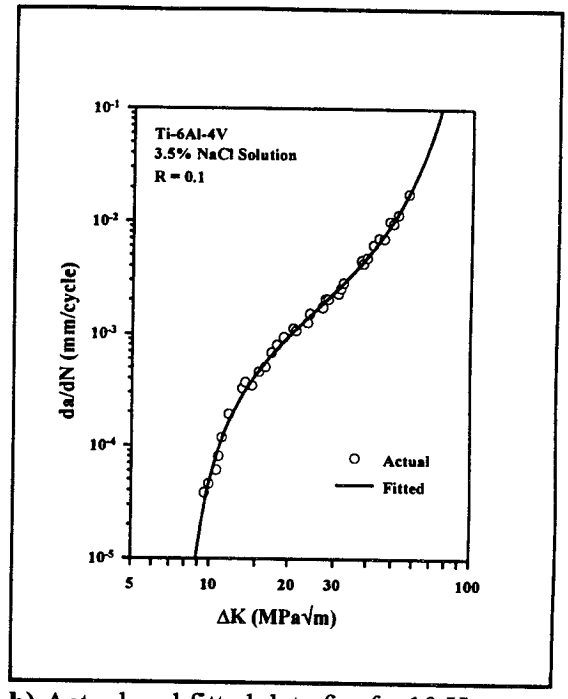

b) Actual and fitted data for f = 10 Hz.

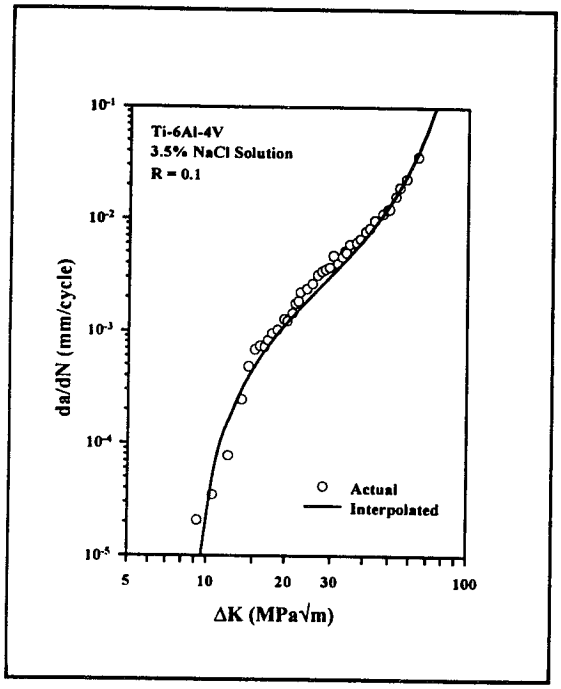

c) Actual and interpolated data for f = 5 Hz.

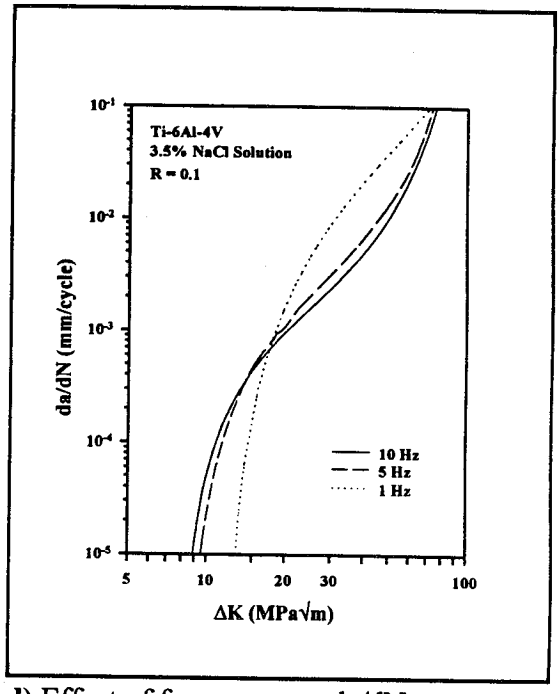

d) Effect of frequency on da/dN.

Figure 5.10: Interpolation results for Ti-6Al-4V (MA) in a 3.5% NaCl solution and R of 0.1 using the Forman Equation without closure (C, n, p, q fit).

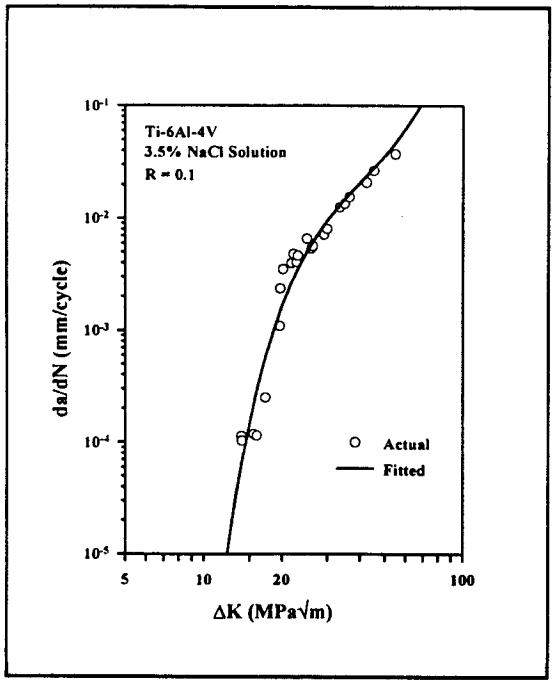

a) Actual and fitted data for f = 1 Hz.

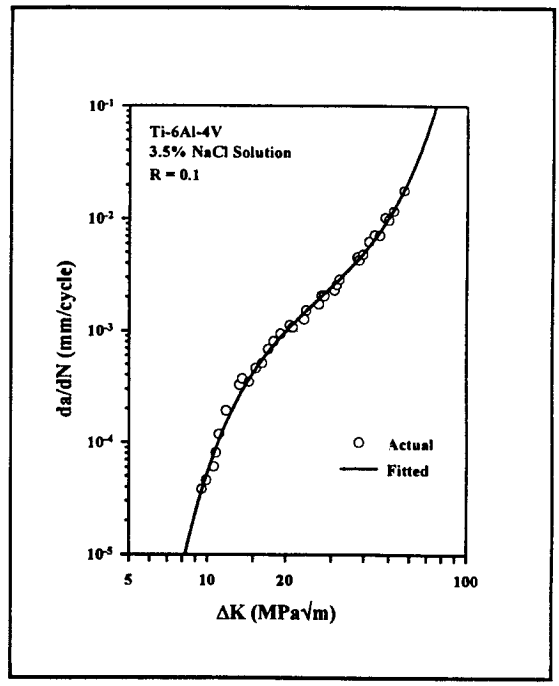

b) Actual and fitted data for f = 10 Hz.

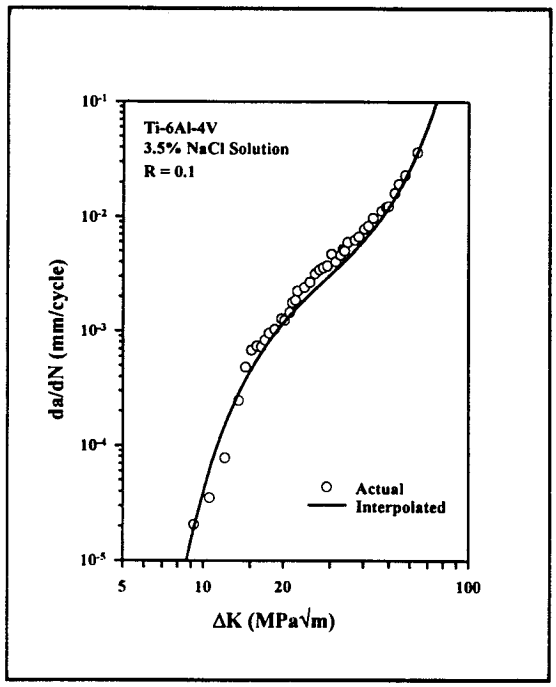

c) Actual and interpolated data for f = 5 Hz.

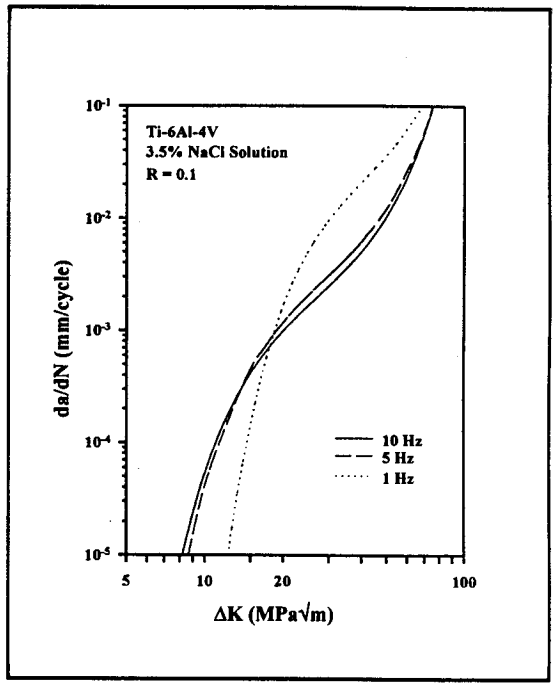

d) Effect of frequency on da/dN.

Figure 5.11: Interpolation results for Ti-6Al-4V (MA) in a 3.5% NaCl solution and R of 0.1 using the SINH Equation with C_1 = 0.5.

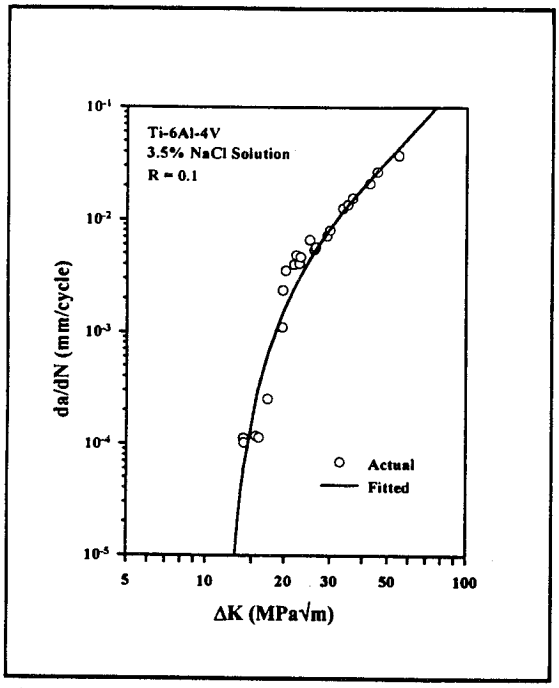

a) Actual and fitted data for $f = 1$ Hz.

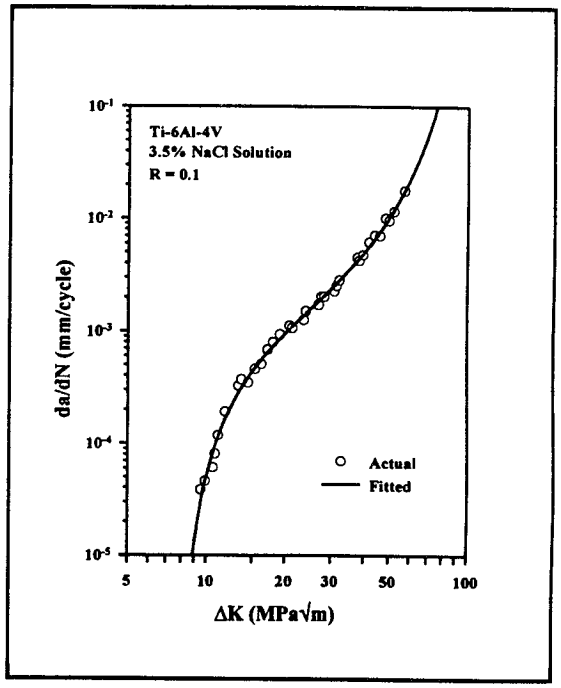

b) Actual and fitted data for $f = 10$ Hz.

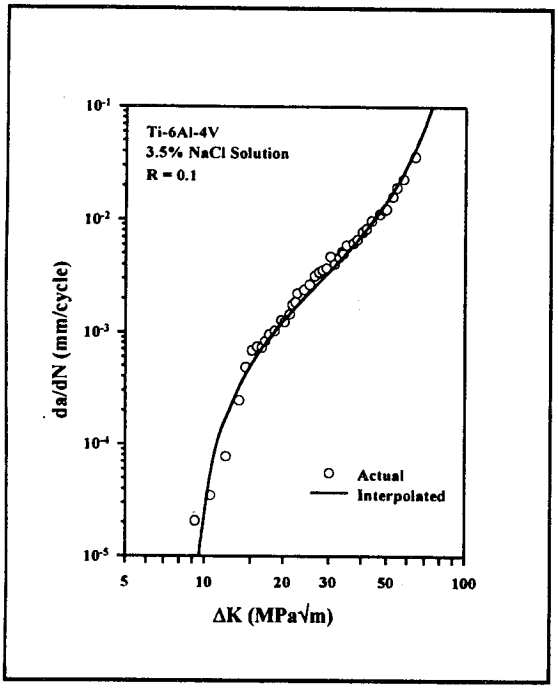

c) Actual and interpolated data for $f = 5$ Hz.

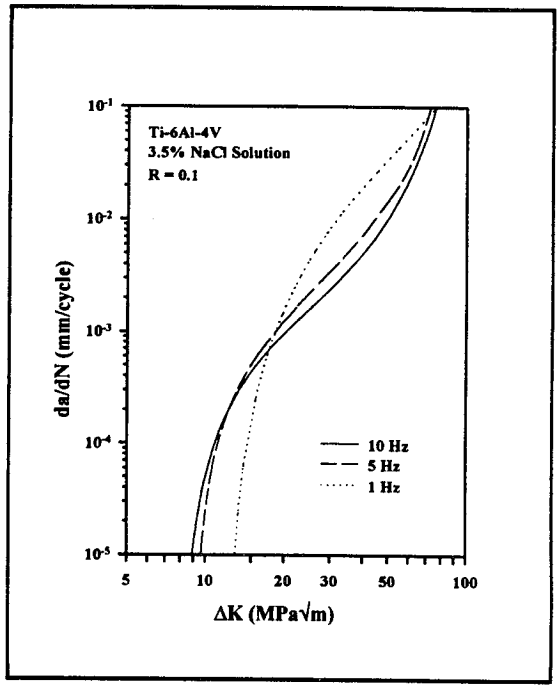

d) Effect of frequency on da/dN.

Figure 5.12: Interpolation results for Ti-6Al-4V (MA) in a 3.5% NaCl solution and R of 0.1 using the Sigmoidal Equation (B, P, Q, D fit).

Table 5.1: Coefficients of Determination for Interpolated Equations

Equation	r^2
Forman Equation without Closure (C, n, p, q fit)	0.9880
Forman Equation with Closure (C, n, p, q fit)	0.9866
Hyperbolic Sine Equation (C_2, C_3, C_4 fit, C_1 = 0.5)	0.9832
Sigmoidal Equation (B, P, Q, D, fit)	0.9717
Forman Equation without closure (C, n, fit, p = 2.0, q = 2.0)	0.9155
Forman Equation with closure (C, n, fit, p = 2.0, q = 2.0)	0.9114
Forman Equation with closure (C, n, p = 0.25, q = 0.75)	0.8706
Forman Equation without closure (C, n, p = 0.25, q = 0.75)	0.8256

fatigue behavior for standard grade Ti-6Al-4V (MA) within the establishing data base. The accuracy of the frequency dependence for interpolation outside the establishing data base was not tested. Notice that the interpolated data (f = 5 Hz) display the frequency "crossover" effect exhibited by the standard grade Ti-6Al-4V. This is due to the fact that the equations fit to the data for frequencies of 1 and 10 Hz displayed the "crossover" effect, and not due to the nature of the logarithmic form of the frequency dependence. The interpolative model assumed that the crack growth rates for f = 5 Hz would lie between the crack growth rates entered for frequencies of 1 and 10 Hz.

Notice in Figures 5.5 through 5.12 that the interpolated data for f = 5 Hz lie closer to the data for a frequency of 10 Hz than a frequency of 1 Hz. This is due to the logarithmic nature of the frequency dependence. The interpolated data often seem to slightly underpredict the measured FCP rates in the middle to upper regions of the data. If a linear

dependence had been utilized, the interpolated growth rates would have increased, as the interpolated data (f = 5 Hz) were shifted vertically, closer to the fitted data for f = 1 Hz. The model would have then slightly overpredicted the FCP rates for f = 5 Hz, resulting in a more conservative model.

5.2.2 ELI Grade Ti-6Al-4V (MA)

5.2.2.1 Modeling the Effect of Stress Ratio

To model the effect of stress ratio, data were taken from a study by Gangloff and Kim for Ti-6Al-4V (MA,ELI) in moist air and a 1.0% NaCl solution (-500 mV_{SCE}).[9] Conditions were constant except R, thus all of the equation parameters were expressed as a function of the stress ratio. Data exist for a frequency of 5 Hz, and stress ratios of 0.1, 0.4, and 0.7 for both environments. To test the model, data for R of 0.1 and 0.7 were fit to the Sigmoidal Equation, and the parameters were set equal to the appropriate interpolation functions given in Appendix C. Using these functions, the equation parameters, including ΔK_{th} were interpolated for a stress ratio of 0.4. EFCP rates were calculated over a range of ΔK values and compared to data. K_C was entered as 78 MPa$\sqrt{m}$, based on the results in Section 4.1.1. ΔK_{th} was calculated from ΔK_o which was taken from the NASA FLAGRO materials files as 3.8 MPa$\sqrt{m}$ for both environments. The value is based on FCP rates in moist air, and is not relevant for other environments. The value was utilized because threshold data were not available for ELI Ti-6Al-4V (MA), and because the value of the threshold would not have a large effect on the quality of the fitted equations. Results are shown in Figure 5.13 for the moist air environment, and in Figure 5.14 for the 1.0% NaCl solution (-500 mV_{SCE}). The

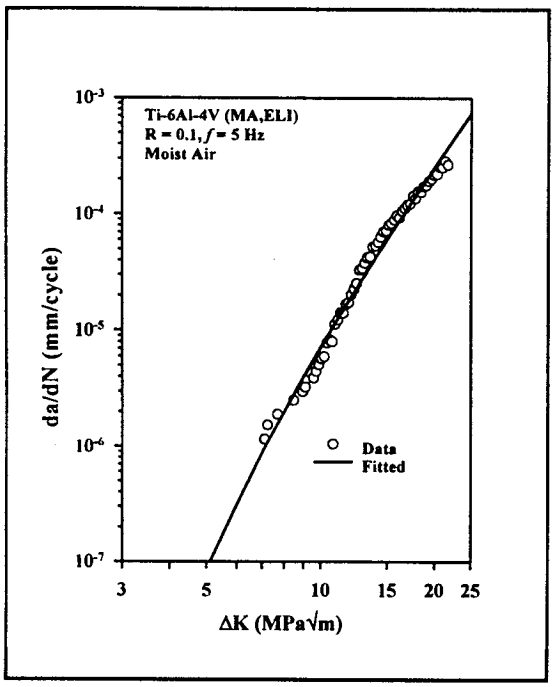

a) Actual and fitted data for R = 0.1.

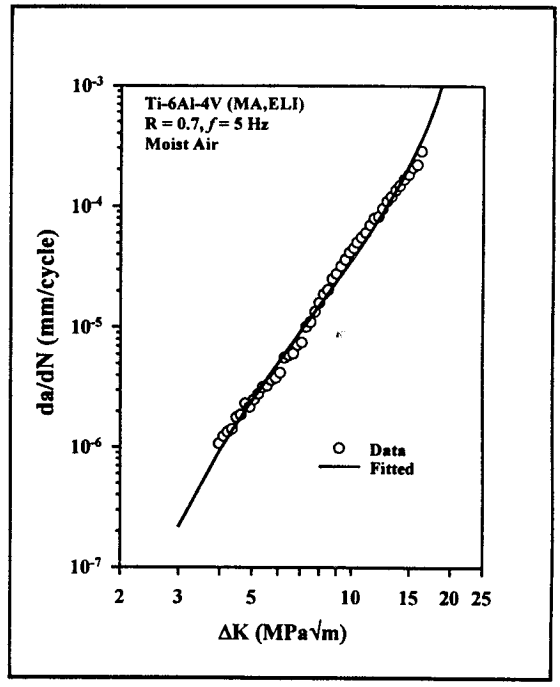

b) Actual and fitted data for R = 0.7.

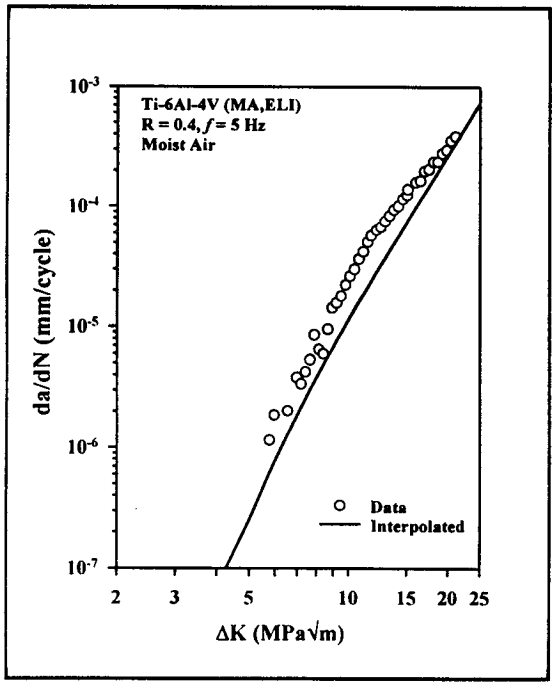

c) Actual and interpolated data for R = 0.4.

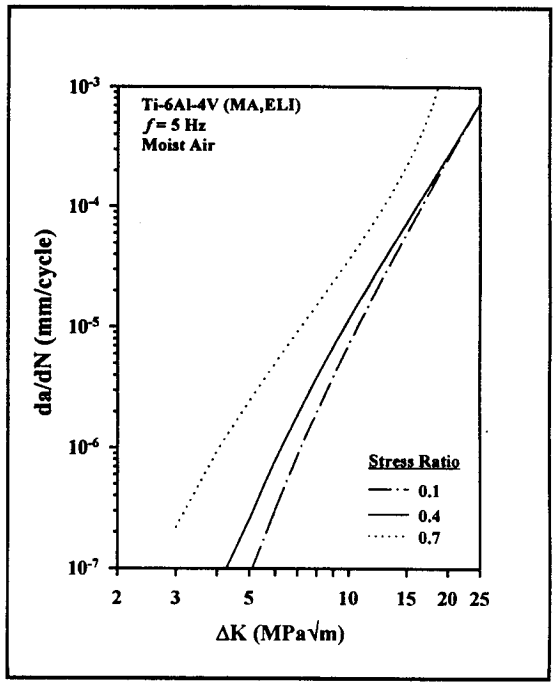

d) Effect of R on da/dN.

Figure 5.13: Interpolation results for Ti-6Al-4V (MA,ELI) in moist air and *f* of 5 Hz using the Sigmoidal Equation (B, P, Q, D fit).

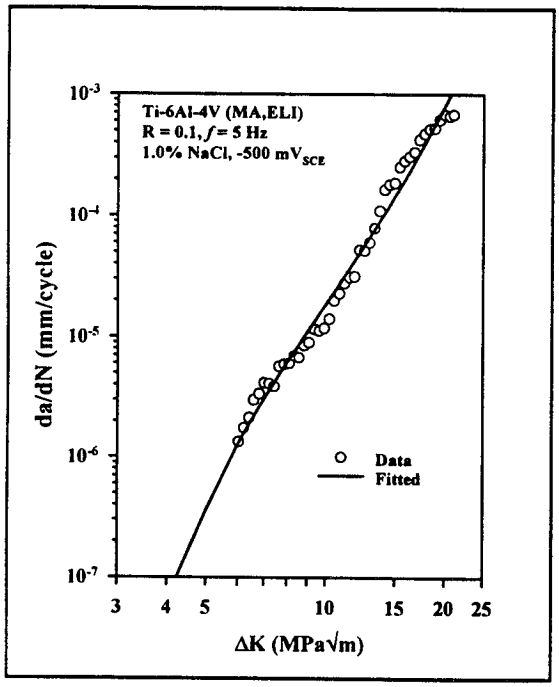

a) Actual and fitted data for R = 0.1.

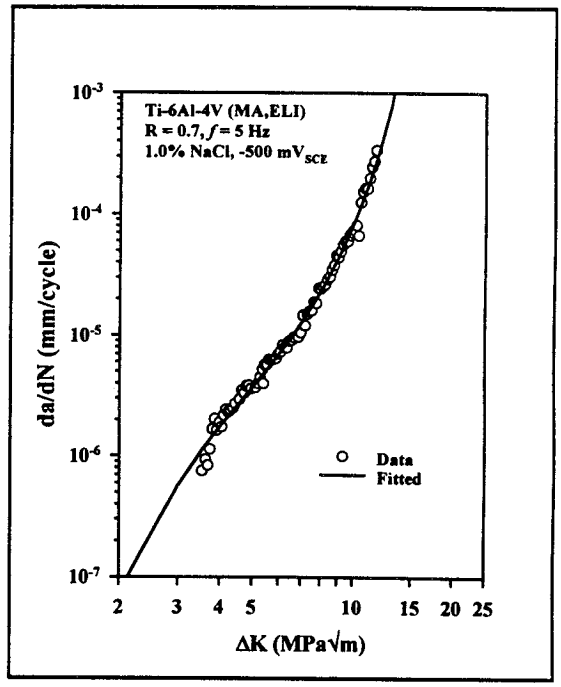

b) Actual and fitted data for R = 0.7.

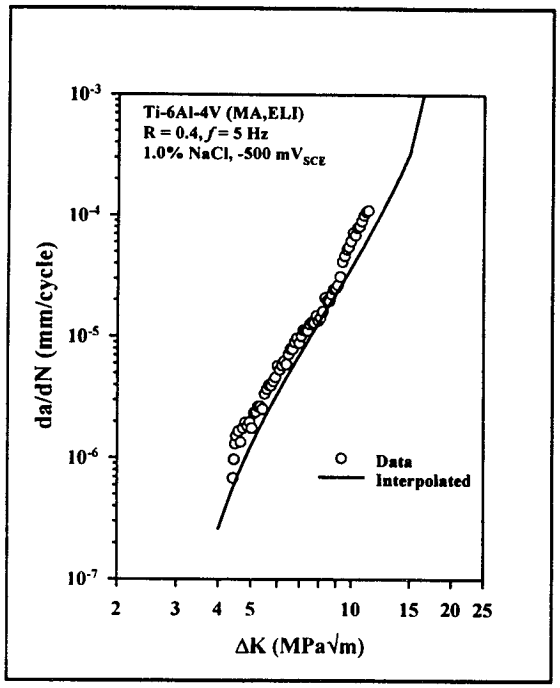

c) Actual and interpolated data for R = 0.4.

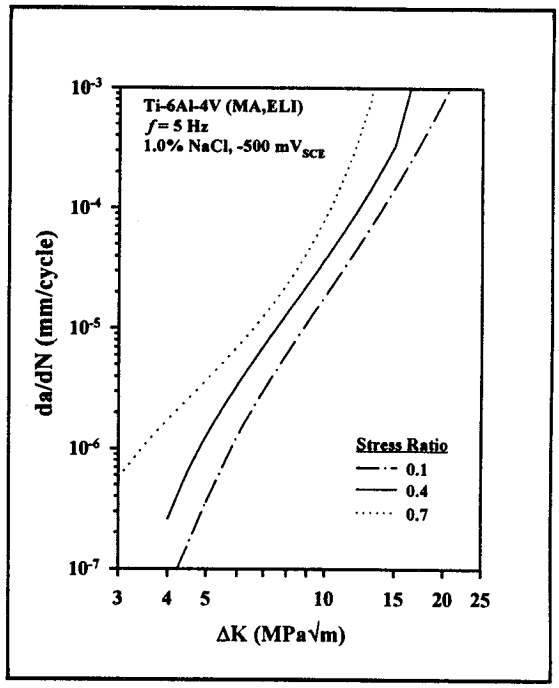

d) Effect of R on da/dN.

Figure 5.14: Interpolation results for Ti-6Al-4V (MA,ELI) in a 1.0% NaCl solution (-500 mV_{SCE}) and f of 5 Hz using the Sigmoidal Equation (B, P, Q, D fit).

coefficients of determination for the interpolated data were calculated; r^2 was 0.7465 for moist air and 0.8794 for 1.0% NaCl (-500 mV_{SCE}).

The effect of stress ratio can be accounted for with the Forman Equation (Equation 2.2) including a plasticity induced crack closure strategy. To analyze the accuracy of this method, the data for R = 0.1 in both the moist air and the 1.0% NaCl solution (-500 mV_{SCE}) were fit to the Forman Equation with closure; fitting C and n, as well as fitting C, n, p, and q. Two cases were analyzed for fitting C and n. In the first test, the value of p was entered as 0.25, while q was 0.75. These values were taken from the NASA FLAGRO materials files for Ti-6Al-4V. In the second test, p and q were entered as 2.0. Using these fitted coefficients, da/dN was predicted for stress ratios of 0.4 and 0.7. K_C was 78 MPa$\sqrt{m}$ for all three stress ratios; only the value of ΔK_{th} and the crack closure function, f, varied as a function of R. ΔK_{th} was calculated from ΔK_o, which was taken from the NASA FLAGRO materials files as 3.8 MPa$\sqrt{m}$, a value determined for moist air. The fitted values for the equation constants are listed in Tables 5.2 through 5.4. Table 5.5 lists the values for the crack closure function, f, and ΔK_{th} as functions of stress ratio. The results for moist air are shown in Figure 5.15; results for 1.0% NaCl (-500 mV_{SCE}) are shown in Figure 5.16.

Table 5.2: Forman Equation Constants (p = 0.25, q = 0.75)*

Environment	C	n
Moist Air	0.2425×10^{-9}	4.958
1.0% NaCl	0.6612×10^{-9}	4.955

* The da/dN versus ΔK data input to the model were in units of mm/cycle and MPa$\sqrt{m}$, respectively. The constants in Table 5.2 through 5.5 can only be used with these units.

Table 5.3: Forman Equation Constants (p = 2.0, q = 2.0)

Environment	C	n
Moist Air	0.3679×10^{-8}	3.937
1.0% NaCl	0.1477×10^{-7}	3.775

Table 5.4: Forman Equation Constants (C, n, p, q fit)

Environment	C	n	p	q
Moist Air	0.533×10^{-23}	20.05	-13.48	-38.44
1.0% NaCl	0.208×10^{-15}	11.94	-6.41	-16.15

Table 5.5: Crack Closure Function and ΔK_{th}

Stress Ratio, R	f	ΔK_{th} (MPa$\sqrt{m}$)
0.1	0.2869	3.59
0.5	0.4392	2.65
0.7	0.6982	1.43

The Forman Equation with closure describes da/dN versus ΔK most effectively for R = 0.1 when all of the equation parameters (C, n, p, and q) are fit. For the air case, r^2 was 0.9798 when fitting C, n, p, and q. When fitting just C and n, r^2 was 0.8478 when p was 0.25 and q was 0.75, and 0.8839 when p and q were equal to 2.0 For the 1.0% NaCl environment, the coefficient of determination was 0.9648 when fitting C, n, p, and q. When fitting just C and n, the coefficient of determination was 0.9320 when p was 0.25 and q was 0.75, and 0.9521 when p and q were set to 2.0. When fitting C, n, p, and q, however, the equation is not always accurate outside the range of the fitted data and often becomes sinusoidal. A

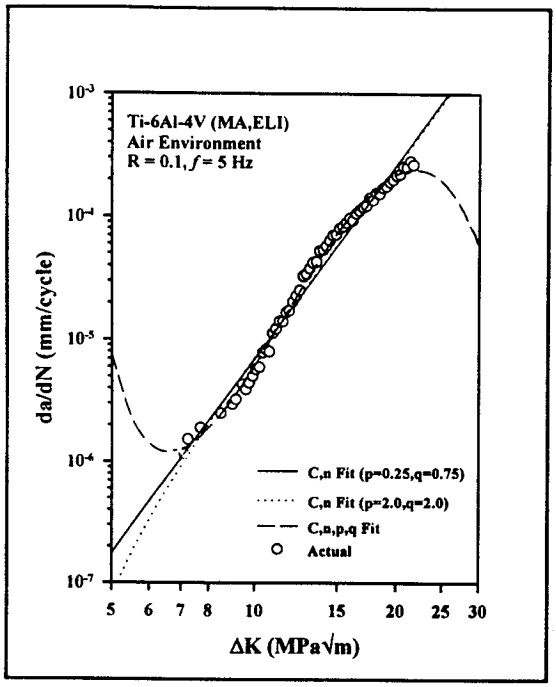

a) Actual and fitted data for R = 0.1.

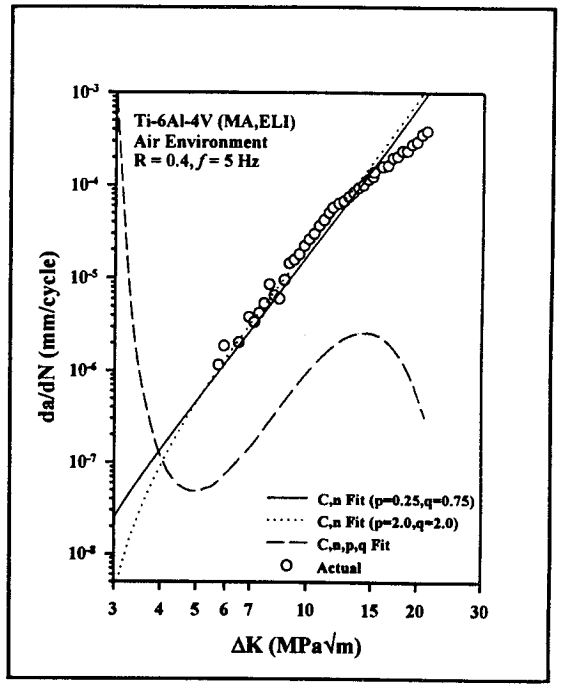

b) Actual and predicted data for R = 0.4.

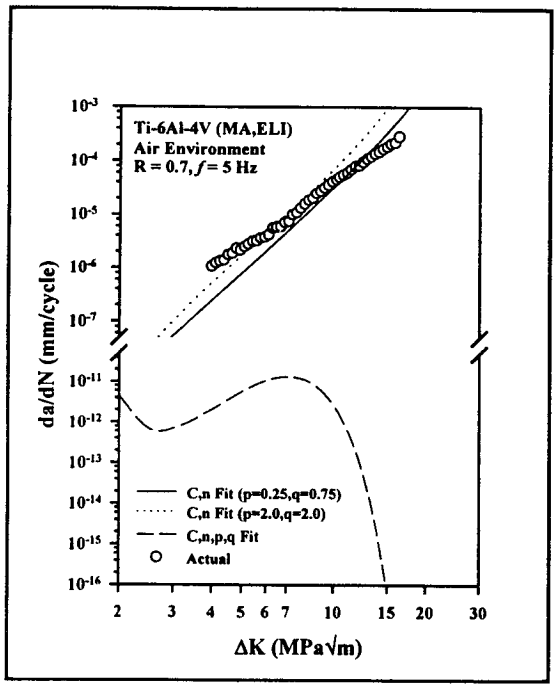

c) Actual and predicted data for R = 0.7.

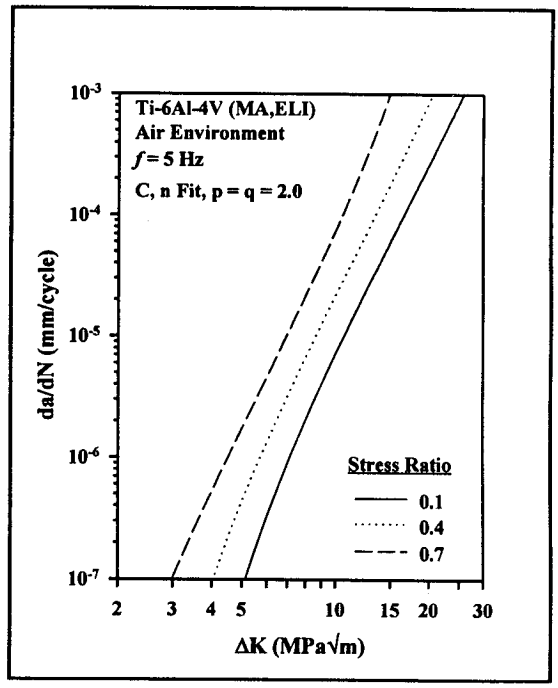

d) Effect of R when C, n fit, p = q = 2.0.

Figure 5.15: Fitted and predicted da/dN values for Ti-6Al-4V (MA,ELI) using the Forman Equation with closure for R = 0.1, 0.4, and 0.7 in moist air for f = 5 Hz.

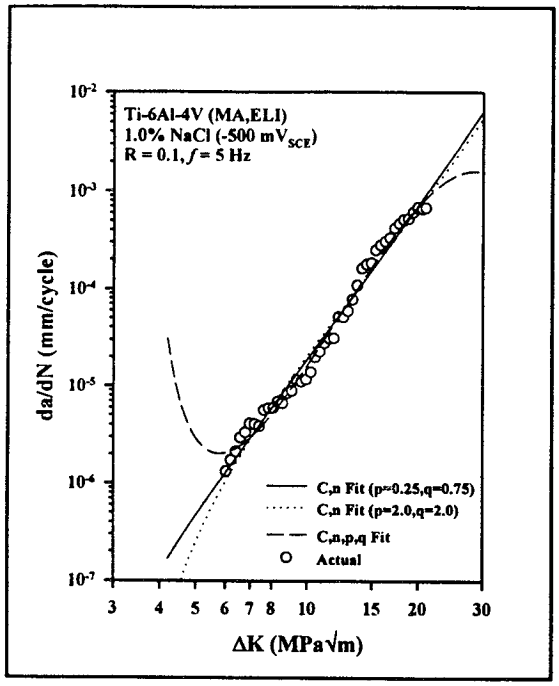

a) Actual and fitted data for R = 0.1.

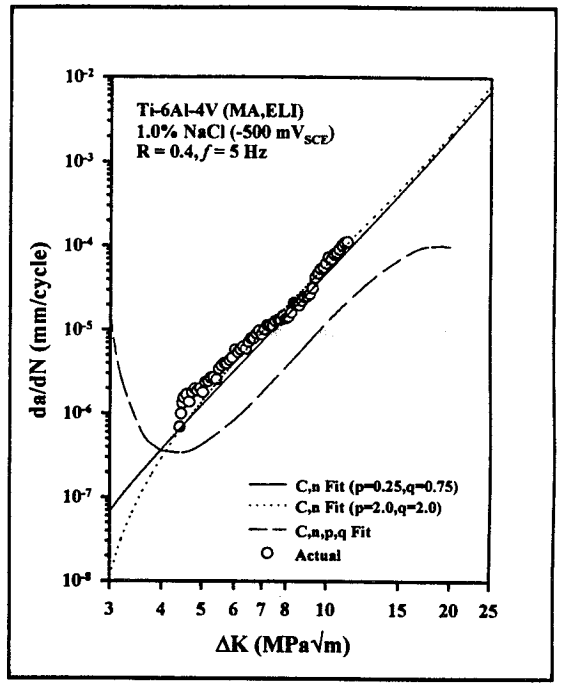

b) Actual and predicted data for R = 0.4

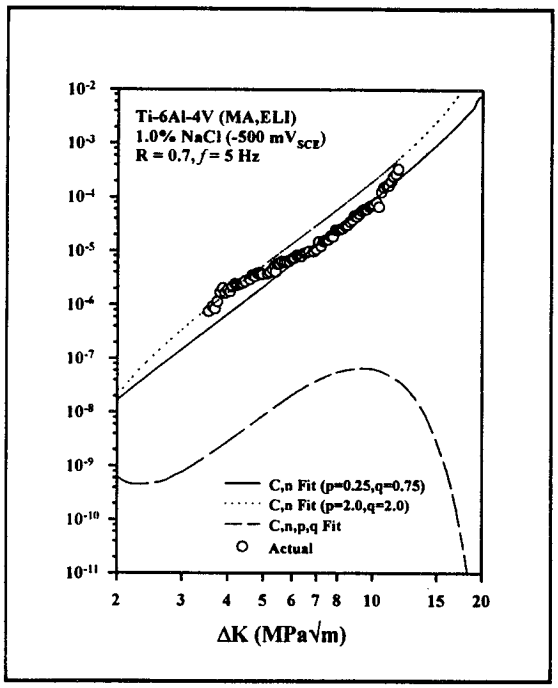

c) Actual and predicted data for R = 0.7.

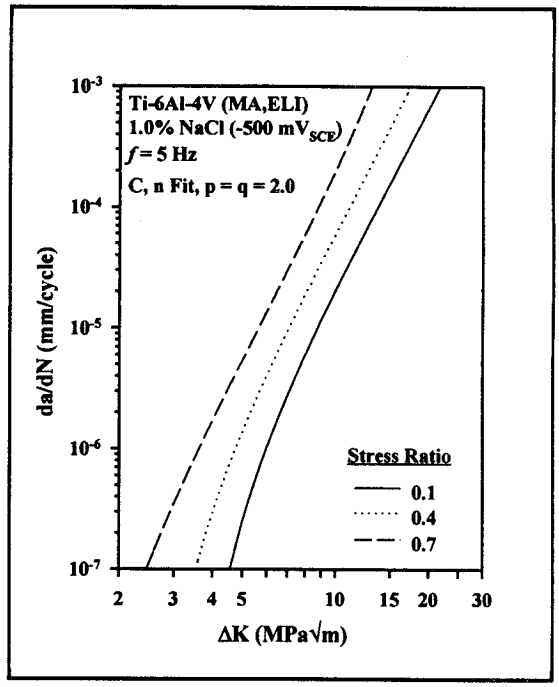

d) Effect of R when C, n fit, p = q = 2.0.

Figure 5.16: Fitted and predicted da/dN values for Ti-6Al-4V (MA,ELI) using the Forman Equation with closure for R = 0.1, 0.4, and 0.7 in 1.0% NaCl (-500 mV$_{SCE}$) for f = 5 Hz.

sinusoidal relationship between da/dN and ΔK is nonsense physically. This problem is corrected by fitting a larger range of data to the equation. The Forman Equation with closure predicted the effect of the stress ratio accurately, via a plasticity induced crack closure strategy, when the parameters C and n were fit, with p and q fixed in both the moist air and 1.0% NaCl (-500 mV_{SCE}) environments.

The Forman Equation with closure was developed to predict the effect of crack closure in moist air. The data shown in Figure 5.16 for the 1.0% NaCl solution (-500 mV_{SCE}) also show good agreement. The Forman Equation should not work for a SCC-sensitive linear superposition case where R affects da/dN by an environmental mechanism not related to plasticity induced closure. The ability of the Forman Equation to accurately predict the effect of stress ratio on EFCP rates via a plasticity induced closure strategy thus strengthens the statements made in Section 4.1.2 that stress corrosion cracking will not affect time or R dependent EFCP of Ti-6Al-4V (MA, ELI) for the range of stress intensities used in this study (5-45 MPa$\sqrt{m}$); the only stress ratio effect on da/dN is plasticity induced closure. The Forman Equation with closure is also effective for Ti-6Al-4V (MA,ELI) because the closure levels measured in both air and NaCl show that plasticity is the dominant factor.

5.2.2.2 Modeling the Effect of Frequency

The interpolative method has been applied to model the effect of frequency on da/dN in Ti-6Al-4V (MA,ELI) in aqueous chloride solutions. Data for Ti-6Al-4V (MA,ELI) in a 1.0% NaCl solution (-500 mV_{SCE}) at a frequency of 5 Hz and R of 0.1 were fit to the Forman Equation with closure. The parameter α was 2.5, while S_{max}/σ_o was 0.3. The parameters C and n were fit, while p and q were 2.0. K_C was 78 MPa$\sqrt{m}$, while ΔK_{th} was calculated from

ΔK_o, which was entered as 3.8 MPa$\sqrt{m}$, for the 5 Hz data, and interpolated for the 40 Hz data. ΔK_o was taken from the NASA FLAGRO materials files, and is based on results for moist air, not a 1.0% NaCl solution. Using the resulting interpolation functions, given in Appendix C, FCP rates were calculated over a range of ΔK values for a frequency of 40 Hz and R of 0.1.

When the interpolative model was originally developed, only the logarithmic form of the frequency dependence was available. This form of the frequency dependence was applied to the data from Dawson and Pelloux[33], and was able to interpolate trends in the data accurately. This same logarithmic dependence was applied to the data for ELI grade Ti-6Al-4V (MA) generated during this research, and yielded unacceptable results. When entering data for a frequency of 5 Hz and interpolating data for 40 Hz, the model substantially underpredicted EFCP rates. Also, when the data for a frequency of 5 Hz were entered into the model, the fitted values of C and n were positive. This resulted in a positive coefficient in the interpolation functions, thus the interpolation functions predicted the wrong trend in da/dN for this alloy class. Since this logarithmic form of the frequency dependence was unacceptable, another function had to be developed. Based on the results of the constant ΔK and variable frequency experiment discussed in Chapter 4, where da/dN was proportional to $f^{0.1 \text{ to } 0.18}$, a frequency dependence of the form f^{α} was selected (α is a user specified constant). This function allows the user to control the frequency dependence; if a linear superposition dependence is desired, the user can enter α as -1.0.

Since only one data set was entered into the model, it is imprecise to call the results an interpolation. In actuality, by entering the data for a frequency of 5 Hz, and

specifying that da/dN is proportional to $f^{0.1}$, the model is forcing curves of da/dN versus ΔK data to pass through the results of the frequency scans presented in Chapter 4. Since the variable frequency experiments revealed only the magnitude of da/dN as a function of frequency for two specific ΔK values, only the parameter C was varied from frequency to frequency, according to the following equation:

$$C = 1.257 \times 10^{-8} f^{0.1} \qquad \textbf{(5.3)}$$

The parameter n was held constant at 3.8, the fitted value for $f = 5$ Hz. ΔK_{th} was also held fixed at 3.6 MPa$\sqrt{m}$ for all frequencies, the value calculated from ΔK_o. Shown in Figure 5.17 are predictions compared to experimental data for Ti-6Al-4V (MA,ELI) in a 3.5% NaCl solution (-500 mV_{SCE}), f of 40 Hz, and R of 0.1. As seen in the figure, the model accurately predicts the effect of frequency. Figure 5.18 presents predictions of da/dN versus ΔK for frequencies in the range of 0.03 to 100 Hz.

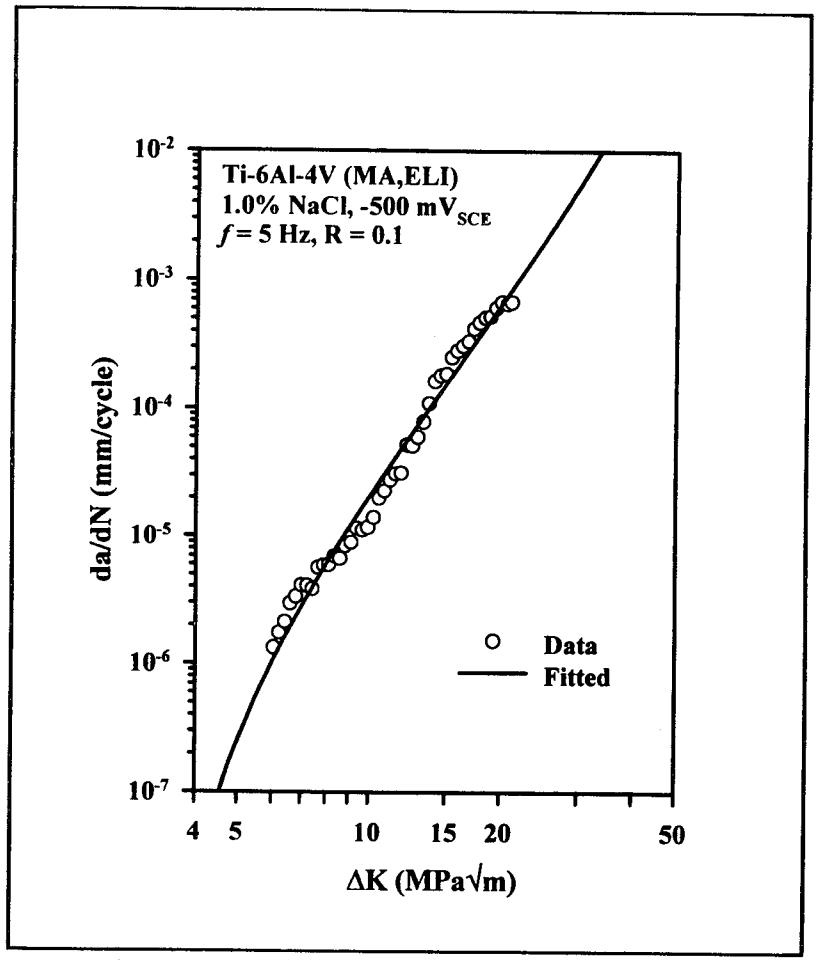

a) Actual and fitted data for f = 5 Hz.

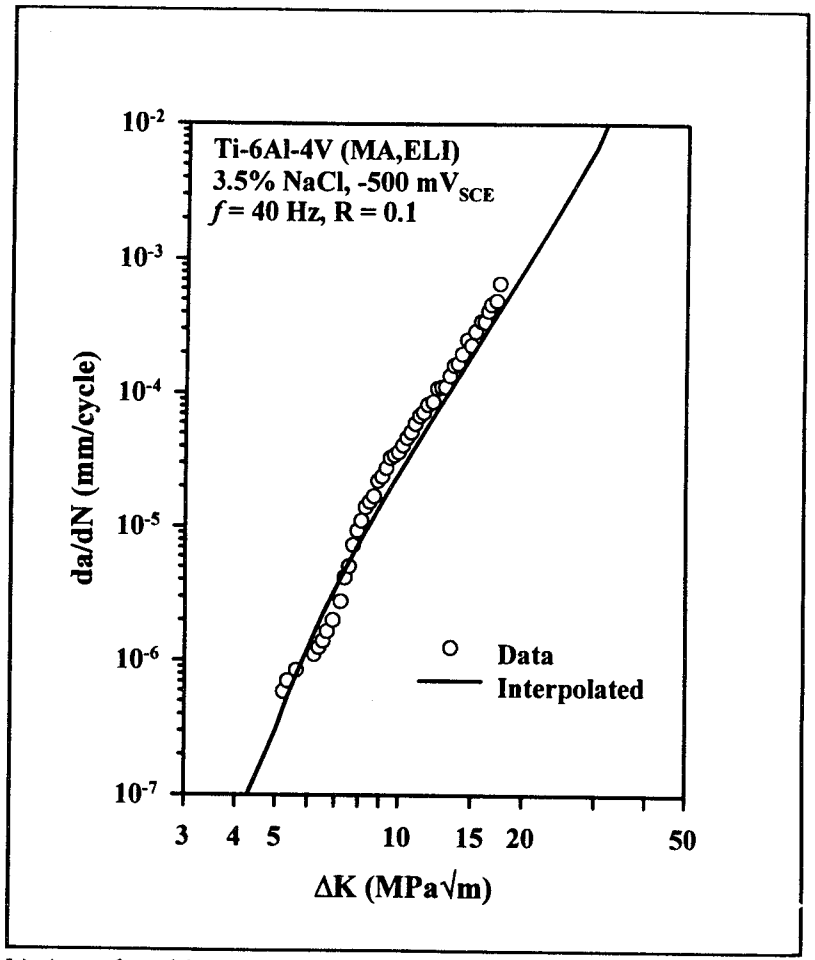

b) Actual and interpolated data for f = 40 Hz.

Figure 5.17: Interpolation results for the effect of frequency on EFCP in Ti-6Al-4V (MA,ELI) in a 3.5% NaCl solution (-500 mV$_{SCE}$) using the Forman Equation with closure (C and n fit, p = q = 2.0).

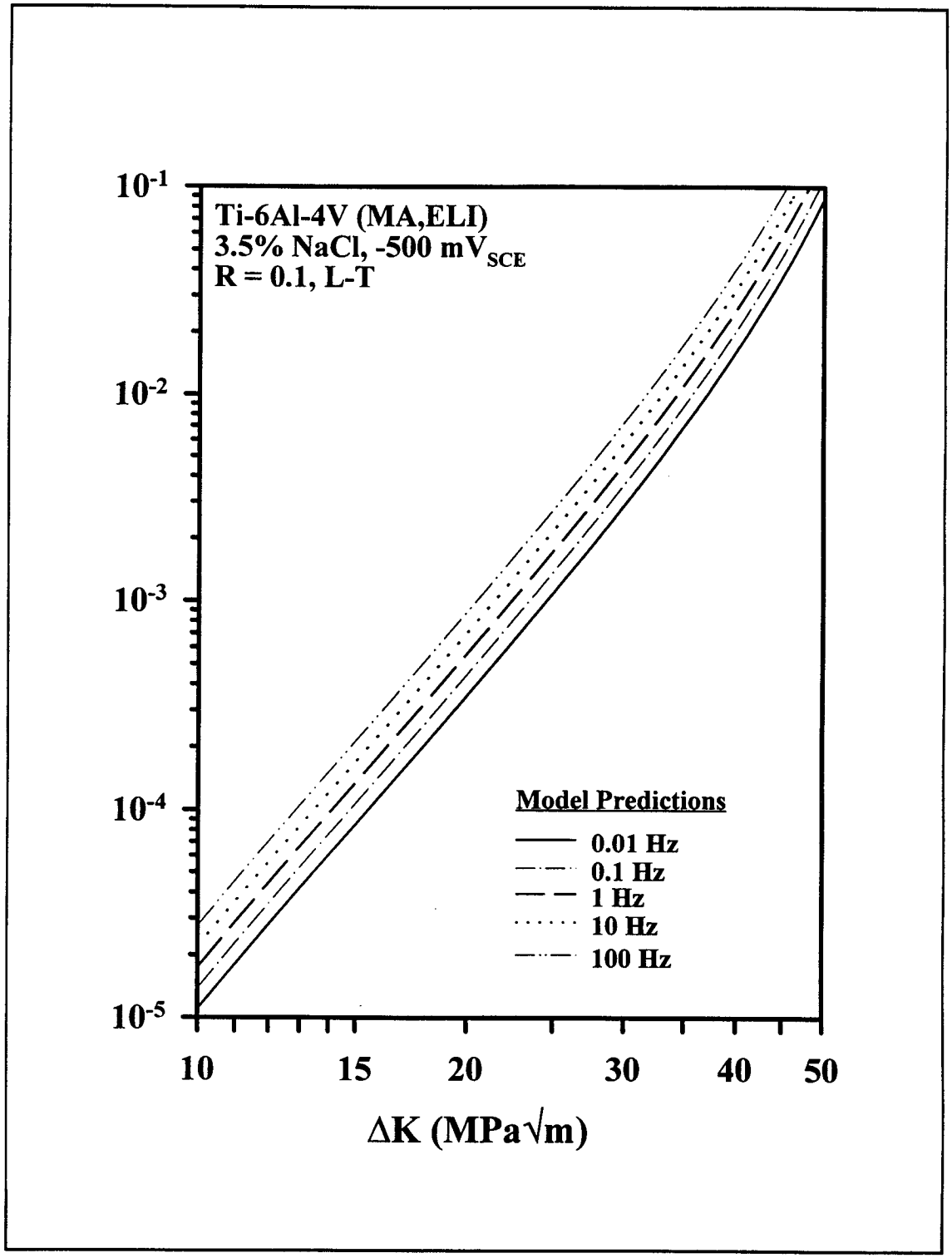

Figure 5.18: Interpolative model predictions of wide range da/dN-ΔK data for Ti-6Al-4V (MA,ELI) in 3.5% NaCl (-500 mV_{SCE}) for frequencies between 0.01 and 100 Hz.

Chapter 6: Discussion

This chapter presents a discussion of the experimental results presented in Chapter 4, as well as the modeling results presented in Chapter 5. The SCC and corrosion fatigue behavior for ELI and standard grade Ti-6Al-4V are compared, and reasons are presented for differences in their behavior. The capability of the computer models to effectively model EFCP rates in Ti-6Al-4V is discussed.

6.1 EAC of Ti-6Al-4V (MA,ELI)

6.1.1 Monotonic Load

The ELI grade of mill-annealed Ti-6Al-4V studied during this research exhibits a greater resistance to SCC in aqueous chloride than standard grade Ti-6Al-4V. ELI Ti-6Al-4V (MA) in a 3.5% NaCl solution (-500 mV_{SCE}) exhibits a K_{TH} between 48 and 55 MPa$\sqrt{m}$; this value is much higher than K_{ISCC} of 23 MPa$\sqrt{m}$ reported by Dawson and Pelloux for standard grade Ti-6Al-4V in essentially the same environment.[33] The ELI grade specimens were held at a fixed electrode potential of -500 mV_{SCE} because titanium alloys exhibit maximum susceptibility to SCC at -500 mV_{SCE} in solutions containing Cl^- ions.[47]

One issue addressed in order to understand the high values of K_{TH} presented in Figure 4.5 is loading rate. Insight into the issue of loading rate can be obtained if the environmental fatigue behavior of Ti-6Al-4V (MA,ELI) and Ti-6Al-6V-2Sn (MA) are examined. Ti-6Al-6V-2Sn exhibits the frequency "crossover" effect[40], ELI grade Ti-6Al-4V does not. Fatigue involves the higher strain rate regime, and if K_{TH} was significantly lower than the measured minimum of 48 MPa$\sqrt{m}$ at this higher strain rate, the ELI grade would exhibit the frequency "crossover" effect. Since the ELI grade does not exhibit the "crossover" effect, K_{TH} remains

above the K_{ISCC} value measured by Dawson and Pelloux,[33] and is not significantly lower than the measured minimum at higher strain rates. This conclusion is supported by the K_{TH} values measured at a stress intensity rate of 0.01 MPa$\sqrt{m}$/s. Several experiments should still be conducted at higher loading rates for the ELI Ti-6Al-4V to address this issue.

One issue addressed in order to understand the increased SCC resistance of the ELI grade is the difference in chemical composition between the two grades. Table 6.1 compares the chemical compositions of ELI and standard grade Ti-6Al-4V. The compositions for the standard grade are given in weight %, either as a range of percents or the maximum percent allowed,[50] while the composition of the ELI grade is for the rolled plate used during this research. As seen in the table, the ELI grade Ti-6Al-4V has significantly less iron (Fe), oxygen (O), nitrogen (N), carbon (C), and hydrogen (H).

Table 6.1: Chemical Compositions of ELI and Standard Grade Ti-6Al-4V

Major Elements		
	Standard Grade	ELI Grade
Al	5.5 - 6.75	6.17
V	3.5 - 4.5	4.33
Fe	0.3	0.19
Interstitial Elements		
	Standard Grade	ELI Grade
O	0.20	0.12
C	0.10	0.025
N	0.05	0.011
H	0.015	0.0055

The α phase in $\alpha + \beta$ alloys is susceptible to SCC in aqueous chloride[47], as governed by the aluminum, oxygen, and tin contents. Figure 6.1 shows the effect of oxygen content on SCC kinetics in Ti-6Al, an α titanium alloy. As quenched specimens with an oxygen content of 0.05% were immune to SCC in 0.6M KCl. Susceptibility to SCC was induced by increasing the oxygen content to 0.15%; increasing the oxygen content to 0.30% further increased the susceptibility. Aging the specimens with an oxygen content of 0.05% at 425°C induced SCC, and accelerated SCC in the alloys with a higher oxygen content. The susceptibility of the specimens with an oxygen content of 0.05%, aged at 425°C, was caused by the precipitation of Ti_3Al (α_2). At high aluminum contents (above ≈ 5%), α_2 precipitates during low temperature aging in the ($\alpha + \alpha_2$) field. These precipitates lower K_{ISCC} and increase SCC velocity.[47]

Since the alloy studied by Dawson and Pelloux[33] and the ELI grade studied during this research are similar in heat treatment (neither alloy was aged), aging is not responsible for the difference in SCC behavior. Strain rates effects are also not responsible. Since the major difference between the ELI grade and the alloy studied by Dawson and Pelloux[33] is the oxygen content, the oxygen content seems to be the controlling factor in determining the SCC resistance of the higher purity alloy.

6.1.2 Fatigue Loading

Figures 6.2 and 6.3 compare da/dN versus frequency for standard and ELI grade Ti-6Al-4V (MA) in a 3.5% NaCl solution for ΔK values of 16 and 22 MPa$\sqrt{m}$ at R = 0.1. The data for standard grade Ti-6Al-4V (MA) were taken from a study by Dawson and Pelloux.[33] The data for Ti-6Al-4V (BA) were taken from a study by Chiou and Wei.[44] The data for the

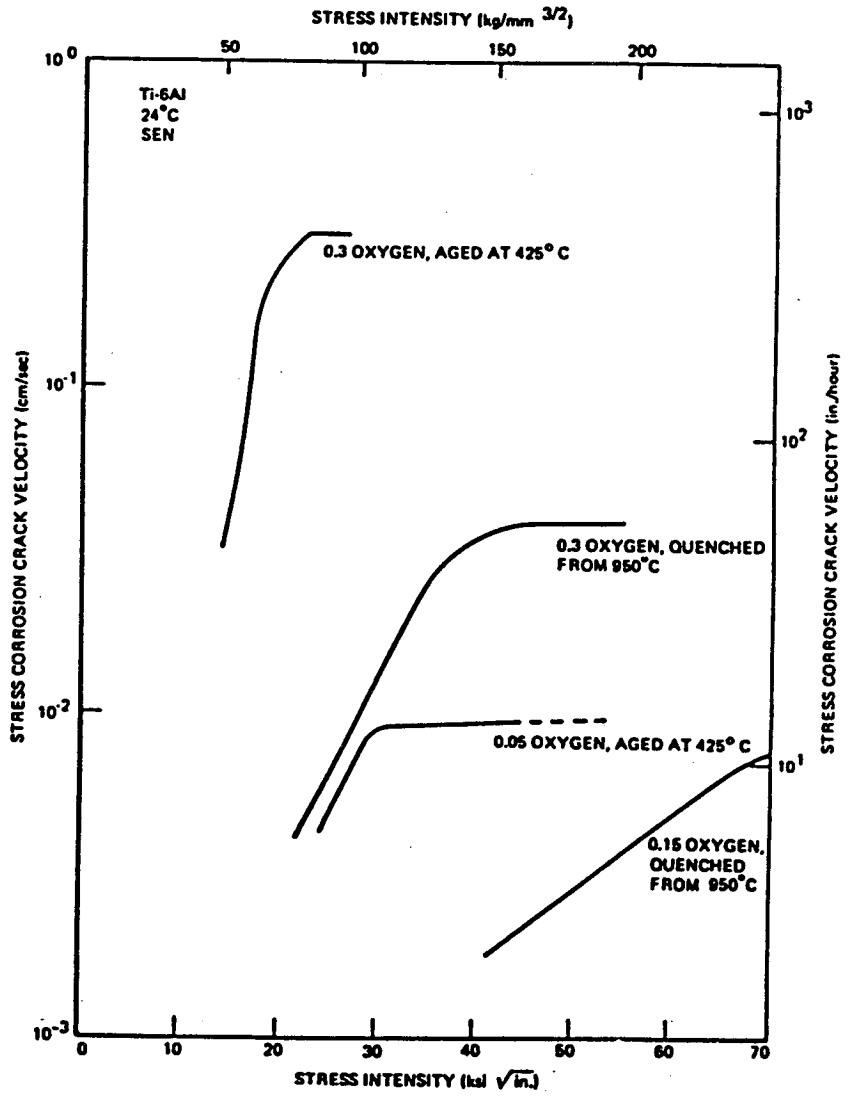

Figure 6.1 Effect of oxygen content on the SCC behavior of Ti-6Al. After Blackburn *et. al.* [47]

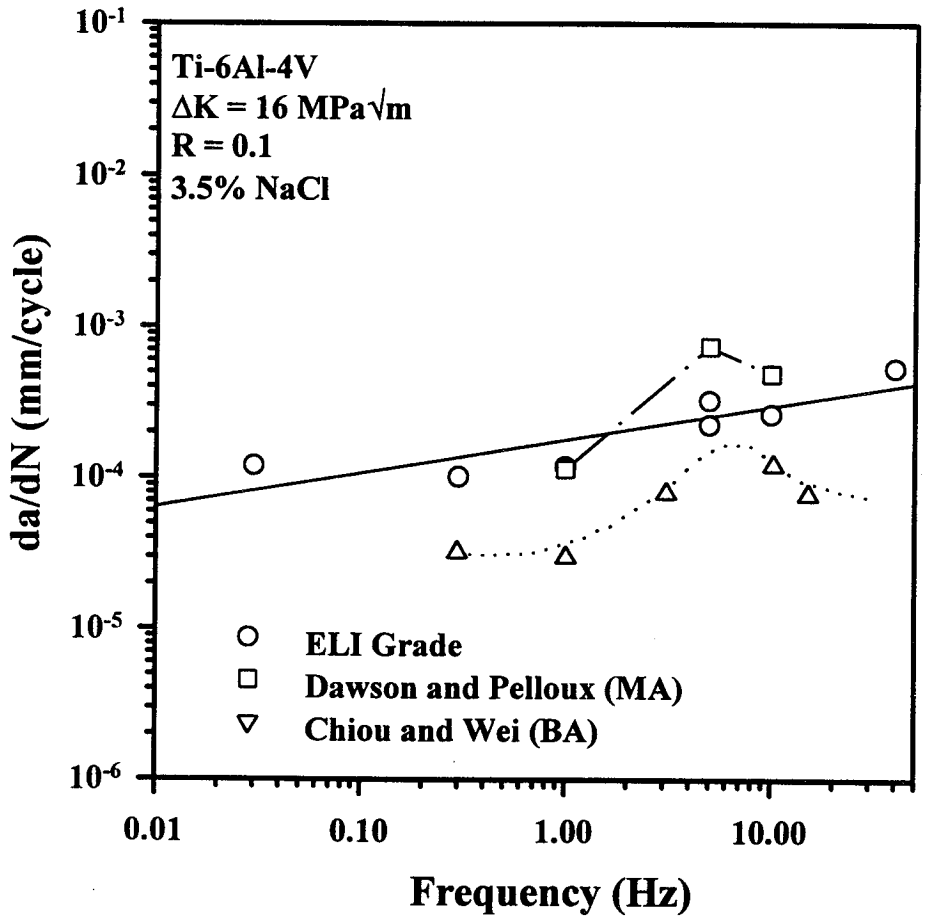

Figure 6.2: Comparison of the frequency response of standard and ELI grade Ti-6Al-4V (MA) and Ti-6Al-4V (BA) in 3.5% NaCl at R = 0.1 and $\Delta K = 16$ MPa$\sqrt{m}$.

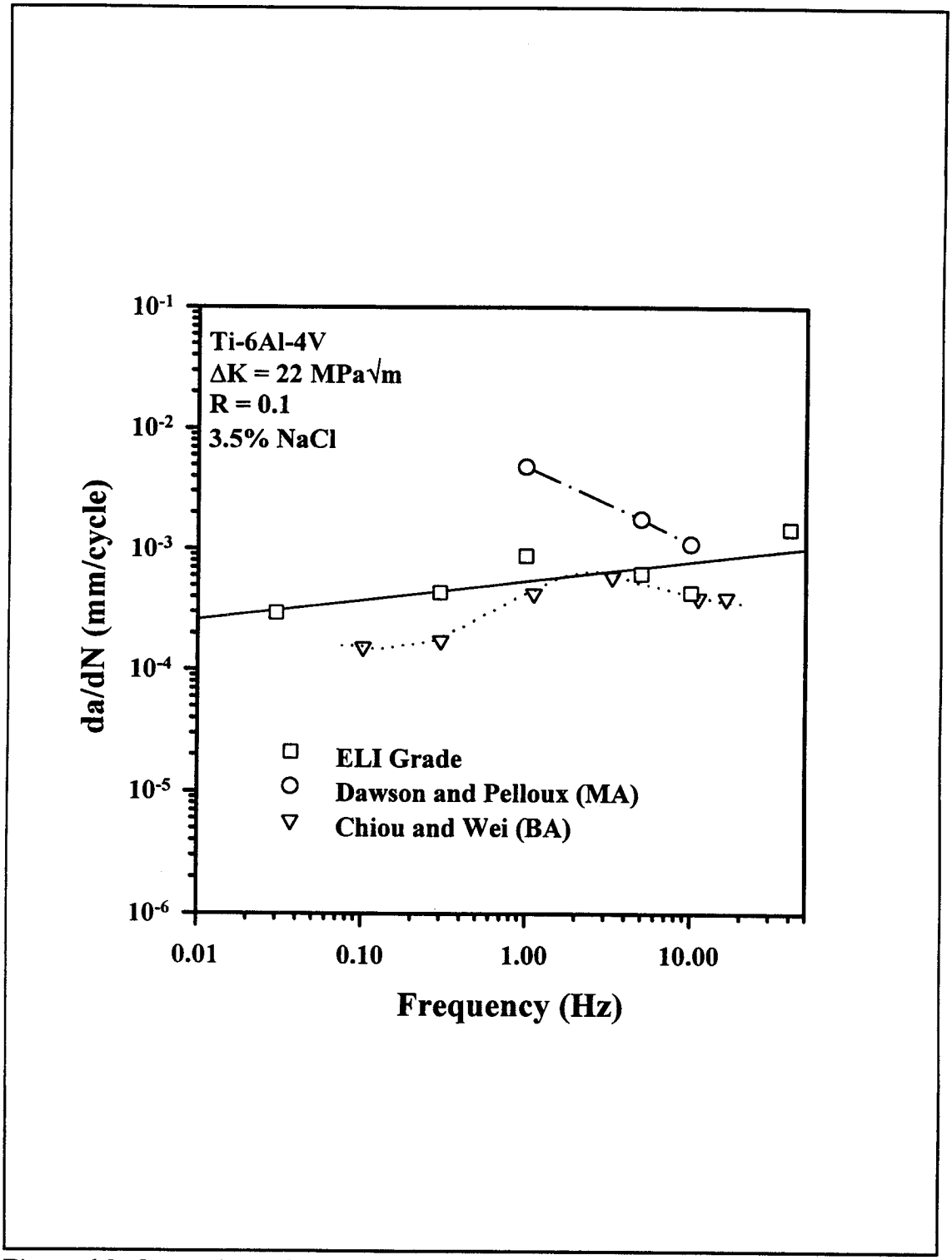

Figure 6.3: Comparison of the frequency response of standard and ELI grade Ti-6Al-4V (MA) and Ti-6Al-4V (BA) in 3.5% NaCl at R = 0.1 and $\Delta K = 22\ MPa\sqrt{m}$.

ELI grade were for a fixed electrode of -500 mV_{SCE}, while the standard grade data were for a free corrosion potential of about -240 mV_{SCE}. When data could not be located for the exact ΔK values needed, values were estimated from trends using a Paris Equation. As seen in the figures, at both ΔK levels of 16 and 22 MPa$\sqrt{m}$, da/dN increases with increasing frequency for the ELI grade. The standard grade exhibits a frequency dependence where da/dN decreases as frequency decreases below a critical frequency, and da/dN decreases as frequency increases above the critical frequency. This is consistent with the frequency "crossover" effect.[33] The behavior exhibited by the ELI grade is not consistent with the frequency "crossover" effect. It should be mentioned that the data for standard grade Ti-6Al-4V seen in Figures 6.2 and 6.3 are limited, and do not extend over a wide range of frequencies. The maximums exhibited by the standard grade could, in fact, be due to scatter in the data. This seems unlikely, since the alloy is known to exhibit the frequency "crossover" effect.[33,41]

One possible explanation for the failure of the ELI grade to exhibit the frequency "crossover" effect is the increased SCC resistance. Standard grade Ti-6Al-4V (MA) exhibits a K_{ISCC} of 23 MPa$\sqrt{m}$[33], and a ΔK of 16 MPa$\sqrt{m}$ is below ΔK_{SCC} for frequencies below 2 Hz, while a ΔK of 22 MPa$\sqrt{m}$ is above ΔK_{SCC}, as seen in Figure 4.13. The minimum value for K_{TH} determined during this research for the ELI grade Ti-6Al-4V (MA) was 48 MPa$\sqrt{m}$; at both the high and low ΔK value, ΔK is above ΔK_{SCC} for all of the frequencies tested, as seen in Figure 4.22. Since the frequency crossover effect is associated with the onset of "cyclic" SCC and the ΔK values did not reach ΔK_{SCC} for the ELI grade Ti-6Al-4V (MA), "cyclic" stress corrosion cracking did not occur.

This explanation is supported by the data seen in Figures 6.2 and 6.3. At both ΔK levels, especially the lower value, the FCP rates measured in the ELI grade Ti-6Al-4V (MA) are lower than those measured in the standard grade. The FCP rates measured in the ELI grade are higher than those seen in Ti-6Al-4V (BA), consistent with the literature.[42] Cyclic SCC is not occurring in the ELI grade, and the ELI grade is thus cracking slower than standard grade Ti-6Al-4V (MA). This implies that cyclic SCC is not controlling the environmental fatigue behavior of the ELI grade below K_{TH}.

6.2 Modeling EFCP of Ti-6Al-4V (MA,ELI)

6.2.1 Linear Superposition Model

The linear superposition model incorporated in UVAFAS.EXE has proven effective for certain, albeit limited, material/environments combinations where the alloy is extremely prone to SCC and $(da/dN)_{\text{stress corrosion}}$ is significantly greater than $(da/dN)_{\text{fatigue.}}$ This is achieved when K_{ISCC} is low and $(da/dt)_{\text{environment}}$ is rapid, or alternatively if $(da/dt)_{\text{environment}}$ is slow but f is also very slow or τ is prolonged.

The linear superposition model is effective for standard grade Ti-6Al-4V (MA) in a 3.5% NaCl solution for ΔK values where K_{max} is above K_{ISCC} and for $f > 1$ Hz. The ELI grade, however, demonstrates the limitations and inaccuracies of the linear superposition model. The linear superposition model incorrectly assumes that da/dN will significantly increase as frequency decreases. Specifically, the model assumes da/dN will be proportional to f^{-1}. The ELI grade Ti-6Al-4V exhibits da/dN which increases mildly with frequency; da/dN is proportional to $f^{0.1 \text{ to } 0.18}$. Linear superposition also assumes the alloy will be prone

to SCC. The ELI grade Ti-6Al-4V (MA) exhibits a resistance to SCC, with K_{TH} values between 48 and 55 MPa$\sqrt{m}$, compared to K_{ISCC} of 23 MPa$\sqrt{m}$ for the standard grade.[33] This results in a small $(da/dN)_{stress\ corrosion}$, and the f dependence of $(da/dN)_{total}$ is not predicted. The frequency independent da/dN, low $(da/dt)_{environment}$, and low SCC susceptibility exhibited by the ELI grade demonstrate that linear superposition is not effective.

6.2.2 Interpolative Model

The interpolative model developed during this research has proven effective in modeling the effects of frequency and stress ratio on FCP rates in standard and ELI grade Ti-6Al-4V when the load characteristics where data were interpolated are within the establishing data base. There are problems, however, associated with the use of an interpolative model.

One major problem is the difficulty encountered with modeling FCP data in the near threshold regime. Fortunately, the ΔK values for the standard and ELI grade where data were interpolated were all above threshold. Presently, the interpolative model allows the user to enter ΔK_{th} manually, calculate ΔK_{th} using an equation from NASA FLAGRO, or optimize the value of ΔK_{th} based on input data. The equation contained in NASA FLAGRO is accurate only for metals in moist air, thus this value is not accurate when modeling EFCP data. The cubic approximation is accurate, however, EFCP rate data are not easily obtained in the near threshold regime particularly for low loading frequencies. The 1 Hz experiment discussed in Chapter 4 required approximately 35 days to complete. The experiment was stopped when the growth rate was approximately 10^{-6} mm/sec, at least an order of magnitude

faster than those typically associated with threshold. The long times involved in obtaining threshold data illustrate the difficulties involved in obtaining EFCP rate data in the low ΔK regimes.

Fortunately, small changes in the value of ΔK_{th} do not greatly affect the fitted values of the equation parameters in the Forman Equation, or have a large effect on the quality of the fitted equation for high ΔK values. Also, the interpolative model will function if ΔK_{SCC} is input into the model instead of ΔK_{th}, the model will simply not interpolate trends in fatigue behavior for the lower ΔK regime. Small changes in the value of ΔK_{th} do seem to have a large effect on the parameter values in the Sigmoidal Equation. This is one reason the Forman Equation was the primary crack growth rate equation utilized in the interpolative model.

Another problem involved in using the interpolative model to describe EFCP rates in Ti-6Al-4V is the empirical nature of the model. A empirical model requires that a large data base be maintained, and that experiments be conducted for the material/environment system where fatigue behavior is to be modeled. More importantly, the model assumes that the damage mechanism for fatigue will not change within or outside the establishing data base, which is not always accurate.

This change in the damage mechanism can be seen by examining standard grade Ti-6Al-4V (MA). The interpolative model was effective for Ti-6Al-4V (MA) in 3.5% NaCl, however, the model ignores one of the primary factors which controls EFCP rates in $\alpha + \beta$ titanium alloys in aqueous chloride solutions, ΔK_{SCC}. The damage mechanism for environmental fatigue changes in Ti-6Al-4V (MA) above and below ΔK_{SCC}. Below ΔK_{SCC},

da/dN is perhaps controlled by the stability of the passive film at the crack tip. Thus, as frequency decreases, and the passive film is ruptured less often, da/dN decreases. Above ΔKSCC, the stability of the passive film no longer controls the fatigue behavior. Instead, hydrogen embrittlement is perhaps the controlling factor. Thus, as frequency decreases and more time is allowed for hydrogen embrittlement to occur, da/dN increases.

This change in the damage mechanism is not considered by the current interpolative model. For example, the model predictions shown in Figure 5.18 assume that da/dN will increase as frequency increases for all frequencies and all ΔK values where data were interpolated. While this trend in da/dN as a function of frequency is accurate over a large portion of the ΔK values where data were interpolated, the model predictions are not accurate at the high ΔK values, where "cyclic" SCC will occur. For these ΔK values, da/dN will decrease as frequency increases, a trend not exhibited by the model predictions.

For Ti-6Al-4V, the current modeling procedure is not sufficient to describe the complex dependence of da/dN on ΔK, and the important effects of ΔK_{SCC} and "cyclic" SCC. The following procedure is thus recommended for standard and ELI Ti-6Al-4V in NaCl. First, determine K_{IC} from a constant CMOD rate experiment with a precracked specimen fractured in moist air. Next, conduct a constant CMOD rate experiment with the alloy of interest in NaCl and where the load is increased monotonically to a stress intensity level of 45 MPa$\sqrt{m}$ in 30 minutes. If cracking does not occur, hold the load constant for 100 hours, and measure crack extension with DCPD or compliance.

Using the data from Dawson and Pelloux[33], construct a plot of ΔK_{SCC} as a functions of frequency, as seen in Figure 4.13. Conduct K-gradient fatigue experiments in moist air

and NaCl at a frequency of 40 Hz to produce wide range da/dN-ΔK data. Collect data for crack growth rates above 4 x 10^{-7} mm/cycle. Next, conduct a second set of K-gradient experiments in moist air and NaCl for a frequency of 0.5 Hz, and growth rates above 10^{-5} mm/cycle. Finally, conduct a variable frequency experiment where ΔK is held constant at either 12 or 25 MPa$\sqrt{m}$, and frequencies range between 0.008 and 100 Hz. Using the results of the K-gradient fatigue experiments, and the variable frequency experiment, the data for ΔK_{SCC} as a function of frequency taken from Dawson and Pelloux can be revised. For example, the data can be scaled so that at the lower frequencies, ΔK_{SCC} approaches the correct value of $(1-R)K_{TH}$ for the titanium alloy being studied.

Once the correct ΔK_{SCC} as a function of frequency is developed, a methodology or algorithm which correctly describes the ΔK_{SCC} transition and "cyclic" SCC can be implemented. This algorithm would have to describe the complex dependence of da/dN on ΔK illustrated in Figure 6.4. The algorithm would involve four interpolation functions. First, ΔK_{th} and ΔK_{SCC} would have to be written as a function of frequency. Next, da/dN for ΔK values below ΔK_{SCC} would be written as a function of frequency, as would da/dN for ΔK values above ΔK_{SCC}. These interpolation functions are:

$$\Delta K_{th} = f_1(f) \tag{6.1}$$

$$\Delta K_{SCC} = f_2(f) = a_0 f^{\gamma} \tag{6.2}$$

$$\frac{da}{dN} = a_2 f^{\beta} \qquad \Delta K > \Delta K_{SCC} \tag{6.3}$$

$$\frac{da}{dN} = a_1 f^{\alpha} \qquad \Delta K < \Delta K_{SCC} \qquad (6.4)$$

where γ ($\gamma < 0$), α ($\alpha > 0$), and β ($\beta < 0$) are empirical constants, as are a_0, a_1, and a_2. Given the lack of near ΔKth environmental FCP data, f_1 is unknown.

Currently, there are no crack growth rate equations contained in the interpolative model (UVAFAS) which exhibit the da/dN-ΔK behavior seen in Figure 6.4. Instead, either a multiple power law equation, or a set of crack growth rate equation could be utilized. Four separate power law segments, or crack growth rate equations would be needed. One segment would be needed for the threshold regime, one for the region between threshold and ΔK_{SCC}, one for the data at ΔK_{SCC}, and one for growth rate above ΔK_{SCC}. If a multiple power law equation was utilized, the locations of the segments corresponding to ΔK_{th} and ΔK_{SCC} could simply be shifted horizontally as a function of frequency according to Equations 6.1 and 6.2. The segments for the region between ΔK_{th} and ΔK_{SCC}, and the segment for data above ΔK_{SCC} could be shifted vertically according to Equations 6.3 and 6.4. The locations of the transition points between each segment could also be calculated using Equations 6.1 through 6.4.

6.3 Implications for Fatigue Life Prediction Including EFCP

The computer models developed during this research have proven effective for certain material/environment systems. The linear superposition model is effective for limited cases where the alloy is extremely sensitive to SCC, and $(da/dN)_{\text{stress corrosion}}$ is significantly

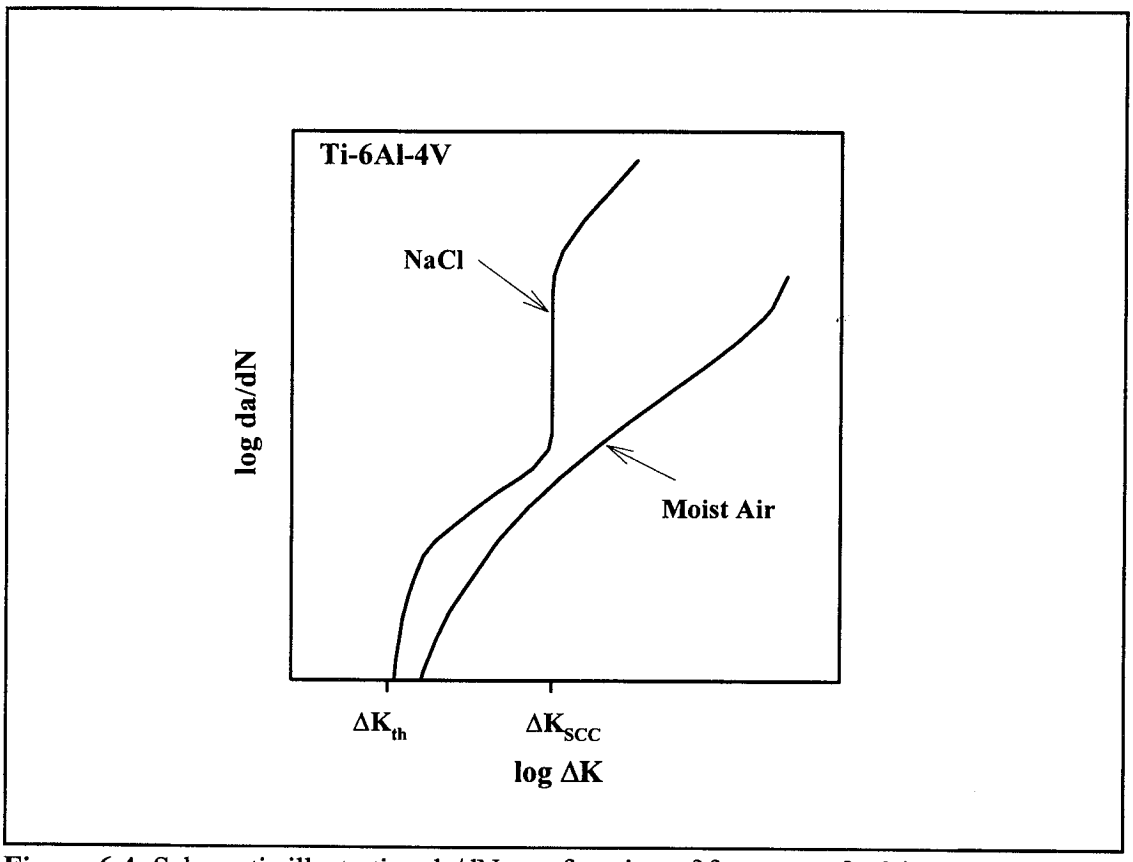

Figure 6.4: Schematic illustrating da/dN as a function of frequency for Ti-6Al-4V in moist air and NaCl environments.

greater than $(da/dN)_{fatigue}$. If these material/environment systems are relevant to aerospace applications, the linear superposition program can be implemented as a NASA FLAGRO module. This approach will describe the effects of R, f, τ, wave form, and ΔK on EFCP rates.

The interpolative model is effective for material/environment systems where the damage mechanism for environmental fatigue does not change within the establishing data base. The interpolative model is able to interpolate trends in fatigue behavior based on load characteristics, the model cannot be used for widespread prediction of da/dN versus ΔK outside the establishing data base.

The interpolative model can be incorporated in NASA FLAGRO. The model requires an extensive data base of da/dN versus ΔK data for various material/environment combinations and a wide range of loading variables. Incorporation of the model in FLAGRO would require the generation of this EFCP data for material/environment systems relevant to aerospace applications.

All of the models used in this research are empirical, and must be utilized with caution. They require a large data base, and are only useful for well-characterized material/environment systems. In order to effectively model and predict EFCP rate data for a wide range of material/environment systems, a more mechanistic approach needs to be developed. Mechanistic models based on an improved understanding of the parameters which affect EFCP must be developed and incorporated into the NASA FLAGRO program.

Chapter 7: Conclusions and Future Work

7.1 Conclusions

7.1.1 Environmental FCP Rate Modeling (UVaFAS)

1. The computer program UVAFAS.EXE provides a reasonable method for modeling time dependent EFCP rates as function of stress ratio, frequency, and hold time.
2. The algorithms used in the computer program UVAFAS.EXE have been bench marked against exact analytical solutions, as well as literature results.
3. The computer models contained in the program UVAFAS.EXE are effective in characterizing EFCP, and can be incorporated in NASA FLAGRO.

7.1.2 EAC of Ti-6Al-4V (MA,ELI)

1. Ti-6Al-4V (MA,ELI) exhibits a greater resistance to SCC than standard grade Ti-6Al-4V (MA) due the lower oxygen content of the ELI grade. Standard Ti-6Al-4V exhibits a K_{ISCC} of 23 MPa$\sqrt{m}$ in 3.5% NaCl, while ELI Ti-6Al-4V exhibits K_{TH} values of 48 and 55 MPa$\sqrt{m}$ depending on loading rate. Ti-6Al-4V (MA,ELI) exhibits a slower $(da/dt)_{environment}$ (of order 10^{-5} mm/sec or less) than standard Ti-6Al-4V.
2. A 1.0% NaCl solution (-500 mV_{SCE}) is detrimental and enhances FCP rates in Ti-6Al-4V (MA,ELI) by approximately two fold compared to fatigue in moist air.
3. ELI Ti-6Al-4V does not exhibit the frequency "crossover" effect for ΔK

values less than 25 MPa$\sqrt{m}$ and frequencies in the range of 0.03 to 40 Hz. Standard Ti-6Al-4V exhibits the frequency "crossover" effect.

4. Ti-6Al-4V (MA,ELI) exhibits a mild frequency dependence for ΔK levels of 12.5 and 25 MPa$\sqrt{m}$ in a 3.5% NaCl solution (-500 mV_{SCE}) for R = 0.1. For both ΔK levels, da/dN increases proportional to $f^{0.1 \text{ to } 0.2}$.

5. The frequency dependence of Ti-6Al-4V (MA,ELI) is governed by the increased resistance to SCC. Standard Ti-6Al-4V exhibits cyclic SCC and FCP rates which are faster than ELI Ti-6Al-4V, where cyclic SCC does not occur.

6. The crack closure levels measured during fatigue are consistent with plasticity induced closure. For ΔK above 10 MPa$\sqrt{m}$, K_{cl}/K_{max} is approximately 0.3, consistent with model predictions by Newman for plasticity induced closure.

7. Crack closure levels are independent of environment; moist air, a 1.0% NaCl solution (-500 mV_{SCE}), and a 3.5% NaCl solution (-500 mV_{SCE}) yield the same levels for K_{cl}/K_{max}.

8. Crack closure levels increase as ΔK decreases for ΔK levels below approximately 10 MPa$\sqrt{m}$. This rise in closure could be due to a change from plasticity induced to roughness or oxide induced closure as the crack tip opening displacement decreases.

7.1.3 Modeling EFCP

1. The linear superposition model is effective for limited material/environment

systems where the alloy is extremely sensitive to stress corrosion cracking and the contribution of stress corrosion to crack growth is significantly greater than that of inert environment mechanical fatigue. This is achieved when the loading frequency is low, the fatigue cycle stress intensity is higher than K_{ISCC}, and $(da/dt)_{environment}$ is relatively rapid.

2. Linear superposition is not effective for describing the fatigue behavior of Ti-6Al-4V (MA,ELI) in aqueous chloride solutions, since the alloy exhibits a high value for K_{TH} and low $(da/dt)_{environment}$ in aqueous chloride, as well as near frequency independent da/dN. The model does work for standard Ti-6Al-4V and Ti-8Al-1Mo-1V when K_{max} is above K_{ISCC}.
3. The interpolative model can be effectively used to model EFCP when the loading variables where data are interpolated lie within the range of the establishing data base. The model is not likely to be effective for predicting EFCP behavior outside the range of the establishing database.
4. Empirical models can be used to effectively model EFCP rates only for particular material/environment systems where substantial data exist. They cannot be used for widespread prediction of EFCP behavior.

7.2 Recommendations for Future Work

7.2.1 EAC of Ti-6Al-4V (MALI)

The results generated during this research for the EAC behavior of Ti-6Al-4V (MA,ELI) have raised questions that need to be addressed. First, the SCC resistance of the

ELI grade alloy needs to be examined, and explained based on a more careful metallurgical examination than provided during this research. The environmental fatigue behavior of the alloy needs to be examined for other time-dependent variables beside loading frequency, and experiments need to be conducted at frequencies above 40 Hz to further explore the "crossover" effect. The effect of loading wave form and hold time need to be explored. Finally, a more detailed closure analysis should be conducted so that the rise in K_{cl}/K_{max} at low ΔK levels is explained and the role of environment is examined.

7.2.2 Modeling EFCP

The conclusions just discussed have led to the following recommendations for future work in regard to modeling EFCP rates. The capability to calculate $(da/dt)_{environment}$ from $(da/dN)_{stress\ corrosion}$ data should be critically assessed and perhaps incorporated into the linear superposition model. This may improve the predictive capability of the model by generating a better set of $(da/dt)_{environment}$ data reflective of crack tip strain rates during fatigue. This involves solving for $(da/dt)_{environment}$ in the following equation:

$$\left(\frac{da}{dN}\right)_{stress\ \ corrosion} = \int_{\tau} \frac{da}{dt}\,[K(t)]\,dt \qquad (7.1)$$

The model should allow the user to choose between sinusoidal, ramp, or square wave forms to represent K(t), and between a Paris Equation and double power law to represent $(da/dt)_{environment}$. The calculations can be completed using linear regression techniques when $(da/dt)_{environment}$ is modeled by a Paris Equation, and a square wave form is utilized with R = 0. The problem quickly becomes more complicated and non linear when other equation and wave forms are utilized.

The functions utilized by the interpolative model need to be examined, to insure that they predict the correct trends in fatigue data for a wide range of material/environment systems as a function of hold time, particularly in titanium alloys. The effect of hold time on da/dN was not examined during this study. Also, the multiple power law model needs to be revised so that the methods used to define power law transitions are less subjective.

References

1. "E647-91 Standard Test Method for Measurement of Fatigue Crack Growth Rates," 1991 Annual Book of ASTM Standards, American Society for Testing and Materials, Philadelphia, PA, 1991, pp. 654-681.

2. P. C. Paris, M. P. Gomez and W. E. Anderson, *The Trend in Engineering*, Washington State University, Vol. 13, No. 1, 1961, pp. 9-14.

3. R. P. Wei and R. P. Gangloff, "Environmentally Assisted Crack Growth in Structural Alloys: Perspectives and New Directions," Fracture Mechanics: Perspectives and Directions, ASTM STP 1020, R. P. Wei and R. P. Gangloff, Eds., American Society for Testing and Materials, Philadelphia, PA, 1989, pp. 233-264.

4. J. A. Feeney, J. C. McMillan and R. P. Wei, "Environmental Fatigue Crack Propagation of Aluminum Alloys at Low Stress Intensity Levels," *Metallurgical Transactions*, Vol. 1, 1970, pp. 1741-1757.

5. R. P. Gangloff, "Corrosion Fatigue Crack Propagation in Metals," Environment Induced Cracking of Metals, R. P. Gangloff and M. B. Ives, Eds., National Association of Corrosion Engineers, Houston, TX, 1990, pp. 55-109.

6. R. G. Forman *et. al.*, NASA FLAGRO User's Manual (Version 2.0, Revision A), Report No. JSC-22267A, National Aeronautics and Space Administration, Lyndon B. Johnson Space Center, Houston, TX, 1994.

7. W. Elber, "Fatigue Crack Closure Under Tension," *Engineering Fracture Mechanics*, Vol. 2, 1970, pp. 37-45.

8. S. Suresh, Fatigue Of Metals, Cambridge University Press, Cambridge, England, 1991, pp. 222-254.

9. R. P. Gangloff and S. S. Kim, "Environment Enhanced Fatigue Crack Propagation in Metals: Inputs to Fracture Mechanics Life Prediction Models," NASA Contractor Report 191538, NASA Langley Research Center, Hampton, VA, 1993.

10. T. L. Anderson, Fracture Mechanics: Fundamentals and Applications, CRC Press, Boca Raton, FL, 1991, p. 607.

11. R. G. Forman *et. al.*, "Development of the NASA/FLAGRO Computer Program," Fracture Mechanics: Eighteenth Symposium, ASTM STP 945, D. T. Reed and R. P. Read, Eds., American Society for Testing and Materials, Philadelphia, PA, 1988, pp. 781-803.

12. Stress Corrosion Cracking and Hydrogen Embrittlement of Iron Based Alloys, J. Hochman, J. Slater, R. D. McCright, and R. W. Staehle, Eds., National Association of Corrosion Engineers, Houston, TX, 1977.

13. Corrosion Fatigue: Mechanics, Metallurgy, Electrochemistry, & Engineering, ASTM STP 801, T. W. Crooker and B. N Leis, Eds., American Society for Testing and Materials, Philadelphia, PA, 1983.

14. R. P. Gangloff, "Corrosion Fatigue Cracking," Manual on Corrosion Tests and Standards: Application and Interpretation, R. Baboian, Ed., American Society for Testing and Materials, Philadelphia, PA, in press 1995.

15. R. W. Hertzberg, Deformation and Fracture Mechanics of Engineering Materials, 3rd Ed, John Wiley & Sons, Inc., New York, NY, 1989, pp. 517-604.

16. R. G. Forman *et. al.*, NASA FLAGRO User's Manual (Version 2.0), Report No. JSC-22267, National Aeronautics and Space Administration, Lyndon B. Johnson Space Center, Houston, TX, 1992.

17. R. G. Forman *et. al.*, NASA FLAGRO User's Manual (Version August 1986), Report No. JSC-22267A, National Aeronautics and Space Administration, Lyndon B. Johnson Space Center, Houston, TX, 1989.

18. G. Haritos, T. Nicholas and G. O. Painter, "Evaluation of Crack Growth Models for Elevated Temperature Fatigue," Fracture Mechanics: Eighteenth Symposium, ASTM STP 945, D. T. Reed and R. P. Read, Eds., American Society for Testing and Materials, Philadelphia, PA, 1988, pp. 206-220.

19. R. H. Van Stone, O. C. Gooden and D. D. Krueger. "Advanced Cumulative Damage Modeling," Materials Laboratory, Air Force Aeronautical Laboratories, Wright Patterson Air Force Base, OH, 1988.

20. M. S. Miller and J. P. Gallagher, "An Analysis of Several Fatigue Crack Growth Rate (FCGR) Descriptions," Fatigue Crack Growth Measurement and Data Analysis, ASTM STP 738, S. J. Hudak, Jr. and R. J. Bucci, Eds., American Society for Testing and Materials, Philadelphia, PA, 1981, pp. 205-251.

21. J. Kuester and J. Mize, Optimization Techniques with FORTRAN, McGraw Hill Book Company, New York, NY, 1973, pp. 240-250.

22. D. M. Marquardt, "An Algorithm for Least Squares Estimation of Non-Linear Parameters," *J. Soc. Indust. Appl. Math*, Vol. 11, 1963, pp. 431-441.

23. R. P. Wei and J. D. Landes, "Correlation Between Sustained-Load and Fatigue Crack Growth in High Strength Steels," Materials Research and Standards, MTRSA, Vol. 9, No. 7, 1969, pp. 25-27,44-46.

24. M. O. Speidel, "Stress Corrosion and Corrosion Fatigue Crack Growth in Aluminum Alloys," Stress Corrosion Research, Hans Arup and R. N. Parkins, Eds., Sijthoff & Noordhoff International Publishers, Leyden, The Netherlands, 1979, pp. 117-176.

25. D. M. Harmon, C. R. Saff and J. G. Burns, "Development of An Elevated Temperature Crack Growth Routine," AIAA Paper 88-2387, American Institute of Aeronautics and Astronautics, 1988.

26. M. E. Mason, "Time-Dependent Fatigue Crack Propagation in 7000 Series Aluminum Alloys," M.S. Thesis, University of Virginia, Charlottesville, VA, 1994.

27. E. Richey, III, A. W. Wilson, J. M. Pope and R. P. Gangloff, "Computer Modeling the Fatigue Behavior of Metals in Corrosive Environments," NASA Contractor Report 194982, NASA Langley Research Center, Hampton, VA, 1994.

28. J. K. Donald, "A Procedure for Standardizing Crack Closure Levels," Mechanics of Fatigue Crack Closure, ASTM STP 982. J. C. Newman, Jr. and W. Elber, Eds., American Society for Testing and Materials, Philadelphia, PA, 1988, pp. 222-229.

29. "E399-90 Standard Test Method for Plane Strain Fracture Toughness of Metallic Materials," 1991 Annual Book of ASTM Standards, American Society for Testing and Materials, Philadelphia, PA, 1991, pp. 485-515.

30. "E-1152-87 Standard Test Method for Determining J-R Curves," 1991 Annual Book of ASTM Standards, American Society for Testing and Materials, Philadelphia, PA, 1991, pp. 825-835.

31. "E813-89 Standard Test Method for J_{IC}, A Measure of Fracture Toughness," 1991 Annual Book of ASTM Standards, American Society for Testing and Materials, Philadelphia, PA, 1991, pp. 713-733.

32. Metals Handbook Ninth Edition, American Society for Metals, Metals Park, OH, 1980, pp. 388-391.

33. D. B. Dawson and R. M. Pelloux, "Corrosion Fatigue Crack Growth of Titanium Alloys in Aqueous Environments," *Metallurgical Transactions*, Vol. 5, March, 1974, pp. 723-731.

34. J. D. Landes, "J Calculation From Front Face Displacement Measurement On A Compact Specimen," *International Journal of Fracture*, Vol. 16, 1980, pp. R183-R186.

35. J. A. Moskovitz and R. M. Pelloux, "Dependence of K_{ISCC} On Loading Rate and Crack Orientation in Ti-6Al-6V-2Sn," *Corrosion*, Vol. 35, 1979, pp. 509-514.

36. G. R. Yoder, L. A. Cooley and T. W. Crooker, "Observations on Microstructurally Sensitive Fatigue Crack Growth in Widmanstatten Ti-6Al-4V Alloy," *Metallurgical Transactions A*, Vol. 8A, 1977, pp. 1737-1743.

37. P. E. Irving and C. J. Beevers, "The Effect of Air and Vacuum Environments on Fatigue Crack Growth Rates in Ti-6Al-4V," *Metallurgical Transactions*, Vol. 5, 1974, pp. 391-398.

38. M. D. Halliday and C. J. Beevers, "Non-Closure of Cracks and Fatigue Crack Growth in β Heat Treated Ti-6Al-4V," *International Journal of Fracture*, Vol. 15, 1979, pp. R27-R30.

39. M. O. Speidel, M. J. Blackburn, T. R. Beck and J. A. Feeney, "Corrosion Fatigue and Stress Corrosion Crack Growth in High Strength Aluminum Alloys, Magnesium Alloys, and Titanium Alloys Exposed to Aqueous Solution," Corrosion Fatigue, Chemistry and Microstructure. O. Devereaux, A. J. McEvily and R. W. Staehle, Eds., National Association of Corrosion Engineers, Houston, TX, 1972, pp. 324-345.

40. D. B. Dawson, "Fatigue Crack Behavior of Ti-6Al-6V-2Sn in Methanol and Methanol Water Solutions," *Metallurgical Transactions A*, Vol. 12A, 1981, pp. 791-800.

41. G. R. Yoder, L. A. Cooley and T. W. Crooker, "Effects of Microstructure and Frequency on Corrosion Fatigue Crack Growth in Ti-8Al-1Mo-1V and Ti-6Al-4V," Corrosion Fatigue: Mechanics, Metallurgy, Electrochemistry, and Engineering, ASTM STP 801, T. W. Crooker and B. N Leis, Eds., American Society for Testing and Materials, 1983, pp. 159-174.

42. R. J. Bucci, "Environment Enhanced Fatigue and Stress Corrosion Cracking of a Titanium Alloy Plus A Simple Model for the Assessment of Environmental Influence on Fatigue Behavior," PhD. Dissertation, Lehigh University, Bethlehem, PA, 1970.

43. D. A. Meyn, "An Analysis of Frequency and Amplitude Effects on Corrosion Fatigue Crack Propagation in Ti-8Al-1Mo-1V," *Metallurgical Transactions*, Vol . 2, 1971, pp. 853-865.

44. S. Chiou and R. P. Wei, "Corrosion Fatigue Cracking Response of Beta Annealed Ti-6Al-4V Alloy in 3.5% NaCl Solution," Report No. NADC-83126-60 (Vol. 5), U. S. Naval Air Development Center, Warminister, PA, 1984.

45. J. C. Newman, Jr., "A Crack Opening Stress Equation for Fatigue Crack Growth," *International Journal of Fracture*, Vol. 24, 1984, pp. R131-R135.

46. T. T. Shih and R. P. Wei, "Load and Environment Interactions in Fatigue Crack Growth," Prospects in Fracture Mechanics, G. C. Sih, H. C. Van Elst, and B. Broek, Eds., Noordhoff International Publishing, Leyden, The Netherlands, 1974, pp. 231-250.

47. M. J. Blackburn, W. H. Smyrl and J. A. Feeney, "Titanium Alloys," Stress Corrosion Cracking in High Strength Steels and in Titanium and Aluminum Alloys, B. F. Brown, Ed., Naval Research Laboratory, Washington, D. C., 1972, pp. 245-363.

48. M. O. Speidel, "Corrosion Fatigue in Fe-Ni-Cr Alloys," Stress Corrosion Cracking and Hydrogen Environment Embrittlement of Iron Based Alloys, J. Hochman, J. Slater, R. D. McCright and R. W. Staehle, Eds., National Association of Corrosion Engineers, Houston, TX, 1977.

49. Private communication with J. C. Newman, Jr., NASA Langley Research Center, Hampton, Va, 1994.

50. Titanium Alloys Handbook, Metals and Ceramics Information Center, Batelle Columbus Laboratories, Columbus, OH, 1972.

Appendix A: University of Virginia Fatigue Analysis Software (UVaFAS)

The programs discussed in this thesis are available in executable form, along with the source code. The models are contained in the program UVAFAS.EXE, a FORTRAN 77 program compiled using a professional compiler from WATCOM, Inc. To execute the program, place the program disk in drive A:\ and type UVAFAS. A main menu will appear which allows the user to select the appropriate model (linear superposition model, interpolative model, or multiple power law model).

The speed of the program is increased if the program is executed from a hard drive. To install the program on a hard drive, copy the files on the program disk into the directory where the program will reside. The program must be executed from the DOS prompt, and cannot be executed from the Windows environment, due to the memory requirements of the program. The program uses the DOS/4GW DOS extender from Rational Systems.

The program files on the disk contain all of the necessary executable files, material data files, and source code. These files are:

UVAFAS.EXE - executable form of the computer models, written in FORTRAN 77

DOS4GW.EXE - DOS extender from Rational Systems

NASMFC, NASMFM, USRMFC, USRMFM - materials files

The source code is contained in the self extracting file SOURCE.EXE. To extract the source code, copy the file SOURCE.EXE into the directory or disk where the code is to reside, and type SOURCE. The source code can be edited using any DOS or Windows ASCII text editor.

The executable programs were compiled using a 32 bit, multi-platform FORTRAN

compiler. The compiler should alleviate memory problems encountered in earlier versions of the program which only utilized the first 640 K of conventional memory. The graphic subroutines utilized by the program are specific to the compiler used to generate the program. If the source code needs to be recompiled, the subroutines necessary to graph the da/dN versus ΔK data, as well as certain other graphic subroutines must be edited.

Appendix B: Interpolation Functions for Ti-6Al-4V (MA)

This appendix contains the values of the equation parameters and the interpolation functions developed when modeling the data for Ti-6Al-4V (MA) taken from a study by Dawson and Pelloux.[33] The first equation tested was the Forman Equation with closure. Results for fitting C and n with p equal to 0.25 and q equal to 0.75 are shown in Table B.1. These function can only be used when ΔK has units of MPa$\sqrt{m}$, and da/dN is in mm/cycles.

Table B.1: Forman Equation with Closure, fitting C and n (p = 0.25, q = 0.75)

Parameter	1 Hz	10 Hz
C	0.3818×10^{-7}	0.5709×10^{-6}
n	3.777	2.596

The following interpolation functions were developed:

$$C = -0.2052 \times 10^{-5} \log\left[\left(\frac{1}{f}\right) + 1\right] + 0.6558 \times 10^{-6} \log\left[\frac{\tau + 1}{0.1}\right] \qquad \textbf{(B.1)}$$

$$n = 4.551 \log\left[\left(\frac{1}{f}\right) + 1\right] + 2.408 \log\left[\frac{\tau + 1}{0.1}\right] \qquad \textbf{(B.2)}$$

$$\Delta K_{th} = 15.406 \log\left[\left(\frac{1}{f}\right) + 1\right] + 7.362 \log\left[\frac{\tau + 1}{0.1}\right] \qquad \textbf{(B.3)}$$

Next, the parameters C and n were fit while entering p and q as 2.0, resulting in the values shown in Table B.2.

Table B.2: Forman Equation with Closure, fitting C and n (p = 2.0, q = 2.0)

Parameter	1 Hz	10 Hz
C	0.9894×10^{-4}	0.1538×10^{-3}
n	1.519	0.919

The following relationships were determined:

$$C = -0.2113 \times 10^{-3} \log\left[\left(\frac{1}{f}\right) + 1\right] + 0.1625 \times 10^{-3} \log\left[\frac{\tau + 1}{0.1}\right] \quad \textbf{(B.4)}$$

$$n = 2.312 \log\left[\left(\frac{1}{f}\right) + 1\right] + 0.823 \log\left[\frac{\tau + 1}{0.1}\right] \quad \textbf{(B.5)}$$

$$\Delta K_{th} = 15.406 \log\left[\left(\frac{1}{f}\right) + 1\right] + 7.362 \log\left[\frac{\tau + 1}{0.1}\right] \quad \textbf{(B.6)}$$

The parameters C, n, p, and q were fit, resulting in the values given in Table B.3.

Table B.3: Forman Equation with Closure, fitting C, n, p, and q

Parameter	1 Hz	10 Hz
C	0.5336×10^{-3}	0.2212×10^{-2}
n	1.272	-0.185
p	2.726	2.378
q	0.696	4.964

The following relationships were determined:

$$C = -0.6465 \times 10^{-2} \log\left[\left(\frac{1}{f}\right) + 1\right] + 0.2480 \times 10^{-2}\left[\frac{\tau + 1}{0.1}\right] \quad \textbf{(B.7)}$$

$$n = 5.610 \log\left[\left(\frac{1}{f}\right) + 1\right] - 0.4172 \log\left[\frac{\tau + 1}{0.1}\right] \quad \textbf{(B.8)}$$

$$p = 1.340 \log\left[\left(\frac{1}{f}\right) + 1\right] + 2.323 \log\left[\frac{\tau + 1}{0.1}\right] \quad \textbf{(B.9)}$$

$$q = -16.440 \log\left[\left(\frac{1}{f}\right) + 1\right] + 5.645 \log\left[\frac{\tau + 1}{0.1}\right] \quad \textbf{(B.10)}$$

$$\Delta K_{th} = 15.406 \log\left[\left(\frac{1}{f}\right) + 1\right] + 7.362 \log\left[\frac{\tau + 1}{0.1}\right] \quad \textbf{(B.11)}$$

The Forman Equation without closure was tested; three cases were studied, fitting C and n with p entered as 0.25 and q as 0.75, fitting C and n with p and q entered as 2.0, and fitting C, n, p, and q. In all three cases, the value of m was 1.0. The results for fitting C and n with p entered as 0.25 and q as 0.75 are shown in Table B.4.

Table B.4: Forman Equation without Closure, fitting C and n (p = 0.25, q = 0.75)

Parameter	1 Hz	10 Hz
C	0.1627×10^{-7}	0.3203×10^{-6}
n	3.777	2.596

The parameters were set equal to the following relationships:

$$C = -0.1171 \times 10^{-5} \log\left[\left(\frac{1}{f}\right) + 1\right] + 0.3687 \times 10^{-6} \log\left[\frac{\tau + 1}{0.1}\right] \quad \textbf{(B.12)}$$

$$n = 4.551 \log\left[\left(\frac{1}{f}\right) + 1\right] + 2.408 \log\left[\frac{\tau + 1}{0.1}\right] \quad \textbf{(B.13)}$$

$$\Delta K_{th} = 15.406 \log\left[\left(\frac{1}{f}\right) + 1\right] + 7.362 \log\left[\frac{\tau + 1}{0.1}\right] \quad \textbf{(B.14)}$$

The parameters C and n were fit while entering p and q as 2.0; the resulting values are displayed in Table B.5.

Table B.5: Forman Equation without Closure, fitting C and n (p = 2.0, q = 2.0)

Parameter	1 Hz	10 Hz
C	0.6252×10^{-4}	0.1118×10^{-3}
n	1.519	0.9185

The following relationships were determined:

$$C = -0.1896 \times 10^{-3} \log\left[\left(\frac{1}{f}\right) + 1\right] + 0.1196 \times 10^{-3} \log\left[\frac{\tau + 1}{0.1}\right] \quad \textbf{(B.15)}$$

$$n = 2.312 \log\left[\left(\frac{1}{f}\right) + 1\right] + 0.823 \log\left[\frac{\tau + 1}{0.1}\right] \quad \textbf{(B.16)}$$

$$\Delta K_{th} = 15.406 \log\left[\left(\frac{1}{f}\right) + 1\right] + 7.362 \log\left[\frac{\tau + 1}{0.1}\right] \quad \textbf{(B.17)}$$

The parameters C, n, p, and q were fit, resulting in the values given in Table B.6.

Table B.6: Forman Equation without Closure, fitting C, n, p, and q

Parameter	1 Hz	10 Hz
C	0.4098×10^{-3}	0.1521×10^{-2}
n	1.272	-0.185
p	2.726	2.378
q	0.696	4.964

The following relationships were determined:

$$C = -0.4280 \times 10^{-2} \log\left[\left(\frac{1}{f}\right) + 1\right] + 0.1698 \times 10^{-2} \log\left[\frac{\tau + 1}{0.1}\right] \quad \textbf{(B.18)}$$

$$n = 5.610 \log\left[\left(\frac{1}{f}\right) + 1\right] - 0.4172 \log\left[\frac{\tau + 1}{0.1}\right] \quad \textbf{(B.19)}$$

$$p = 1.340 \log\left[\left(\frac{1}{f}\right) + 1\right] + 2.323 \log\left[\frac{\tau + 1}{0.1}\right] \quad \textbf{(B.20)}$$

$$q = -16.440 \log\left[\left(\frac{1}{f}\right) + 1\right] + 5.645 \log\left[\frac{\tau + 1}{0.1}\right] \quad \textbf{(B.21)}$$

$$\Delta K_{th} = 15.406 \log\left[\left(\frac{1}{f}\right) + 1\right] + 7.362 \log\left[\frac{\tau + 1}{0.1}\right] \quad \textbf{(B.22)}$$

The Hyperbolic Sine Equation was tested. The parameters C_2, C_3, and C_4 were fit, while C_1 was held constant at 0.5. The resulting values are shown in Table B.7.

Table B.7: Hyperbolic Sine Equation ($C_1 = 0.5$)

Parameter	1 Hz	10 Hz
C_2	4.914	4.326
C_3	-1.620	-1.429
C_4	-1.639	-2.714

The following relationships were determined:

$$C_2 = 2.265 \log\left[\left(\frac{1}{f}\right) + 1\right] - 92.493 \log\left[1 - R\right] \quad \textbf{(B.23)}$$

$$C_3 = -0.736 \log\left[\left(\frac{1}{f}\right) + 1\right] + 30.564 \log\left[1 - R\right] \quad \textbf{(B.24)}$$

$$C_4 = 4.140 \log\left[\left(\frac{1}{f}\right) + 1\right] + 63.058 \log\left[1 - R\right] \quad \textbf{(B.25)}$$

The Sigmoidal Equation was tested fitting B, P, Q, and D. Values determined for the equation parameters are given in Table B.8.

Table B.8: Sigmoidal Equation

Parameter	1 Hz	10 Hz
B	-4.097	-1.423
P	-0.1265	-2.816
Q	2.674	2.404
D	-0.7475	-4.635

The following relationships were determined:

$$B = -10.300 \log\left[\left(\frac{1}{f}\right) + 1\right] + 21.777 \log\left[1 - R\right] \quad \textbf{(B.26)}$$

$$P = 10.360 \log\left[\left(\frac{1}{f}\right) + 1\right] + 70.923\left[1 - R\right] \quad \textbf{(B.27)}$$

$$Q = 1.041 \log\left[\left(\frac{1}{f}\right) + 1\right] - 51.595 \log\left[1 - R\right] \quad \textbf{(B.28)}$$

$$D = 14.971 \log\left[\left(\frac{1}{f}\right) + 1\right] + 114.828 \log\left[1 - R\right] \quad \textbf{(B.29)}$$

$$\Delta K_{th} = 15.406 \log\left[\left(\frac{1}{f}\right) + 1\right] - 160.898 \log\left[1 - R\right] \quad \textbf{(B.30)}$$

Appendix C: Interpolation Functions for Ti-6Al-4V (MA,ELI)

The parameter values and interpolation functions in this appendix were determined for Ti-6Al-4V (MA,ELI) data taken from a study by Gangloff and Kim[9], as well as the Ti-6Al-4V (MA,ELI) data generated during this study. The first set of interpolation functions was utilized to interpolate the effect of stress ratio. Since f was constant, the form of the dependence on f is unimportant, the dependence is simply replaced by a constant. For the moist air environment, the following relationships were determined:

$$B = -203.15 \log\left[\left(\frac{1}{f}\right) + 1\right] - 5.27 \log\left[1 - R\right] \quad \textbf{(C.1)}$$

$$P = 53.27 \log\left[\left(\frac{1}{f}\right) + 1\right] + 7.54 \log\left[1 - R\right] \quad \textbf{(C.2)}$$

$$Q = 18.95 \log\left[\left(\frac{1}{f}\right) + 1\right] - 3.74 \log\left[1 - R\right] \quad \textbf{(C.3)}$$

$$D = 1.51 \log\left[\left(\frac{1}{f}\right) + 1\right] + 3.37 \log\left[1 - R\right] \quad \textbf{(C.4)}$$

$$\Delta K_{th} = 47.93 \log\left[\left(\frac{1}{f}\right) + 1\right] + 4.53 \log\left[1 - R\right] \quad \textbf{(C.5)}$$

For the 1.0% NaCl solution (-500 mV_{SCE}), the following relationships were determined:

$$B = -43.60 \log\left[\left(\frac{1}{f}\right) + 1\right] - 2.40 \log\left[1 - R\right] \quad \textbf{(C.6)}$$

$$P = -16.55 \log\left[\left(\frac{1}{f}\right) + 1\right] + 9.04 \log\left[1 - R\right] \quad \textbf{(C.7)}$$

$$Q = 24.65 \log\left[\left(\frac{1}{f}\right) + 1\right] - 5.20 \log\left[1 - R\right] \quad \textbf{(C.8)}$$

$$D = -110.72 \log\left[\left(\frac{1}{f}\right) + 1\right] - 0.0013 \log\left[1 - R\right] \quad \textbf{(C.9)}$$

$$\Delta K_{th} = 47.93 \log\left[\left(\frac{1}{f}\right) + 1\right] + 4.53 \log\left[1 - R\right] \quad \textbf{(C.10)}$$

REPORT DOCUMENTATION PAGE

Form Approved
OMB No. 0704-0188

1. AGENCY USE ONLY (Leave blank)	2. REPORT DATE	3. REPORT TYPE AND DATES COVERED
	October 1995	Contractor Report

4. TITLE AND SUBTITLE

Empirical Modeling of Environment-Enhanced Fatigue Crack Propagation in Structural Alloys for Component Life Prediction

5. FUNDING NUMBERS

G NAG1-745

WU 297-40-00-01

6. AUTHOR(S)

Edward Richey III

7. PERFORMING ORGANIZATION NAME(S) AND ADDRESS(ES)

University of Virginia
School of Engineering and Applied Science
Charlottesville, VA 22903

8. PERFORMING ORGANIZATION REPORT NUMBER

9. SPONSORING / MONITORING AGENCY NAME(S) AND ADDRESS(ES)

National Aeronautics and Space Administration
Langley Research Center
Hampton, VA 23681-0001

10. SPONSORING / MONITORING AGENCY REPORT NUMBER

NASA CR-198231

11. SUPPLEMENTARY NOTES

Final Report - Langley Technical Monitor: Robert S. Piascik
The information in this report was offered as a thesis in partial fulfillment of the requirements for the Degree of Master of Science in Mechanical Engineering, University of Virginia, May 1995.

12a. DISTRIBUTION / AVAILABILITY STATEMENT

Unclassified - Unlimited

Subject Category - 24

12b. DISTRIBUTION CODE

13. ABSTRACT *(Maximum 200 words)*

This research aims to develop the methods and understanding needed to incorporate time and loading variable dependent environmental effects on fatigue crack propagation (FCP) into computerized fatigue life predication codes such as NASA FLAGRO (NASGRO). In particular, the effect of loading frequency on FCP rates in $\alpha+\beta$ titanium alloys exposed to an aqueous chloride solution is investigated. The approach couples empirical modeling of environmental FCP with corrosion fatigue experiments.

Three different computer models have been developed and incorporated in the DOS executable program, UVAFAS. A multiple power law model is available, and can fit a set of fatigue data to a multiple power law equation. A model has also been developed which implements the Wei and Landes linear superposition model, as well as an interpolative model which can be utilized to interpolate trends in fatigue behavior based on changes in loading characteristics (stress ratio, frequency, and hold times).

14. SUBJECT TERMS

Empirical modeling; Superposition; Interpolative; Corrosion Fatigue; Environmental fatigue; NASGRO; Crack propagation

15. NUMBER OF PAGES

173

16. PRICE CODE

A08

17. SECURITY CLASSIFICATION OF REPORT	18. SECURITY CLASSIFICATION OF THIS PAGE	19. SECURITY CLASSIFICATION OF ABSTRACT	20. LIMITATION OF ABSTRACT
Unclassified	Unclassified		